SPECTROSCOPIC STUDIES OF THE HELIUM-CADMIUM LASER DISCHARGE

Peter G. Browne

A Thesis Submitted for the Degree of PhD
at the
University of St Andrews

1974

Full metadata for this item is available in
St Andrews Research Repository
at:
http://research-repository.st-andrews.ac.uk/

Please use this identifier to cite or link to this item:
http://hdl.handle.net/10023/14157

This item is protected by original copyright

SPECTROSCOPIC STUDIES OF THE HELIUM - CADMIUM LASER DISCHARGE

A thesis

presented by

P. G. Browne, BSc

to the

University of St. Andrews

in application for the degree of

Doctor of Philosophy

ProQuest Number: 10166309

All rights reserved

INFORMATION TO ALL USERS
The quality of this reproduction is dependent upon the quality of the copy submitted.

In the unlikely event that the author did not send a complete manuscript and there are missing pages, these will be noted. Also, if material had to be removed, a note will indicate the deletion.

ProQuest 10166309

Published by ProQuest LLC (2017). Copyright of the Dissertation is held by the Author.

All rights reserved.
This work is protected against unauthorized copying under Title 17, United States Code
Microform Edition © ProQuest LLC.

ProQuest LLC.
789 East Eisenhower Parkway
P.O. Box 1346
Ann Arbor, MI 48106 – 1346

Th 8214

However, if I had waited long enough I probably never would have written anything at all since there is a tendency when you really begin to learn something about a thing not to want to write about it but rather to keep on learning about it always and at no time, unless you are very egotistical, which, of course, accounts for many books, will you be able to say: now I know all about this and will write about it.

Ernest Hemingway
"Death in the Afternoon"

DECLARATION

I hereby certify that this thesis has been composed by me, and is a record of work done by me, and has not previously been presented for a higher degree.

This research was carried out in the School of Physical Sciences, in the University of St. Andrews, under the supervision of Mr M H Dunn and Dr A Maitland.

P G Browne

CERTIFICATE

We certify that Peter G Browne, BSc, has spent nine terms at research work in the School of Physical Sciences, in the University of St Andrews, under our direction, that he has fulfilled the conditions of the Resolution of the University Court, 1967, No 1, and that he is qualified to submit the accompanying thesis in application for the degree of Doctor of Philosophy.

M H Dunn

A Maitland

CAREER

P G Browne was born in Tamworth, N.S.W., on 7 June 1948 and educated at Newcastle Boys' High School N.S.W. He was awarded a National Undergraduate Scholarship to the Australian National University, Canberra, and obtained the degree of BSc with first class Honours in Physics in 1968. After seven months as a Research Assistant in the Department of Engineering Physics at the A.N.U. he commenced postgraduate studies at the University of St. Andrews in August 1969. Since July 1972 he has been a Postdoctoral Fellow at St. Andrews, collaborating with Dr. A L S Smith on the development of sealed carbon dioxide lasers.

ACKNOWLEDGMENTS

I thank:

My supervisors, M H Dunn and A Maitland, for their advice, interest and encouragement throughout this work.

The other members of the Laser Group, particularly J N Ross and A J Kinnear, for their advice and valuable criticism.

R McCraw of the Mechanical Workshop, and F Akerboom, the glassblower. This work owes much to their various skills.

Messrs Laser Associates, for financial support.

Mrs N Pacholek, for typing this thesis.

My wife, Liz, for her encouragement and understanding.

ABSTRACT

The techniques of absorption and perturbation spectroscopy have been applied to the He-Cd laser discharge to determine species densities, excitation rates and de-excitation rates of relevance to laser oscillation on transitions in the cadmium ion.

The first section of this work describes the use of a line absorption technique to measure helium singlet and triplet metastable densities in a 3 mm bore capillary tube for both pure helium discharges (current range 10 - 200 mA, pressure range 0.5 - 15 torr) and for He-Cd discharges. For the pure helium discharge, with constant discharge current, the singlet and triplet densities show pronounced maxima of 2×10^{12} cm^{-3} and 9×10^{12} cm^{-3} respectively around 2 torr. At constant pressure the metastable densities saturate for currents above about 20 mA. The measured triplet densities are in fair agreement with values calculated using known cross-sections for production and loss processes.

The addition of cadmium vapour has two principal effects: the metastable populations are almost halved when the optimum cadmium pressure for lasing is present while the current saturation is displaced towards higher currents (60 - 120 mA). The observed optimum performance of the He-Cd laser with respect to discharge current, helium filling pressure and cadmium partial pressure is related directly to the behaviour of the helium metastable densities as these parameters are varied.

The second section describes the application of the technique of perturbation spectroscopy to the helium-cadmium laser. Chopping the radiation field inside the cavity of the laser operating at 4416Å induces perturbations in the populations of the $5s^2\ ^2D_{3/2,5/2}$ and $5p\ ^2P_{3/2}$ levels of the cadmium ion. Analysis of the perturbations of the $5p\ ^2P_{3/2}$ and $5s^2\ ^2D_{5/2}$ populations shows that the ratio of non-radiative

to radiative de-excitation rates for the latter level (the upper level of the 4416Å laser transition) is 0.9 ± 0.2, with little dependence on discharge conditions. From the $5s^2\ ^2D_{3/2}$ population changes the cross-section for excitation of this level from the $5s^2\ ^2D_{5/2}$ level by electron collisions is found to be $\sim 7 \times 10^{-16}$ cm^2.

NOTE:

The principal results of the experiments described in this thesis have been published as follows:

(a) Browne P G and Dunn M H 'Metastable densities and excitation processes in the He-Cd laser discharge' J Phys B:Atom Molec Phys 6 1103-1117 June 1973

(b) Browne P G and Dunn M H 'Perturbation spectroscopy of the He-Cd laser discharge' J Phys B:Atom Molec Phys 7 May 1974

TABLE OF CONTENTS

		Page
CHAPTER I	INTRODUCTION	1.1
CHAPTER II	THEORETICAL ANALYSIS OF THE ABSORPTION EXPERIMENT	2.1
2.1	Introduction	2.2
2.2	Optical Design Criteria	2.3
2.3	Diffraction Effects at Stop	2.7
2.4	Analysis of the Re-absorption Technique	2.7
2.5	Factors Influencing Line Profiles	2.9
2.6	Experimental Examination of Line Widths	2.10
2.7	Structure of the Examined Lines and Absorption of a Line with Overlapping Components	2.11
	Figures 2.1 - 2.8	2.15-2.18
CHAPTER III	METASTABLE POPULATIONS IN THE PURE HELIUM DISCHARGE	3.1
3.1	Introduction	3.2
3.2	Apparatus and Experiment	3.3
3.3	Results for the Pure Helium Discharge	3.6
3.4	Discussion for the case of a Pure Helium Discharge	3.12
	Figures 3.1 - 3.11	3.19-3.23
CHAPTER IV	EFFECT OF CADMIUM VAPOUR ON THE METASTABLE POPULATIONS	4.1
4.1	Introduction	4.2
4.2	Cadmium Neutral Density	4.2
4.3	Metastable Densities in the Presence of Cadmium Vapour	4.3
	Figures 4.1 - 4.7	4.9-4.12

		Page
CHAPTER V	PERTURBATION SPECTROSCOPY OF THE HELIUM - CADMIUM DISCHARGE	5.1
5.1	Introduction	5.2
5.2	Preliminary Considerations	5.3
	5.2.1 Spatial Anisotropy in the Sidelight	5.3
	5.2.2 Calibration of the Optical System	5.4
5.3	Experiment	5.6
5.4	Results and Discussion	5.7
	5.4.1 General Remarks	5.7
	5.4.2 Perturbation at 2144Å	5.9
	5.4.3 Perturbation at 3250Å	5.17
	Figures 5.1 - 5,13	5.23-5.29
CHAPTER VI	SUMMARY AND CONCLUSIONS	6.1
6.1	Introduction	6.2
6.2	Absorption Spectroscopy	6.2
6.3	Perturbation Spectroscopy	6.7
APPENDIX I	CONSTRUCTION OF A CATAPHORETIC HELIUM-CADMIUM LASER	A1.1
A1.1	Introduction	A1.2
A1.2	The Laser Tube and Vacuum System	A1.2
A1.3	Cadmium Oven Design	A1.4
A1.4	Cathode Requirements	A1.4
A1.5	Operating Characteristics and Laser Power	A1.5
	Figures A1.1-A1.3	A1.7-A1.8
APPENDIX II	COMPUTER CALCULATION OF THE ABSORPTION FOR A LINE WITH OVERLAPPING COMPONENTS	A2.1
	Figures AII.I - AII.2	A2.4-A2.5
REFERENCES		R1-R3

CHAPTER I

INTRODUCTION

Prior to 1968, metal vapour lasers were little studied. The principal work concerned only the discovery of new lasing transitions with pulsed excitation. Very little diagnostic examination of particular systems was reported. The basis of the antipathy to metal vapour lasers was twofold: first, these systems did not exhibit any outstanding features in their performance compared to single gas or gas-mixture lasers then available and second, the containment of corrosive and poisonous metal vapours at temperatures up to 1000°C posed many experimental problems.

This situation was radically changed by the two papers of Silfvast (1), (2), in which continuous laser oscillation was reported on the 4416Å and 3250Å transitions of the cadmium ion ($5s^2\ ^2D_{5/2}$ - $5p^2\ P_{3/2}$ and $5s^2\ ^2D_{3/2}$ - $5p\ ^2P_{1/2}$ respectively). The latter transition remains the shortest wavelength at which continuous laser oscillation has been obtained. Laser powers of the order of 100 mW at 4416Å and 20 mW at 3250Å are now commonplace. The active medium of this laser is the positive column of a helium capillary discharge which is seeded with the metal vapour.

Shortly after the above reports a simple and elegant technological development by Sosnowski (3) and Goldsborough (4) eliminated the need for a continuous oven along the length of the discharge tube. It has long been known that in a discharge in a mixture of gases the constituent with the lowest ionization potential is pumped towards the cathode - an effect known as cataphoresis (5). Sosnowski (3) and Goldsborough (4) found that if a few pellets of the metal were placed inside the laser tube at the anode end of the capillary discharge and heated by a small oven the metal vapour was distributed uniformly along the tube by cataphoresis. Further, by making a short section of the tube near the cathode with a much larger diameter than the capillary, the metal

could be condensed as the walls of the enlarged section were much cooler than the walls of the capillary tube.

Three parameters are found to affect the laser power produced by cataphoretic lasers - the cadmium oven temperature, the discharge current and the helium filling pressure. Pronounced maxima are observed in the output power as a function of each variable (with the other two fixed). Optimum power is obtained for currents of about 100 mA, oven temperatures about 200°C and helium filling pressures of 3 torr.

The He-Cd laser is therefore a convenient source of coherent radiation in the deep blue and ultraviolet regions of the spectrum. Output powers are in the range between those of the low power He-Ne laser (1 - 10 mW) and the argon ion laser (1 - 10 W). Naturally this inspired various studies of the laser discharge to clarify the excitation processes producing the population inversion necessary for laser oscillation. These studies will now be briefly reviewed.

Silfvast proposed (1), and it is now generally accepted, that Penning collisions between helium atoms in the singlet and triplet metastable states and ground state cadmium atoms simultaneously ionize the metal and excite the upper laser levels, according to the reaction

$$He_m + Cd_g \rightarrow Cd^+ (5s^2\ {}^2D_{3/2,5/2}) + He_g + e^- + \Delta E \quad (1.1)$$

The subscripts m,g denote metastable and ground states respectively, and ΔE the excess energy of the reaction.

Schearer and Padovani (6) and Riseberg and Schearer (7), by measuring decay rates of spectral lines in a He-Cd static afterglow, determined a value of 4.5×10^{-15} cm^2 for the total de-excitation cross-section of helium triplet metastables by cadmium ground state atoms. Čermak (8) deduced cross-sections for excitation into individual states of the cadmium ion (including the ground state) by an analysis of the

kinetic energy of the electrons produced in Penning collisions.

Cross-sections for the excitation of cadmium ion levels by electron collisions with ground state atoms were determined by Varshavskii et al (9), while the electron densities under lasing conditions were measured by Dunn (10).

Using a flowing afterglow technique Webb et al (11), determined the relative contributions of Penning collisions and charge transfer collisions to the excitation of upper laser levels in a wide range of metals. For the laser transitions of interest here it was found that the contribution of charge transfer excitation was negligible.

Because of their role in the excitation of the upper laser levels it is important to know the number densities of the helium metastable atoms under conditions appropriate to laser oscillation, and also their dependence on the discharge parameters : current and the partial pressures of helium and cadmium. The validity of the excitation mechanism (equ. (1.1)) can then be further checked by comparing the parametric behaviour of the metastable species and the laser output power.

As there are no radiative transitions from the helium metastable levels, their densities can be measured only by absorption techniques. The first section of this thesis describes the application of the re-absorption technique of Harrison (12) to measure the absorption coefficients of transitions terminating on the metastable levels ($3p\ ^1P$ - $2s\ ^1S$ at 5016Å, $4p\ ^1P$ - $2s\ ^1S$ at 3965Å and $3p\ ^3P$ - $2s\ ^3S$ at 3889Å). From the absorption coefficients, the Einstein A - coefficients and the transition line shapes, helium singlet and triplet metastable densities have been determined. Chapter II discusses the theory of the absorption experiments and Chapter III its application to the determination of metastable densities in a pure helium discharge. In Chapter IV the influence of cadmium vapour on the metastable densities

is then considered. Appendix I describes the construction and operation of a cataphoretic He-Cd laser. The laser power at 4416Å is shown as a function of the operating parameters.

The second section, Chapter V, concerns the perturbation spectrum of the He-Cd discharge. Chopping the 4416Å laser radiation perturbs the populations of the $5s^2\ ^2D_{5/2}$ level (the upper laser level), and the $5p\ ^2P_{3/2}$ and $5s^2\ ^2D_{3/2}$ levels of CdII. Analysis of these perturbations with two- and three-level models and the appropriate rate equations enables the relative pumping rates of the upper and lower laser levels ($5s^2\ ^2D_{5/2}$, $5p\ ^2P_{3/2}$ respectively) to be determined, as well as the rate of non-radiative de-excitation of the upper laser level. Analysis of the perturbations of the $5s^2\ ^2D_{3/2}$ level population allows the cross-sections for excitation to this level from the $5p\ ^2P_{3/2}$ and $5s^2\ ^2D_{5/2}$ levels by electron collisions to be estimated.

CHAPTER II

THEORETICAL ANALYSIS OF THE ABSORPTION EXPERIMENT

2.1 Introduction

All the methods for determining metastable densities involve measurement of the absorption of lines terminating on the metastable levels. Emission spectroscopy cannot be used because of the low transition probabilities for radiative decay from metastable levels. Line absorption techniques usually require two separate but identical discharges - one acts as a source and the other as absorber. This ensures similar line profiles for emission and absorption and is one of the few cases where the analysis of results is relatively simple (the Ladenburg - Reiche case (13)).

As the eventual object of this work is the study of the helium-cadmium discharge the problem arises of maintaining two such discharges identical over the time periods required for the absorption experiments. Experience with the laser system (Appendix I) has shown this to be rather difficult.

It was decided, therefore, to use the reabsorption technique described by Harrison (12), in which one discharge acts as both source and absorber. In this technique the light emerging from one end of the discharge tube is reflected back into the tube by a plane front-aluminised mirror with calibrated reflectivity. The fractional absorption of the discharge is then determined by comparing the signal due to the light entering a spectrometer directly along the tube axis (with mirror covered) with the signal due to the additional light reflected back through the tube when the mirror is uncovered.

Stops are necessary in the light collection arrangement to ensure that reflections from the tube walls are avoided and that each volume element along the axis of the discharge (and its image in the mirror) radiates the same amount of light into the spectrometer.

With the light collection system thus defined, the absorption

coefficient, k_ν, for the transition under investigation can be calculated from the measured fractional absorption, knowing the active length of the discharge and the transition line profile (13).

This chapter discusses the optical design criteria of the absorption experiment including diffraction effects at the stops involved. The re-absorption technique is analysed for a simple Doppler-broadened line, and the analysis is extended to a line consisting of overlapping fine-structure components. Factors influencing the line profile in a capillary discharge in helium are discussed and experimental measurements of the Doppler width of the 5016Å ($3p\ ^1P - 2s\ ^1S$) helium line considered.

2.2 Optical Design Criteria

In order that the absorption coefficient for a particular spectral line may be determined from the changes in its intensity produced by the presence of the mirror, stops must be placed in the optical system to ensure that similar volume elements of the plasma along the axis of the discharge contribute similar intensities to the spectrometer slit (in the absence of absorption), ie the effective volume element must be independent of x, the distance from stop A (Fig. 2.1).

This is arranged by placing two circular stops between the tube and the spectrometer slit. The principal stop, A, is in contact with the tube end nearer the spectrometer and the smaller stop, B, is immediately in front of the spectrometer slit.

The analysis of the geometry of such an arrangement is a modification of that of Harrison (12) to apply to a system with circular (instead of rectangular) stops.

The plasma is taken to be a uniform cylinder of length d and diameter 2D (Fig. 2.1). The plasma tube is separated from the mirror by a distance a, and stop A from the spectrometer by a distance z.

The acceptance angle θ defined by the stops A,B must be small enough to ensure that the light collected comes wholly from within the tube (or its mirror image) and not indirectly by reflections from the walls,

ie $$2\theta \leqslant \frac{2D}{2a+2d+\frac{zR}{r+R}}$$

where r,R are the radii of stops B,A respectively.

But $$2\theta = \frac{2R(R+r)}{zR}$$

$$\therefore \quad \frac{2(R+r)}{z} \leqslant \frac{2D}{2a+2d+\frac{zR}{r+R}}$$

ie $$2(R+r)(a+d) + zR \leqslant Dz$$

But $$2(a+d) = L$$

$$\therefore \quad L(R+r) + zR \leqslant Dz \qquad (2.1)$$

We require further that the fraction of light gathered from each volume element is limited by the smaller stop B.

ie $$\frac{2R}{L} \geqslant \frac{2r}{L+z} \qquad (2.2)$$

If both conditions (2.1) and (2.2) are fulfilled, the volume dV' of the element at x (of thickness dx) in the discharge contributing light to the slit is given by

$$dV' = \pi\{R + x(\frac{R+r}{z})\}^2 \, dx$$

and the fraction of light, emitted by any source within this element, which enters the spectrometer slit is (assuming no absorption along its path)

$$\frac{\pi r^2}{4\pi(z+x)^2}$$

Thus the 'effective volume' dV of this element is

$$\frac{\pi r^2}{4\pi(z+x)^2} \; \pi\{R + x(\frac{R+r}{z})\}^2 \, dx \; . \qquad (2.2a)$$

For $r \ll R$, dV is given by

$$dV = \frac{\pi r^2}{4\pi(z+x)^2} \; \pi \{R + \frac{x}{z} R\}^2 \, dx,$$

$$= \frac{\pi r^2 R^2}{4z^2} dx \ , \qquad (2.3)$$

which is independent of x.

From (2.2) we have, $R \geqslant \frac{rL}{L+z}$.

From (2.1) we have $\frac{Dz}{L+z} \geqslant R$. Hence the limits on R are given by

$$\frac{rL}{L+z} \leqslant R \leqslant \frac{Dz}{L+z} .$$

Since $r << R$, the left hand inequality is always fulfilled and the condition on R becomes

$$R \leqslant \frac{Dz}{L+z} .$$

The geometry for optimum light gathering is now determined. Let $r = kR$ (where $k << 1$). Substituting

$$R = \frac{Dz}{L+z}$$

in equation (2.3) gives

$$dV = \frac{\pi}{4} D^4 k^2 \frac{z^2}{(L+z)^4} dx .$$

Differentiating dV with respect to z gives the value of z for optimum light gathering,

ie $$\frac{d}{dz} \{\frac{z^2}{(L+z)^4}\} = 0$$

whence, for optimisation, $L = z$ and $R = \frac{D}{2}$. Further $r \sim \frac{D}{10}$ for $k = 1/5$.

Thus we obtain the arrangement of stops for optimum light collection, at the same time ensuring that the light received from each volume element in the discharge is independent of the distance from the slit.

In the experiment described in the next chapter convenience in the experimental lay-out necessitated deviations from this optimum arrangement. Specifically, the following values were used:

spectrometer-stop distance $z = L/2$ (= 22 cm)

tube diameter $2D = 3$ mm

radius of principal stop $R = D/3 = 0.5$ mm

radius of smaller stop $r = D/15 = 0.1$ mm .

With this geometrical arrangement the condition that dV is independent of x will now be re-examined.

From equation (2.2a), without the approximation $r << R$ being made,

we obtain after re-arrangement

$$dV = \frac{\pi r^2 R^2}{4z^2} \{1 + \frac{xr}{R(z+x)}\}^2 \, dx$$

whence we have

$$dV \approx \frac{\pi r^2 R^2}{4z^2} \{1 + \frac{2r}{R} \frac{x}{z+x}\} \, dx \, . \qquad (2.2b)$$

The second term in brackets in equation (2.2b) is the correction term giving the dependence of dV on x. For the extremes of the geometrical arrangement defined above, ie x = 44 cm for z = 22 cm and $\frac{r}{R} = \frac{1}{5}$ we have

$$2 \frac{r}{R} \frac{x}{z+x} = 0.27 \, .$$

Thus at the point in the mirror image of the tube farthest from the monochromator there is an additional contribution of 27% to dV due to the dependence of dV on x.

For given values of R, x and z this additional term may be made as small as desired by reducing r, the radius of the stop at the spectrometer, since the correction term $2 \frac{r}{R} \frac{x}{z+x}$ is linear in r. However, the light collected by the stop at the spectrometer is proportional to r^2, so that as r is reduced to weaken the dependence of dV on x the amount of light collected is reduced even faster.

The choice of stop size, r, is therefore a compromise between that which defines a precise geometry and that which enables sufficient light to be collected.

For the absorption cell to be described in the following chapter (Section 3.2) the discharge occupies the central 3 cm of a tube 20 cm long. With the above geometry the correction term, $2 \frac{r}{R} \frac{z}{z+x}$, is 0.13 for volume elements within the cell and 0.27 for volume elements in the mirror image of the cell. Thus the signal from the mirror image is overestimated by ∿11%, which leads to an underestimate of the metastable densities. This is offset, to a certain extent, by the overestimate of metastable densities produced by uncertainties in the precise absorption length (see Section 3.2).

2.3 Diffraction Effects at Stop A

Having placed a small stop at A it is necessary to ensure that diffraction effects at this stop do not lead to a significant loss of light-collecting capability. Fig. 2.2 illustrates the situation and defines the co-ordinate axes.

θ_D, the angular extent of the Airy disc of the diffraction pattern produced by the stop, is

$$\theta_D \sim 1.2 \frac{\lambda}{\Delta x}$$

For the experiments described here $\Delta x = 1$ mm and the maximum value used for λ is approximately 5000Å. Hence θ_D has a maximum value of 6×10^{-4} radians.

The minimum collection angle Θ_C is given by (Fig. 2.1)

$$\theta_C \sim \frac{2R}{L} .$$

Thus, for these experiments, θ_C has a minimum value of 3×10^{-3} radians and diffraction effects at stop A may be neglected.

2.4 Analysis of the re-absorption technique

Having established the optical design criteria the theory of the Ladenburg-Reiche line absorption technique (13) as applied by Harrison (12) will now be discussed.

As described above the experiment is arranged so that $2\theta(z+2d+2a)<2D$ (Fig.2.1). Let F be the fraction of normally incident light reflected by the mirror, and F_q the fraction of normally incident light transmitted through the quartz window. From section 2.2 the volume of an element dV of plasma which can radiate into the spectrometer is

$$dV = \frac{\pi r^2 R^2}{4z^2} dx .$$

If the intensity emitted in the frequency interval $d\nu$ is $I_\nu \, d\nu$ per unit volume of plasma, the total intensity of the emitted line is $I = \int I_\nu \, d\nu$ where the integral is performed over the line profile.

If the light from the volume element is absorbed according to

$$I_{\nu x} = I_{\nu o} \exp(-k_\nu x)$$

where k_ν is the absorption coefficient (in cm^{-1}) for light of frequency ν and x is the absorption path-length, then the total intensity of light reaching the spectrometer directly is

$$I_o = \int_\nu \int_o^d F_q I_\nu \pi r^2 \frac{R^2}{4z^2} \exp(-k_\nu x)\, dx\, d\nu .$$

Similarly the intensity of light reaching the spectrometer after reflection from the mirror is

$$I_R = \int_\nu \int_o^d F F_q^3 I_\nu \pi r^2 \frac{R^2}{4z^2} \exp\{-k_\nu (d-x)\} \exp(-k_\nu d)\, dx\, d\nu .$$

The ratio I_R/I_o is measured experimentally and it is from this ratio that the absorption coefficient at line centre and hence the number density of the absorbing species may be determined.

Consider first a single isolated Doppler-broadened line. For this case we may write

$$k_\nu = k_o \exp(-p^2)$$

$$I_\nu = I_o \exp(-p^2)$$

where

$$p = \frac{2(\nu-\nu_o)}{\Delta\nu_D} (\ell n 2)^{\frac{1}{2}}$$

and

$$\Delta\nu_D = \frac{2(2\mathcal{R}\, \ell n 2)^{\frac{1}{2}}}{c} \nu_o \left(\frac{T}{M}\right)^{\frac{1}{2}} .$$

$\Delta\nu_D$ is the (full) Doppler width between half intensity points of the line centred at ν_o, c the velocity of light, $\mathcal{R}$ the universal gas constant, M the molecular weight of the gas and T its absolute temperature.

With the above substitutions the ratio I_R/I_o reduces to

$$\frac{I_R}{I_o} = F F_q^2 G(k_o d)$$

where

$$G(k_o d) = \frac{\int_p (1-A) A\, dp}{\int_p (1-A)\, dp} \qquad (2.4)$$

and

$$A = \exp(-k_o d \exp(-p^2)).$$

Mitchell and Zemansky (13) tabulate values of $G(k_o d)$ as a function of $k_o d$ calculated by Ladenburg and Reiche for a single Doppler broadened

line. The $k_o d$ values determined from the experimental $G(k_o d)$ measurements are then related to the number density of the absorbing atoms N_1 by the equation

$$k_o d = \frac{2}{\Delta\nu_D}\sqrt{\frac{\ell n 2}{\pi}}\,\frac{\lambda_o^2}{8\pi}\,\frac{g_u}{g_1}\,N_1\left(1 - \frac{g_1}{g_u}\frac{N_u}{N_1}\right) A_{u1}\, d \qquad (2.5)$$

where A_{u1} is the Einstein coefficient for the transition at wavelength λ_o (frequency ν_o) from the upper level u (population N_u, statistical weight g_u) to the lower level 1 (population N_1, statistical weight g_1).

Thus, if $\Delta\nu_D$ and A_{u1} are known, and if the condition $g_1 N_u << g_u N_1$ is fulfilled, the k_o values derived from the measured fractional absorption yield values for the density, N_1, of the absorbing species. In our case the absorbing species are the metastable levels of helium. If the condition $g_1 N_u << g_u N_1$ is not fulfilled then only the reduced number density $N_1(1 - \frac{g_1 N_u}{g_u N_1})$ can be determined.

2.5 Factors Influencing Line Profiles

The causes of the broadening of the individual components of spectral lines will be considered first. Fine structure effects are considered in a later section.

For low pressure glow discharges the principal mechanisms which must be considered are Stark broadening, natural (or homogeneous) broadening, collision broadening and Doppler broadening.

The width of helium lines due to Stark broadening can be calculated from the theoretical broadening constants tabulated by Griem (14). For an electron density of 10^{12} cm^{-3} (10) the Stark widths lie in the range 3-30 MHz.

Fugol et al (15) show that the natural widths of the helium lines are in the range 1-4 MHz, and derive empirical relations for the widths due to collision broadening. For a temperature of 600K and helium pressure of 10 torr the widths of the helium lines due to collision broadening are in the range 70-130 MHz.

The Doppler effect, arising from the random thermal velocities

of the emitting atoms, produces in spectral lines a frequency distribution whose full width $\Delta\nu_D$ at half-power points is given by

$$\frac{\Delta\nu_D}{\nu_o} = 7.16 \times 10^{-7} \left(\frac{T}{M}\right)^{\frac{1}{2}}$$

where ν_o is the centre frequency of the line and M is the molecular weight of the gas whose absolute temperature is T.

For the He-Cd discharge where $T \approx 600K$, the resulting Doppler widths in both helium and cadmium lines are of the order of 1 GHz at 5000Å.

Thus it is clear that the Doppler widths of the studied lines are much greater than the widths produced by other broadening mechanisms and the above analysis of the line absorption technique for a Doppler broadened line may be applied.

2.6 Experimental Examination of Line Widths

Line widths of the order of several gigahertz can be measured most conveniently with a scanning Fabry-Perot interferometer. The 5016Å helium line ($3p\ ^1P - 2s\ ^1S$) from a pure helium discharge was examined using such a device with a reflection finesse of 50. This line has the advantage of being a singlet-singlet transition and thus it exhibits no fine structure which would complicate the line-shape. It is also one of the more intense lines in the spectrum emitted by the helium discharge.

The experimental arrangement is shown in Fig. 2.3. The mirrors of the interferometer were separated by 6 mm giving a free spectral range of 25 GHz. One mirror was mounted on a piezoceramic transducer which could be scanned over approximately $1\frac{1}{3}$ free spectral ranges with the 150 V sawtooth from the oscilloscope. A lens of focal length 105 mm focused the fringe pattern so that the central spot lay symmetrically around a 50 μ pinhole at the monochromator input slit. (The central spot diameter was approximately 2 mm, thus the pinhole

finesse is 40). The output of the photomultiplier, with the monochromator set at 5016Å, was displayed on an X-Y recorder as the piezoceramic was scanned by the sawtooth voltage. Sufficient intensity was available that recourse to more sophisticated detection systems (such as lock-in amplifiers) was unnecessary.

Typical results are shown in Figs. 2.4a,b for line widths as a function of current at constant pressure, and as a function of pressure at constant current. The experimental accuracy is of the order of 10%, due principally to thermal drift of the interferometer.

It is evident that the line widths vary little over the current range 50 - 150 mA and the pressure range 1 - 10 torr. The full width at half maximum under these conditions is about 5 GHz.

This observed line width must be ascribable to Doppler broadening since the 5016Å transition in helium at 600K has a theoretical Doppler width of 5.2 GHz, which is much larger than the width produced by any other broadening mechanism. (600K is a value for the temperature inside the discharge obtained from the measured outside wall temperature and the calculated temperature drop across the quartz wall of the discharge tube.)

The Doppler effect is also the most significant source of line broadening for the other lines examined in this work. In the analysis of the absorption measurements a constant Doppler width corresponding to a gas temperature of 600K has been assumed for all lines.

It should be noted that a change in gas temperature from 480K to 740K changes the Doppler width by only 10% and so the calculation of metastable densities from fractional absorption measurements is only weakly dependent on the gas temperature.

2.7 Structure of the Examined Lines and Absorption of a Line with Overlapping Components

Of the lines investigated, at 5016Å, 3965Å and 3889Å in helium

and 3261Å in cadmium, only the first two are simple single Doppler-broadened lines for which the analysis of Ladenburg and Reiche may be directly applied. These two lines arise from transitions between levels in the singlet spectrum of helium which exhibit no fine structure.

When the components of a line overlap, the absorption can be evaluated only by numerical integration. Values for $G(k_o d)$ can be found once the form of $k_\nu d$ as a function of frequency is known.

The $k_o d$ value is calculated first for each component in the line structure, and each component is assumed to have a Doppler profile. If there are n components to the structure, their relative intensities $I^{(i)}$ $(i = 1 \ldots n)$ give the equation

$$(k_o d)^{(1)} : (k_o d)^{(2)} : \ldots\ldots (k_o d)^{(n)} = I^{(1)} : I^{(2)} : \ldots I^{(n)}$$

The relative intensities are obtained from the theoretical intensity rules for multiplets together with, in the case of the cadmium line, the relative abundances of the isotopes.

The one remaining equation necessary to find all the $k_o d$ values is given by a modified form of equation (2.5):

$$\frac{1}{2}\sqrt{\frac{\pi}{\ell n 2}}\ \Delta\nu_D \sum_{i=1}^{n} (k_o d)^{(i)} = \frac{\lambda_o^2}{8\pi} A_{ul} \frac{g_u}{g_l} N_l \left(1 - \frac{g_l}{g_u}\frac{N_u}{N_l}\right) d$$

$N_{u,l}$ are now the total populations over all components of the structure of the levels. (For the 3889Å He line the upper level (^3P) has sublevels with J = 0,1,2. The g_u value for this case is the sum of the g values of the individual sublevels, ie 9).

The required number of Doppler profiles ~~are~~ is drawn so that each curve has a maximum value equal to one of the $k_o d$ values and a width of $\Delta\nu_D$. The separations between the centres of the curves are equated to the measured separations of the components of the line. The individual profiles are then added, giving a resultant curve of $k_\nu d$ as a function of ν. Then the integrals of (1-A) and A(1-A) are found

(where the general form $A = \exp(-k_\nu l)$ is used in equation 2.4) and the absorption evaluated as a function of Nd (or more correctly $N_1(1 - \frac{g_1}{g_u}\frac{N_u}{N_1})d$, the product of the reduced number density of the absorbing level and the absorption length).

The helium line at 3889Å is found, when examined with a high resolution interferometer (16), to be a closely spaced triplet. This triplet structure arises from the different energies possessed by the J = 0,1,2 sublevels of the ^3P upper level of the transition. The splittings of the components are 5-6 GHz (16) which is slightly less than the Doppler width of 6.8 GHz for each component at 600K.

The structure of the CdI resonance line at 3261Å ($5\ ^3P_1 - 5^1S_0$) has different origins. First, the isotope shifts of the line must be considered since the cadmium used was of normal isotopic composition with eight stable isotopes. Second, the hyperfine splitting of the line due to nuclear spin must be considered for the two stable isotopes with odd atomic number. The other isotopes with even atomic numbers have zero nuclear spin, which has no effect on the structure of the line. The detailed structure of the line was derived from the results of Brix and Steudel (17), Kelly and Tomchuk (18), and Kuhn and Ramsden (19).

The structures of the 3889Å helium line and 3261Å cadmium line together with the theoretical intensity ratios of the components are shown in Figs. 2.5 and 2.7 respectively.

The above integration procedure was performed for each line by an IBM 1130 computer. Details of the computer programmes are given in Appendix II. The results of these calculations, ie graphs of the absorption function $G(k_0 d)$ versus the product of the reduced number density of the absorbing level and the absorption length, are shown in Fig. 2.6 for the helium triplet metastable level (absorption at

3889Å) and Fig. 2.8 for the cadmium ground state neutral density (absorption at 3261Å). It must be emphasised, however, that these curves are valid only for a Doppler width corresponding to 600K.

Further, the influence on the absorption coefficient of collisional broadening up to 200 MHz in addition to Doppler broadening of 5.2 GHz was examined (20) for the 5016Å singlet line by computer integration over the resulting Voigt profile. It was found that for the range of values of fractional absorption observed in the experiments, the approximation of a simple Doppler profile was adequate.

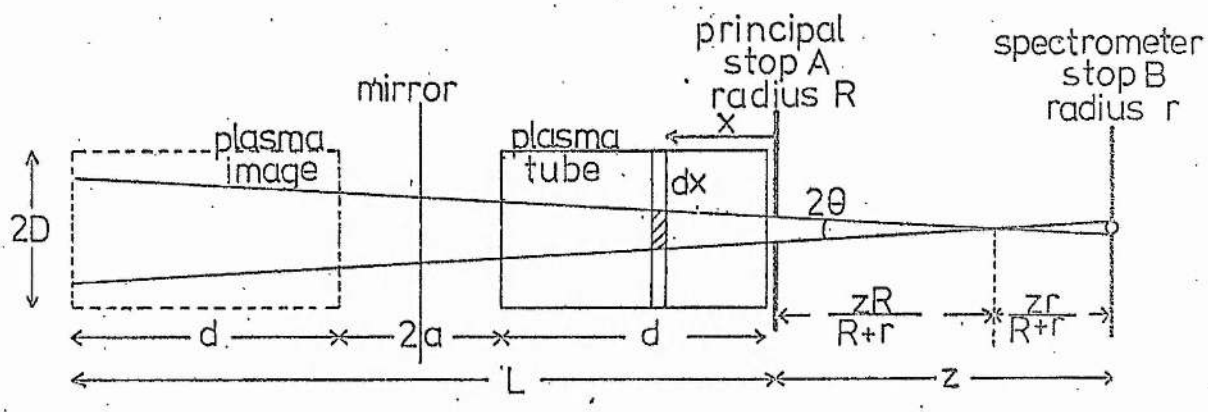

Fig. 2.1 Optical arrangement of the absorption experiment

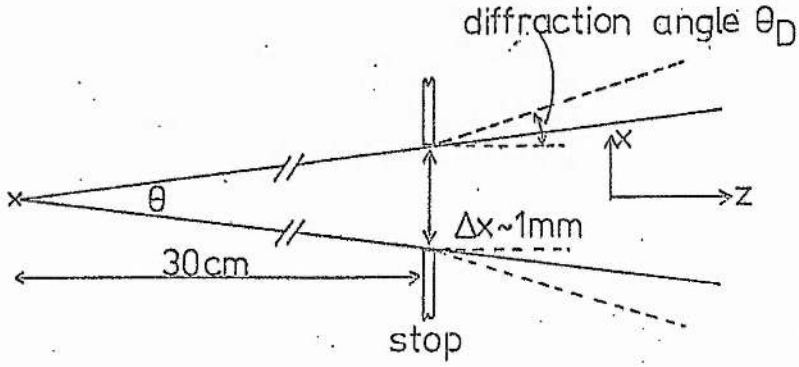

Fig. 2.2 Illustration of diffraction effects at the principal stop

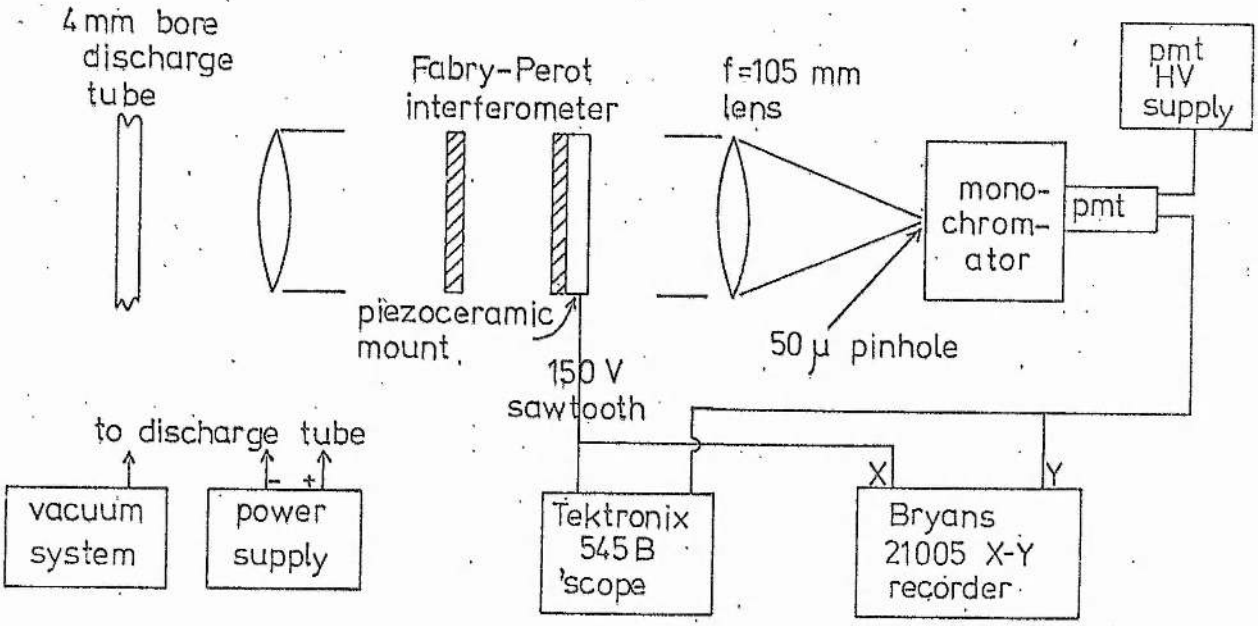

Fig. 2.3 Schematic diagram of the system used for measuring the linewidth of the HeI line at 5016Å.

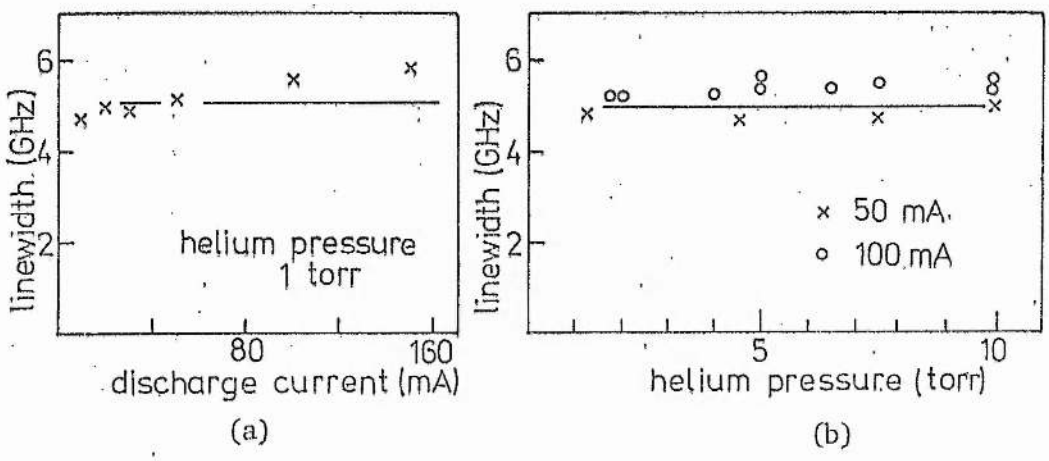

Fig. 2.4 Linewidth of the 5016Å line of HeI in a pure helium discharge

(a) as a function of current at a fixed pressure

(b) as a function of pressure at fixed current

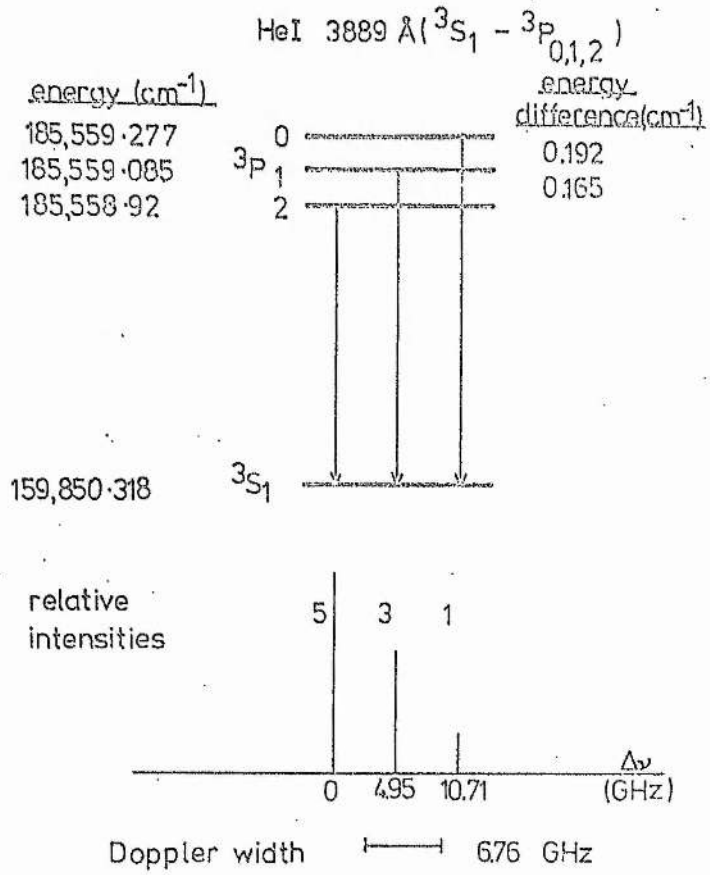

Fig. 2.5 Structure of the HeI line at 3889Å, together with the intensity ratios of the components

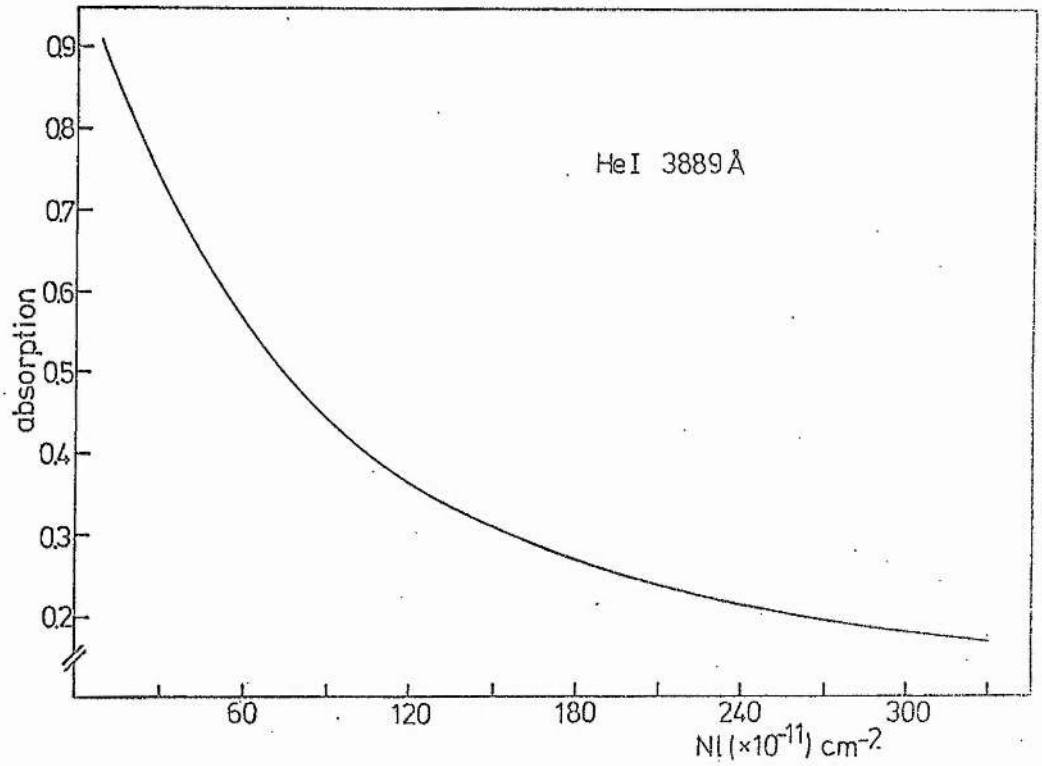

Fig. 2.6 Computer derived relation between absorption at 3889Å HeI and the product of the absorption length and reduced helium triplet metastable density. Valid for 600 K only.

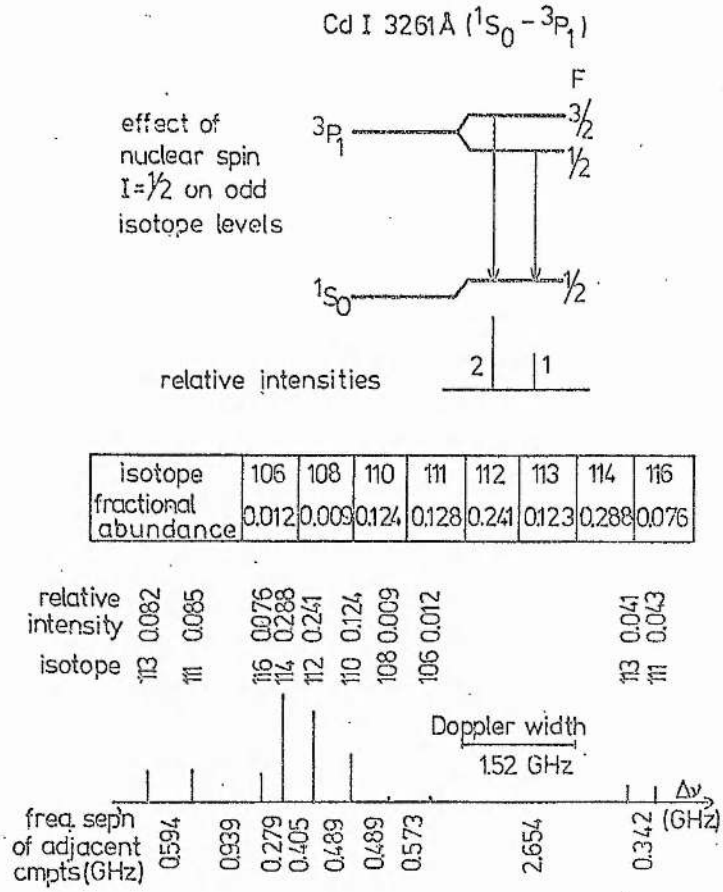

Fig. 2.7 Structure of the CdI resonance line at 3261Å arising from isotope and nuclear spin effects, together with intensity ratios of the components.

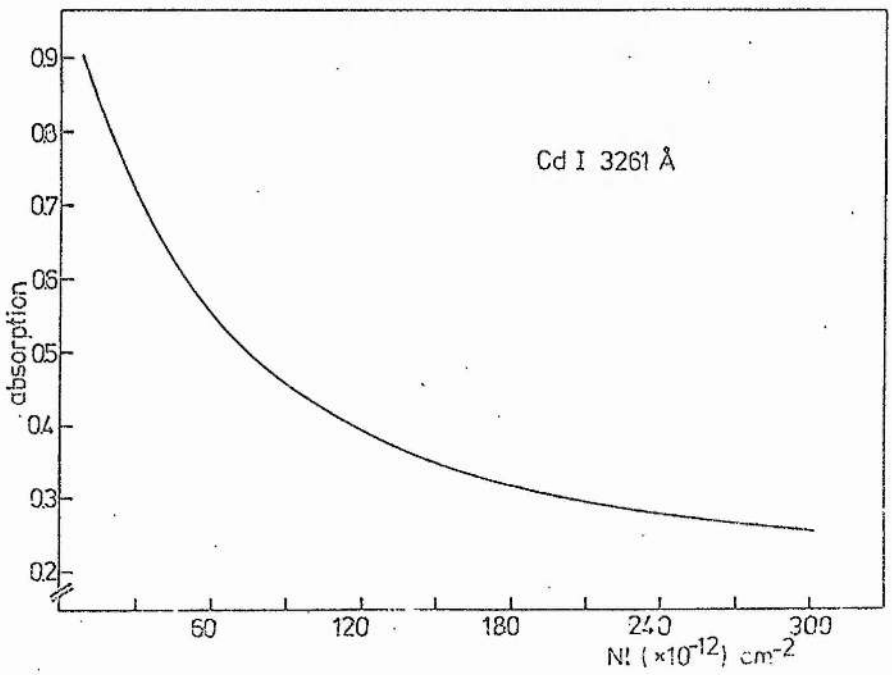

Fig. 2.8 Computer derived relation between absorption at 3261Å (CdI) and the product of the absorption length and density of cadmium ground state neutral atoms. Valid for 600 K only.

CHAPTER III

METASTABLE POPULATIONS IN THE PURE HELIUM DISCHARGE

3.1 Introduction

This chapter considers the measurement of metastable densities in a pure helium discharge, after describing the construction and operation of the capillary discharge cell in which the metastable densities in both pure helium and helium-cadmium discharges were measured.

The results for singlet and triplet metastable densities in pure helium discharges are presented. The two principal features of these results are:

(i) Both the 2 ^3S and 2 ^1S metastable densities initially increase rapidly with increasing discharge current, but for currents above 20 mA and pressures below 2 torr they become independent of the discharge current. A decrease in measured metastable densities with increasing current for pressures above 2 torr is shown to be caused by the presence of significant populations ($\geq$ 10% of the metastable populations) in the upper levels of the transitions on which the absorption is measured.

(ii) The saturated populations are dependent on helium pressure, initially rising rapidly with increasing pressure to a maximum around 2 torr, and thereafter decreasing slowly as the pressure increases further.

In the final section, the triplet metastable density is derived theoretically by considering the various documented production and loss processes for this level. The broad features of the behaviour of the triplet metastables are explained, and satisfactory agreement is obtained between calculated saturated densities and the measured values. A similar treatment is then applied to estimate the populations of the 3 ^1P level, to allow a comparison with the metastable population.

3.2 Apparatus and Experiment

The construction and operation of several trial absorption cells with diameters 5-25 mm and lengths 3-15 cm showed that three requirements had to be fulfilled by the final design of the capillary absorption cell. First, the length of the positive column along which the absorption was measured had not to exceed 3 cm. Lengths greater than 3 cm gave a large amount of absorption ($G(k_0 d) < (0.3)$) and, in consequence, little variation in this quantity with large changes in metastable density (see Fig. 2.6). Second, as the ultimate aim of this work was to examine the He-Cd laser discharge, a means of introducing cadmium vapour into the discharge had to be provided as near as possible to the anode end of the absorbing region. Third, flaring of the discharge at discontinuities had to be prevented since this could produce considerable uncertainty in the absorption length. The flaring effect was particularly evident for pressures less than 2 torr. (Even if flaring is completely avoided there still remains uncertainty as to the exact absorption length owing to diffusion of the metastables from the ends of the discharge region. The effective absorption length is therefore greater than the discharge length by approximately twice the capillary diameter. Diffusion effects may make the absolute values of the metastable populations uncertain by 20%.)

The final design of the absorption tube is shown in Fig. 3.1. The tube was of quartz. At each end of the tube a quartz disc of Schlieren quality was attached by 'Torr-Seal' such that the disc was perpendicular to the tube axis. At the anode end of the absorption region (of length 3 cm and diameter 3 mm) a sharp boundary to the discharge was obtained by forcing it to run into the capillary through a gap of 0.5 mm. It was found that by making the side arm connection to the cathode of approximately the same diameter as the capillary,

flaring of the discharge was avoided. When cadmium was present in the discharge most of it was found also to turn the corner and condense in the cathode bulb, although a much smaller amount condensed on the capillary walls beyond the discharge region.

Cadmium wire (5N purity) of natural isotopic composition was placed inside the outer jacket which was surrounded by a flexible oven (Electrothermal HR 5/2/4) whose temperature was stabilised to $\pm 1C^{o}$ by a temperature controller (Ether "Digi"). The metal vapour entered the discharge through a 2 mm wide slit cut in the wall of the capillary with a diamond saw. As this hole was less than 2 mm from the anode end of the capillary discharge, the absorbing length was taken to be the same (3 cm) for both pure helium and He-Cd discharges.

The overall experimental arrangement is shown in Fig. 3.2. The tube was rigidly mounted on an aluminium base, which was clamped onto an optical bench with saddles allowing accurate positioning in the vertical and transverse directions. The optical bench supported the grating monochromator (Carl Zeiss SPM2) whose output was detected with a photomultiplier (EMI type 9594 QUB). The photomultiplier was found to have a linear response for output voltages up to 500 mV across the 100 kΩ anode load resistor. The exit slits of the monochromator were always set sufficiently wide to allow the light from the entire profile of the chosen line to be incident on the photomultiplier.

The principal stop, of ebonite (with a black and non-reflective roughened surface) glued to one quartz window of the cell, was 22 cm from the 200 μ pinhole at the monochromator inlet slits. At the other end of the cell the plane front-aluminised mirror was supported by a laser-mirror mount to obtain fine adjustment of its alignment.

The capillary tube and the stops were aligned using a

cathetometer (Wild) to define the optical axis of the system. The mirror was then mounted in position and, with the discharge running adjusted to obtain maximum reflected signal on a line showing little absorption. The reflectivity of the mirror was measured by Optical Coatings Ltd over the range 3200 - 6500Å using a spectrophotometer (Cary) Manufacturer's specifications for the transmission, F_q, of the quartz windows were used (see Section 2.4). These values were found later to be in precise agreement with values measured with a Pye-Unicam spectrophotometer in this department. Further, the value of the reflected signal measured for the 4416Å laser line when cadmium was present in the discharge was compared with the value derived from the above transmission and reflection data (but ignoring the slight gain in the intensity of the line along 3 cm). Agreement to 2% was found. Monitoring the magnitude of the 4416Å reflected signal was a convenient means of checking that cadmium deposition was not altering the transmission of the quartz window near the mirror.

Helium of 4N5 purity was used (BDH "Labgas") and the filling pressure measured with a Bourdon gauge which had been calibrated against a McLeod gauge over the range 0-15 torr. The discharge current was provided by a 5 kV, 200 mA smoothed but unregulated power supply.

The output of the photomultiplier (taken across the 100 kΩ anode resistor) was recorded directly on a Servoscribe chart recorder with a 10 μF capacitor across the input terminals to reduce discharge noise. With a black card inserted between the mirror and the tube end, the signal entering the spectrometer directly was measured for approximately 1 minute. The card was then removed and the additional signal due to light reflected from the mirror was measured for a similar time. Each measurement was repeated several times in turn. Under any set

of conditions the reproducibility of these several measurements was within 5%, while the day-to-day reproducibility of measurements was also within 5%.

The values obtained for the ratio I_R/I_o were corrected for mirror reflectivity and quartz window transmission to give a final value for the absorption. The absorption measurements on a particular transition allowed the value of the reduced number density η of metastables, where

$$\eta = N_m(1 - \frac{g_l}{g_u}\frac{N_u}{N_m}), \qquad (3.1)$$

to be found for that transition from the appropriate graph (Figs. 2.6,2.8 and (13)).

3.3 Results for the Pure Helium Discharge

Measurements of reduced number densities for the pure helium discharge are summarised in Figs. 3.3, 4, 5, 6. With constant discharge current, singlet and triplet (Fig. 3.3) metastable densities show a sharp peak in their dependence on helium filling pressure. Both metastable densities reach their maximum values, of 2×10^{12} cm^{-3} for singlets and 9×10^{12} cm^{-3} for triplets, at pressures around 2 torr (for a current of 100 mA). For helium pressures below 2 torr singlet and triplet metastable densities rapidly saturate with increasing discharge current and show constant values (2×10^{12} cm^{-3} for singlets at 1 torr, 8×10^{12} cm^{-3} for triplets at 2 torr) for currents above 10 - 20 mA.

The saturated triplet metastable density at 1 torr is in close agreement with the results of Kruse (21) who measured the density by Rozdestvensky's 'hook' method in a 1 cm bore tube with current densities in the range 0 - 650 mA cm^{-2}. Assuming that the E/p value for both experiments is the same, current density is the most important scaling parameter since it is proportional to the electron density. The saturated triplet metastable density found by Kruse was $(6.0 \pm 0.5) \times 10^{12}$ cm^{-3} for current densities above 200 mA cm^{-2}, which is similar

to the present value of 6.2×10^{12} cm^{-3} for current densities above 560 mA cm^{-2}. The difference in the current densities at which the metastable densities saturate is due to the different tube diameters and the consequent difference in diffusion losses for the metastable species. Kruse obtained results at only one pressure, so further comparison is not possible.

At pressures greater than 2 torr the reduced metastable densities show an apparent decrease with increasing current (Figs. 3.5, 6). If this decrease represents a real decrease in the metastable populations it implies the existence of a destruction process for metastable species which is proportional to the electron density raised to some power greater than unity. A search of the literature (see following section) showed that no such process is known. Thus, other reasons for the decrease must be considered - in particular the effects of changes in the Doppler width, gas pumping effects along the tube, and the influence of significant populations in the upper levels of the transitions at which absorption is measured.

Since $k_o \propto \frac{1}{\Delta\nu_D}$ (equation 2.5), increases in the Doppler width of the transitions as the current is increased would lead to a reduction in the measured absorption, which could be interpreted as a decrease in the metastable populations. However, it has already been shown (section 2.6) that the Doppler width of the transitions is approximately constant over the range of currents considered here.

Gas pumping effects (22) in the capillary discharge could reduce the number density of helium ground state atoms in the absorption region at higher currents, thus giving rise to a decrease in metastable species. To test for pumping effects a return path was provided between the anode and cathode side-arms. A valve in this path enabled the absorption to be measured with the return path open or closed.

At 5 torr and 140 mA no change was observed in the absorption when the valve in the return path was opened. Thus gas pumping effects and changes in the Doppler width are not responsible for the apparent decrease in metastable densities.

The influence of upper level effects can be examined by considering the absorption results for the singlet metastable density. There is sufficient light intensity with the present experimental arrangement to measure the absorption on the helium transitions at 3965Å and 5016Å which have the 2 ^{1}S lower level in common. Denoting the 5016Å line by λ_1 and the 3965Å line by λ_2, the ratio of the absorption coefficients at line centre for the two lines may be written

$$\frac{k_o^{\lambda_1}}{k_o^{\lambda_2}} = \frac{\lambda_1^3}{\lambda_2^3} \frac{A_{\lambda_1}}{A_{\lambda_2}} \frac{(1 - N(3^1P)/3N_m)}{(1 - N(4^1P)/3N_m)} \qquad (3.2)$$

where A_{λ_1,λ_2} are the Einstein coefficients of the transitions, $N(3^1P,4^1P)$ are the populations of the upper levels of these transitions, N_m is the singlet metastable density, and the factor 3 is the ratio of the statistical weights $g(3,4^1P)/g(2^1S)$.

In the absence of significant populations in the upper levels, or if they are equal, the last quotient on the right hand side of equation (3.2) has the value 1, and the ratio of the absorption coefficients (substituting for $\lambda_{1,2}$ and $A_{\lambda_{1,2}}$) is 3.7. In Fig. 3.7 the experimentally determined values of this ratio are plotted as a function of current for various helium pressures. The errors for each point may be as high as 20% since two quantities, each known to 10%, are divided. Even so, at the higher pressures the reduction in the ratio from the theoretical value of 3.7 indicates that the upper level populations are becoming comparable to the population of the 2^1S metastable level.

If the ratio of the terms involving upper level populations in equation (3.2) is approximated as follows,

$$\frac{1 - N(3^1P)/3N_m}{1 - N(4^1P)/3N_m} \sim (1 - \frac{N(3^1P)}{3N_m})(1 + \frac{N(4^1P)}{3N_m})$$

$$\sim (1 - \frac{1}{N_m}(\frac{N(3^1P)}{3} - \frac{N(4^1P)}{3})) \qquad (3.3),$$

then the reduction in $k_o^{\lambda_1}/k_o^{\lambda_2}$ by approximately one third at 10 torr (Fig. 3.7) implies that, at this pressure, $N(3^1P) - N(4^1P) \sim N_m$. Thus $N(3^1P)$ and $N(4^1P)$, while different, are individually of the order of N_m.

The spontaneous emission intensities at 5016Å and 3965Å, measured at right angles to the axis of the tube to minimise absorption, are directly proportional to $N(3^1P)$ and $N(4^1P)$ respectively. From measured spontaneous emissions $N(3^1P)$ and $N(4^1P)$ are seen to increase by a factor of 2 as the pressure is reduced from 10 to 2 torr at a current of 100 mA. At the same time N_m increases by a factor of about 3. Thus, at the lower pressures, $N(3^1P)$ and $N(4^1P)$ are still comparable to N_m. The value of $k_o^{\lambda_1}/k_o^{\lambda_2}$ at the lower pressures is very close to its theoretical value of 3.7. Thus $N(3^1P)$ and $N(4^1P)$ must be approximately equal at this pressure.

For the sake of argument the spontaneous emission intensities at 5016Å and 3965Å have been normalised so that $N(3^1P)$ equals $N(4^1P)$ at 1 torr and 100 mA. The normalised population densities are shown in Figs. 3.8, 9 as a function of current and helium pressure. By multiplying $N(3^1P)$ and $N(4^1P)$ by a scaling factor so that at 10 torr $N(3^1P)-N(4^1P)$ is equal to N_m, the pressure variation of $N(3^1P)$, $N(4^1P)$ and N_m may be displayed on the one graph (Fig. 3.10) and approximate values for $N(3,4^1P)$ derived.

Fig. 3.10 then illustrates the pressure behaviour of $k_o^{\lambda_1}/k_o^{\lambda_2}$, whose deviation from 3.7 is proportional to $\frac{1}{N_m}(N(3^1P) - N(4^1P))$.

$N(4^1P)$ is seen to reach a maximum value in the pressure region 1-2 torr and then decrease. $N(3^1P)$, however, shows a broad maximum in the range 2-6 torr and then decreases, but more slowly than $N(4^1P)$. For pressures less than 2 torr there is little change in $N(3^1P) - N(4^1P)$ while above 2 torr this difference steadily increases with pressure. N_m is a decreasing function of pressure so that the deviation $k_o^{\lambda_1}/k_o^{\lambda_2}$ from its value of 3.7 steadily increases with pressure, as is seen in Fig. 3.7.

The current dependence of the normalised spontaneous emissions (Fig. 3.8) shows that the difference $N(3^1P) - N(4^1P)$ is almost constant in the range 100 - 200 mA. Thus the ratio $k_o^{\lambda_1}/k_o^{\lambda_2}$ is constant with current over this range, as is seen in Fig. 3.7. There should, however, be less deviation of $k_o^{\lambda_1}/k_o^{\lambda_2}$ at 50 mA from its theoretical value than is observed. This is possibly due to the errors in the experimental points.

In principle, further use can be made of the spontaneous emission measurements to determine absolute values of the upper level populations according to the following method. The spontaneous emission intensity, S, for each line is related to the population of the upper level of the transition by

$$\begin{aligned} N(4^1P) &= K(3965)\ S(3965) \\ N(3^1P) &= K(5016)\ S(5016) \end{aligned} \qquad (3.4)$$

where, for the two lines, K(3965,5016) are calibration constants which depend on viewing geometry, the transmission of the discharge tube wall, the sensitivity of the monochromator-photomultiplier arrangement, the frequency of the lines and the Einstein coefficients.

Substitution of equation (3.4) into equation (3.1) for the two transitions and re-arranging the resulting equations gives

$$K(5016)\ S(5016) - K(3965)\ S(3965) = 3\eta(3965) - 3\eta(5016) \qquad (3.5)$$

where the factors of 3 take account of the ratio of statistical weights

of the levels. It is then possible, in theory, to evaluate the constants K(5016,3965) and thus to determine the upper and lower level populations absolutely by comparing measured values for η and S under (at least two) different experimental conditions.

A computer programme was written to select each pair of results from those taken under thirty six different experimental conditions (50 - 200 mA, ½ - 7 torr) and to calculate the appropriate constants. The results, however, showed that the errors in the reduced number densities (± 10%) allowed only order of magnitude estimates to be made of the constants, since the right hand side of equation (3.5) is a small difference between two large quantities, with consequent large errors. The estimates suggest 3^1P and 4^1P populations of the order of 10^{12} cm^{-3}, as expected, for discharge currents around 150 mA in a discharge at 4 torr.

Because of the large errors in the values obtained for the calibration constants singlet metastable densities have not been extracted explicitly from the reduced number densities shown in Fig. 3.6. However, apart from the apparent decrease with increasing current at higher pressures, which is explained by the effects of significant upper level populations, the principal features of the reduced number density results are determined by changes in the population of the metastable levels.

Since there was insufficient light intensity to measure the triplet metastable density by absorption on any line other than that at 3889Å, detailed evaluation of upper level effects is not possible for the triplet states. The general shape of the reduced triplet metastable densities, however, suggests similar behaviour to the singlets.

Absorption measurements transverse to the discharge were also carried out using a cell which had had part of its cylindrical wall ground away on opposite sides and replaced by optically-contacted quartz

flats, thereby removing the lens effects of the tube wall. The absorption length was 5 mm (the tube diameter). Singlet and triplet metastable densities obtained from measurements with this tube showed a similar functional dependence on discharge parameters to the densities obtained from measurements along the tube axis, while the densities obtained from absorption in the transverse direction were a factor of two higher than those obtained from absorption along the axis. In view of the different spatial averages in the two cases, and the variation (which was not taken into account) of the transmission of the quartz window due to discharge damage on the surface, such differences in absolute value are not unexpected.

3.4 Discussion for the Case of a Pure Helium Discharge

Since the processes in the discharge determining singlet and triplet metastable state densities are mostly similar, attention will be restricted in this discussion to a closer consideration of the triplet state population. In the case of the pure helium discharge the excitation and destruction processes determining the population of the triplet metastable state are generally well documented.

The excitation process is through electron collisions with the helium ground state atoms leading either to direct excitation of the metastable state or to excitation to higher states with subsequent radiative decay to the metastable state. Destruction of the triplet metastables can take place by diffusion to the tube walls, by collisions with ground state helium atoms, by collisions with electrons or collisions between the metastable atoms. The rate equation describing the population is therefore of the form

$$\alpha N_o n_e - N_m \tau_D^{-1} - \beta N_m N_o - \gamma N_m n_e - \delta N_m^2 = 0 \qquad (3.6)$$

where N_o, N_m and n_e are the densities of the helium ground state atoms, triplet metastable species and electrons respectively, τ_D is the

characteristic diffusion time for the metastables and the coefficients α, β, γ, and δ describe the other processes listed above.

The coefficient α describing the electron excitation is of the form

$$\alpha = \langle \sigma(v_e) v_e \rangle$$

where the brackets < > denote the average over the electron energy distribution and $\sigma(v_e)$ is a composite cross-section describing both direct and indirect excitation to the metastable state as a function of the electron velocity, v_e. Cross-section data for the excitation of metastable and higher states of helium by electron collision with ground state atoms have been reviewed by Corrigan and von Engel (23) and Miller et al (24), while electron energy distributions in helium have been calculated by Smit (25), Heylen and Lewis (26), Reder and Brown (27), and Englert (28) for the range of E/p values of interest here (5-20 V cm^{-1} $torr^{-1}$). The composite cross-section rises rapidly to a mean value of about 3×10^{-18} cm^2 just above threshold (20.4 eV) while the fraction of electrons with energies greater than 20 eV can be derived from the distribution function as approximately $6 \times 10^{-3}(E/p-4)$ for E/p values between 5 and 20 V cm^{-1} $torr^{-1}$. The coefficient for electron excitation, α, is therefore approximately $5 \times 10^{-12}(E/p-4)$ cm^3 s^{-1}.

Phelps (29) has determined metastable diffusion rates, and for the 3 mm diameter tube used here the characteristic diffusion time , τ_D, is approximately 3×10^{-5} p s, where p is the helium filling pressure in torr.

Phelps (29) has also studied the collisional destruction of the triplet metastable state through collisions with ground state helium. There is no evidence that the two body process,

$$He(2^3S) + He \rightarrow 2\ He,$$

occurs, while for the pressure range of interest here the three body process,

$$He(2^3S) + 2\ He \rightarrow He_2^* + He,$$

is insignificant compared to the diffusion loss. The third term in equation (3.6) can therefore be ignored.

Electronic destruction of the triplet metastables is principally through ionization (30). The cross-section for de-excitation back to the ground state, derived from the electron excitation cross-section by detailed balancing (31), is an order of magnitude smaller than the ionization cross-section, while excitation to higher HeI triplet states can be neglected since radiative decay from these states is predominantly back to the triplet metastable state. By combining the cross-section determined by Long and Geballe (30) with the electron distribution data previously mentioned the ionization coefficient, γ, is calculated as 6×10^{-8} cm^3 s^{-1}, approximately independent of E/p in the range 5 - 20 V cm^{-1} $torr^{-1}$. It has been mentioned (32) that the destruction rate of metastables by electron collisions leading to ionization may be higher than the above value by a factor of up to five when stepwise, in addition to direct, ionization is taken into account. At present, however, no published results are available. This higher rate of loss through ionization would lead to a reduction in the final value of the saturated metastable density, and the current at which saturation occurs, by the same factor.

More difficult to estimate is the role of electron collisions in destroying the triplet state by converting it to the singlet metastable state. Morrison and Rudge (33) have calculated cross-sections as a function of electron energy, as well as reviewing previous work. Values proposed by different investigators differ by nearly three orders of magnitude for 1 eV electrons, making the contribution of this effect to the coefficient γ between 10^{-10} and 10^{-8} cm^3 s^{-1}. The influence of this process as a destruction mechanism for triplet metastables is to

a certain extent offset by the reverse process of singlet to triplet conversion, but since singlet densities are between one quarter and one fifth of triplet densities, the net effect is still a loss process for the triplet metastable population.

Metastable-metastable collisions leading to ionization,

$$He(2^3S) + He(2^3S) \rightarrow He + He^+ + e,$$

can become a significant loss mechanism for the metastable densities (10^{12} - 10^{13} cm^{-3}) involved here. The coefficient δ in equation (3.6) has been determined by Phelps and Molnar (34), Bell et al (35), Miller et al (36) and Fugol et al (37) as approximately 2×10^{-9} cm^3 s^{-1} at 300 K.

If the various coefficients in equation (3.6) are evaluated numerically, the following equation describing the triplet metastable population is obtained:

$$(E/p - 4)n_e p = 2 \times 10^{-14} N_m^2 + 0.3 N_m p^{-1} + 6 \times 10^{-13} n_e N_m \quad (3.7).$$

In this equation the neutral density, N_o, has been substituted using a gas temperature of 600 K and a pressure equal to the tube filling pressure. Also, triplet-singlet conversion is ignored. Inclusion of this effect is to increase the last term on the right hand side. The electron density in the capillary helium discharge of the dimensions involved here can be summarised by (10)

$$n_e(cm^{-3}) \sim 10^{11} I(E/p)^{-1} \quad (3.8)$$

where I is the discharge current in mA, and E/p is measured in V cm^{-1} $torr^{-1}$. Substitution of (3.8) into (3.7) enables the metastable density to be expressed purely as a function of the plasma parameters I and E/p as

$$N_m(6I(E/p)^{-1} + 30 p^{-1} + 2 \times 10^{-12} N_m) = 10^{13}(E/p-4)Ip(E/p)^{-1}. \quad (3.9)$$

As the current is increased at constant E/p, a point is reached when the first term on the left-hand side of equation (3.9) dominates over the other two terms - ie loss of metastables by collisions with electrons dominates over the other loss processes. The metastable

population then saturates with respect to discharge current at a value given by

$$(N_m)_{sat} \approx 2 \times 10^{12} \left(\frac{E}{p} - 4\right)p \qquad (3.10)$$

At a pressure of 2 torr, E/p is 10 V cm^{-1} $torr^{-1}$, so that the saturated triplet metastable population predicted by the above equation is about 2×10^{13} cm^{-3} in reasonable agreement with the experimental value of 8×10^{12} cm^{-3}. In figure 3.11 the function (E/p-4)p is plotted as a function of helium pressure,p, using experimentally determined E/p values appropriate to a 100 mA discharge in a 3 mm bore capillary. Comparison of figures 3.11 and 3.3 shows that the experimentally observed peak in metastable population with changing pressure can be explained by the excitation and destruction processes described by equation (3.6).

The threshold current for saturation of the metastable population can be predicted using equation (3.9). If the metastable-metastable collisions are disregarded as a loss process (this will lead to an underestimate) then the metastable population saturates for currents given by $I \geq \left(\frac{5}{p}\right)\left(\frac{E}{p}\right)$.

At 2 torr, therefore, saturation should occur at about 25 mA, while with increasing pressure the current at which the population saturates should rapidly decrease. This behaviour is illustrated by the results in Figs. 3.4, 5.

The behaviour of the triplet metastable state with discharge conditions in the pure helium discharge is therefore reasonably well described by the processes incorporated in equation (3.6).

A similar procedure may be applied to estimate the population of the 3^1P levels in helium. At 2 torr with discharge current 100 mA, n_e is 6×10^{11} cm^{-3} (10), N_o is 6×10^{16} cm^{-3} and the density of singlet metastables is 2×10^{12} cm^{-3}.

Using the cross-sections of Corrigan and von Engel (23) and van Eck and de Jongh (38), the rate of direct excitation to the 3^1P level from the helium ground state is calculated as 2.6×10^{17} cm^{-3} s^{-1}. There is also a significant pumping rate from the singlet metastable level, for which Kim and Inokuti (39) have calculated a cross-section of $\sim 10^{-15}$ cm^2 for electron energies in the range 5 - 35 eV. The production rate for the 3^1P state via this process is 1.2×10^{17} cm^{-3} s^{-1}. Therefore the production rate of the 3^1P level, neglecting radiative and collisional cascade processes, is 4×10^{17} cm^{-3} s^{-1}.

The principal decay of the 3^1P level is via the radiative transition at 5016Å to the 2^1S level ($A \sim 10^7$ s^{-1}). The vacuum-ultra-violet transition at 537Å from the 3^1P level is trapped with a trapping factor $\sim 10^3$ (40) so that the effective Einstein coefficient is $\sim 0.2 \times 10^6$ s^{-1}. Taking the 5016Å radiative path as the only method of destruction of the 3^1P level gives the steady state population of the 3^1P level as 4×10^{10} cm^{-3} under the stated conditions. This is in poor agreement with the values of $\sim 10^{12}$ cm^{-3} implied by the absorption measurements.

The present values of 3, 4^1P populations are supported by the results of Kruse (21) for the triplet levels of helium at 1 torr under the discharge conditions already described in Section 3.3. Kruse found that for $N(2^3S) = 6 \times 10^{12}$ cm^{-3} the values of $N(3^3D)$, $N(2^3P)$ and $N(3^3P)$ were 12×10^{12} cm^{-3}, 8×10^{12} cm^{-3} and 3×10^{12} cm^{-3} respectively. The most likely cause of the discrepancy between measured and calculated densities of the 3^1P level is uncertainty in the excitation cross-section from the singlet metastable level, for which only the one set of calculated data is available.

As the populations of the 3^1P and 4^1P excited helium levels are of the order of 10^{12} cm^{-3}, the populations of other helium levels with similar excitation energies (3^1S, 4^1S, 2^1P, 3^1D, 4^1D, 2^3P, 3^3P, 3^3D, 3^3S..)

will probably be of this order of magnitude also. Summing over all these states, there will be a large density of excited species with sufficient energy to ionize and excite cadmium atoms by Penning collisions. Thus the possibility that atoms in these higher helium levels, in addition to metastable species, contribute to the excitation of the upper laser levels in the cadmium ion cannot be excluded.

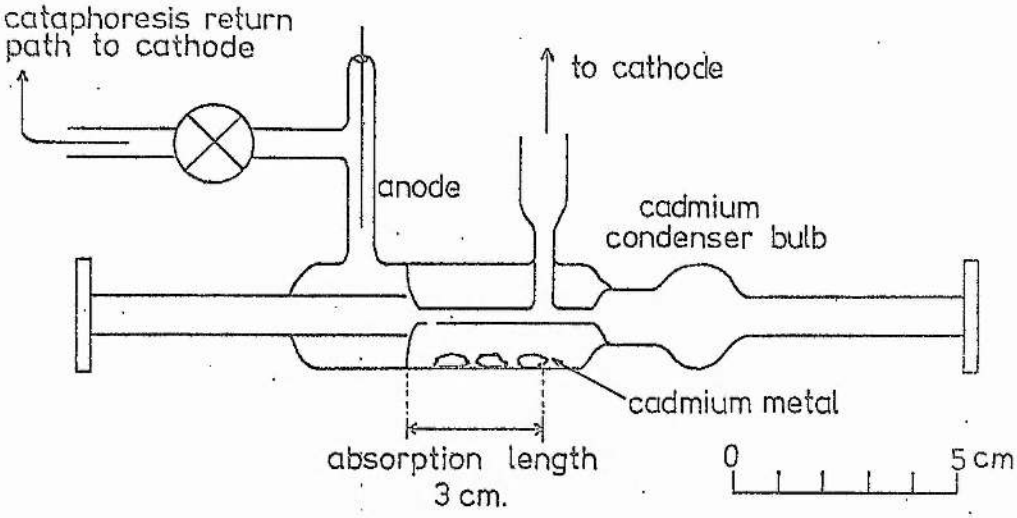

Fig. 3.1 Scale drawing of the absorption cell

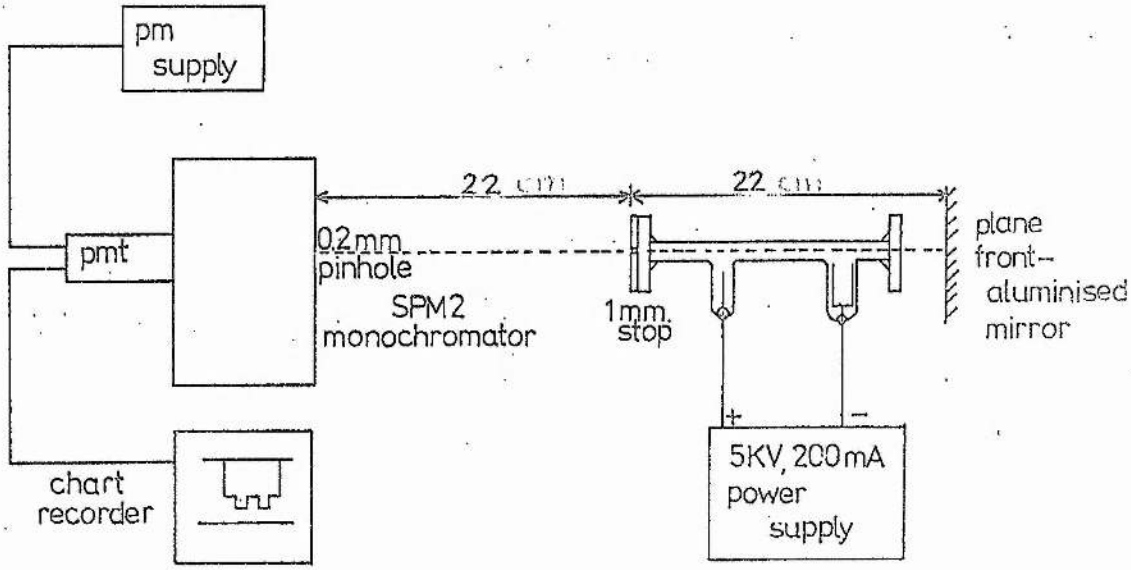

schematic diagram of line absorption experiment

Fig. 3.2 Schematic diagram of the absorption experiment

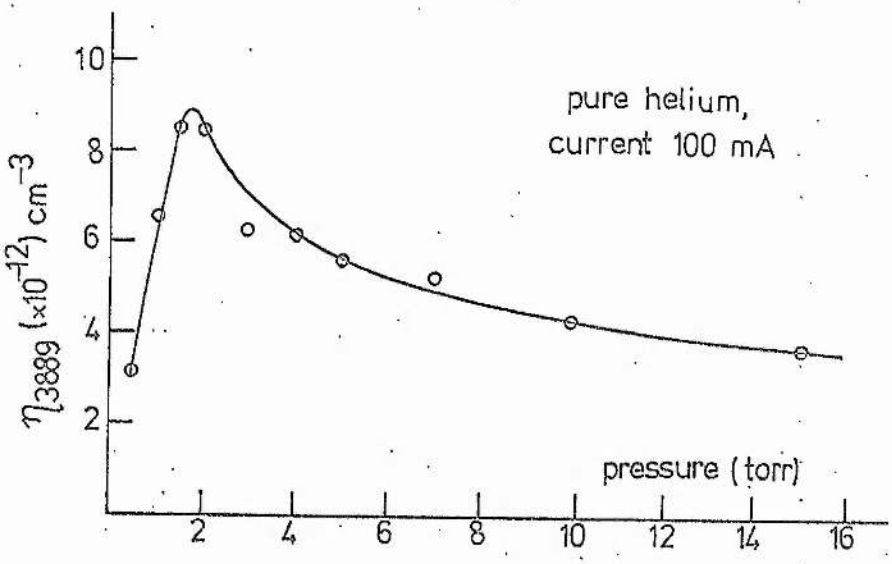

Fig. 3.3 The reduced triplet metastable density, n_{3889}, as a function of helium pressure. Results derived from absorption at 3889Å.

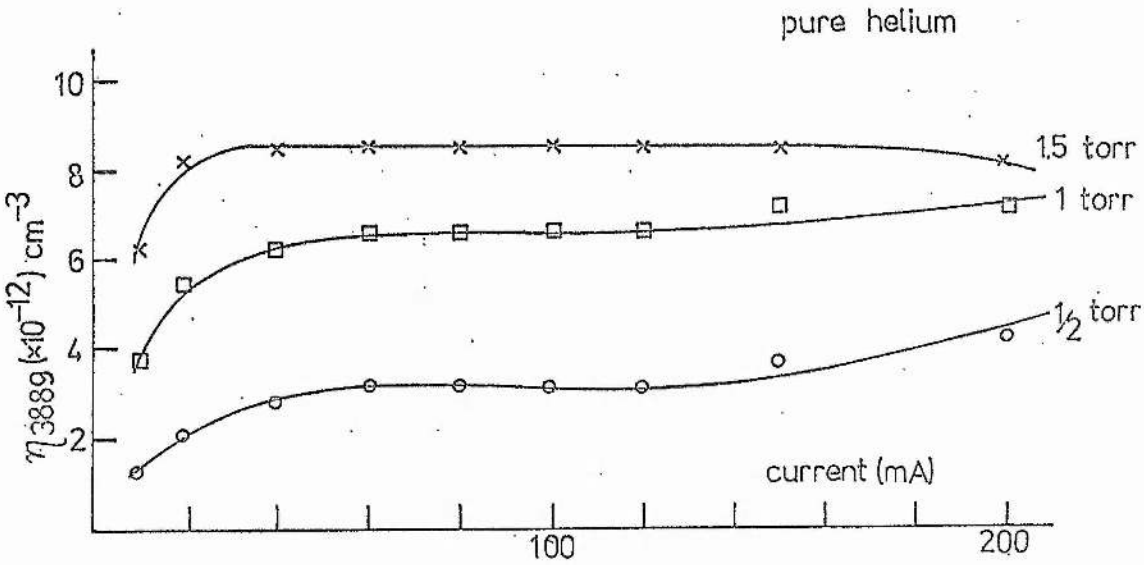

Fig. 3.4 The reduced triplet metastable density, n_{3889}, as a function of discharge current for helium pressures ½ - 1.5 torr. Results derived from absorption at 3889Å.

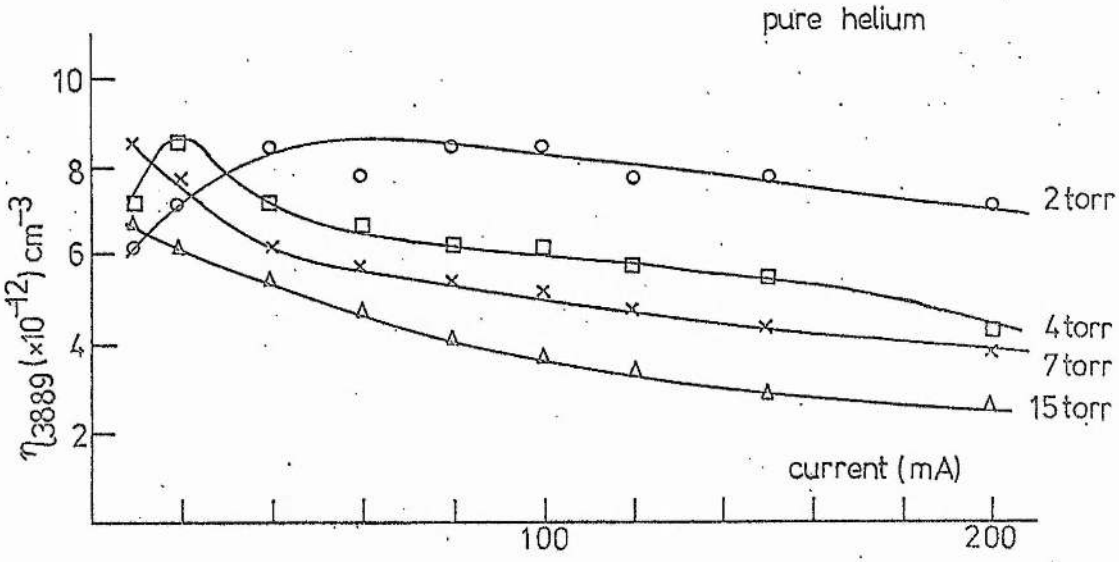

Fig. 3.5 The reduced triplet metastable density, η_{3889}, as a function of discharge current for helium pressures 2-7 torr. Results derived from absorption at 3889Å.

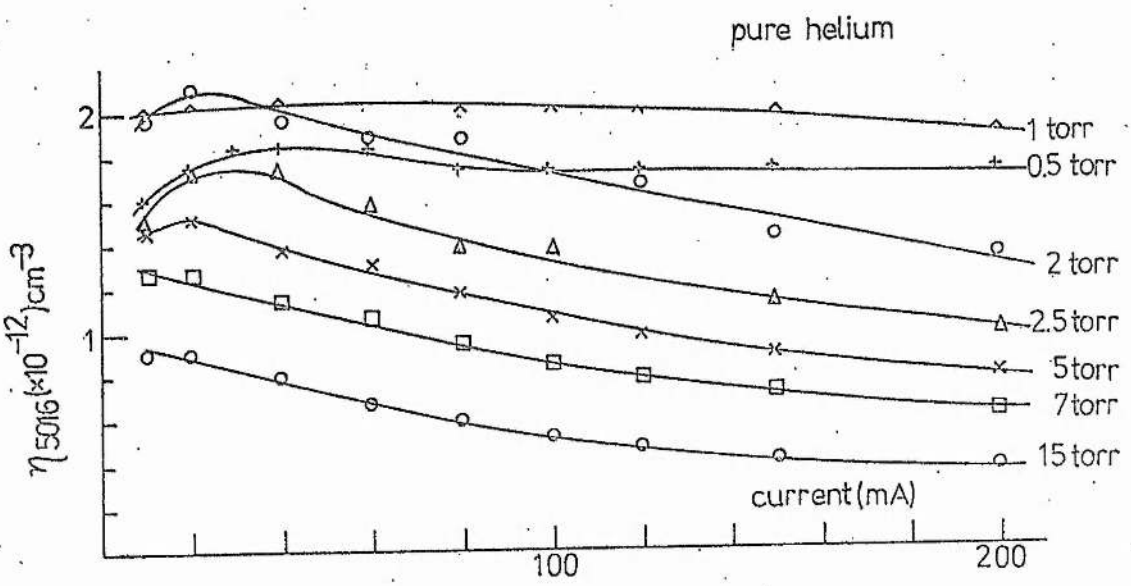

Fig. 3.6 The reduced singlet metastable densities, η_{5016}, as a function of discharge current for helium pressures in the range 0.5 - 7 torr. Results derived from absorption at 5016Å.

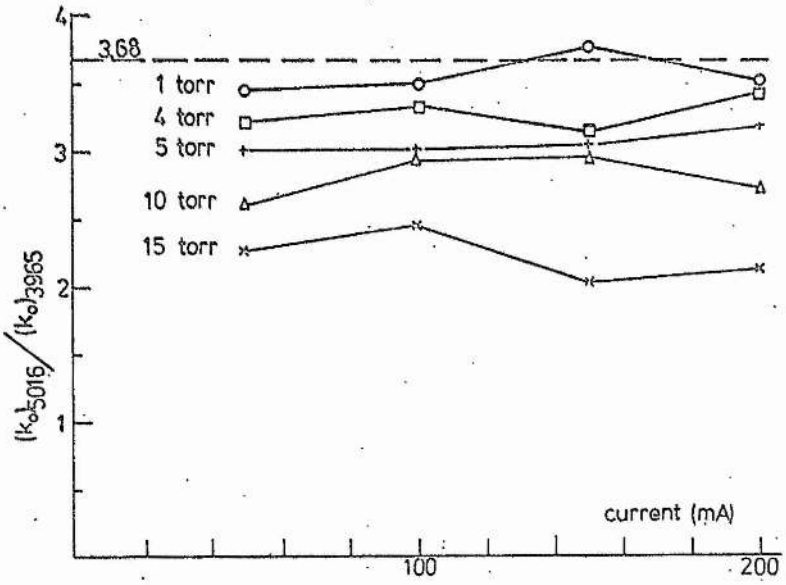

Fig. 3.7

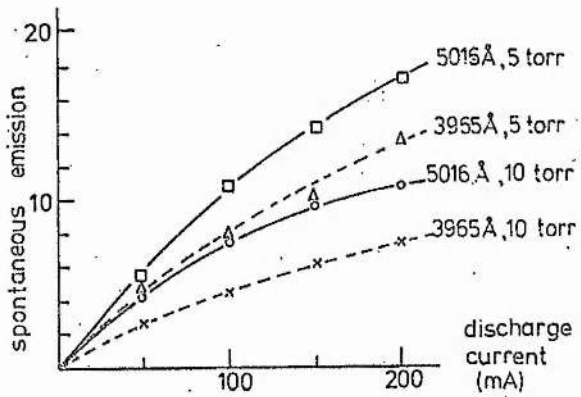

Fig. 3.8

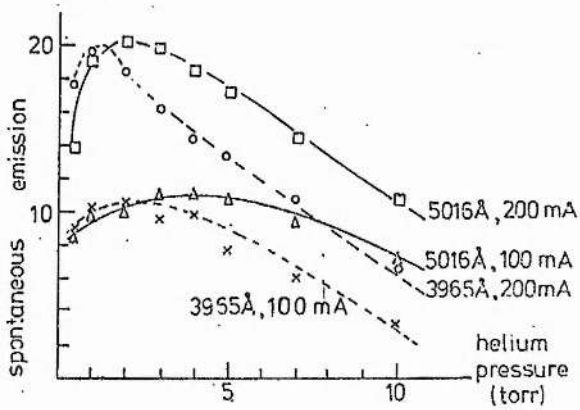

Fig. 3.9

Fig. 3.7 The ratio of the absorption coefficient at line centre for the 5016Å line to that for the 3965Å line as a function of current for various pressures in the pure helium discharge. The broken line indicates the value of 3.7 expected in the absence of upper level effects.

Fig. 3.8, 3.9 Spontaneous emission intensities of the 3965Å and 5016Å lines of HeI as a function of discharge current and helium pressure respectively. The intensities are proportional to the densities of the 4^1P (3965Å) and 3^1P (5016Å) levels of HeI and have been normalised such that the densities $N(3^1P)$ and $N(4^1P)$ are equal at 1 torr and 100 mA.

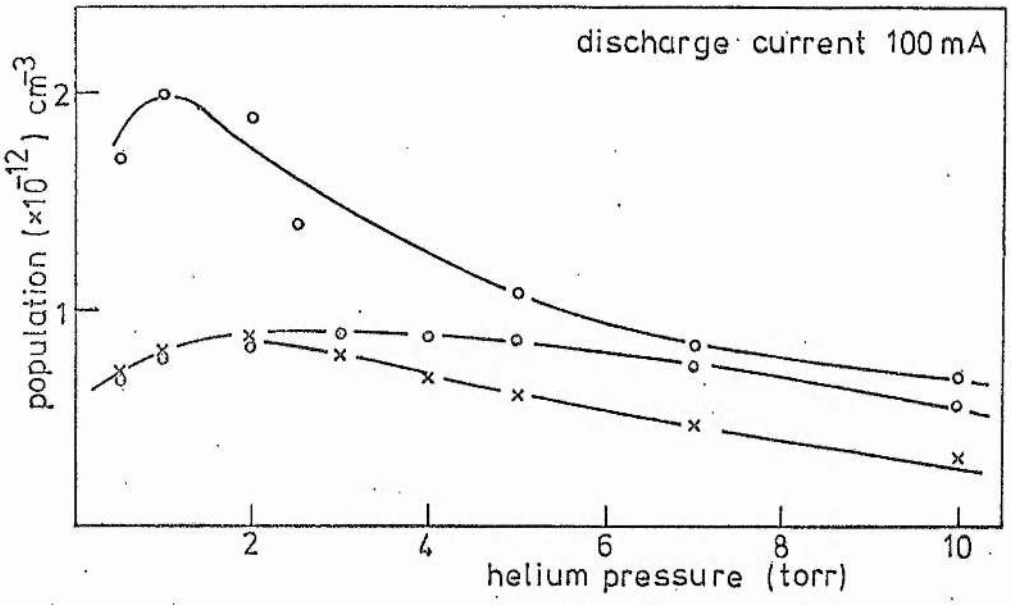

Fig. 3.10 Populations of the 2^1S (o), 3^1P (⊙) and 4^2P (x) levels of HeI, per unit statistical weight. The values for the 2^1S density are from absorption at 5016Å, while the 3^1P and 4^1P densities are tentative, based on the arguments of Section 3.3.

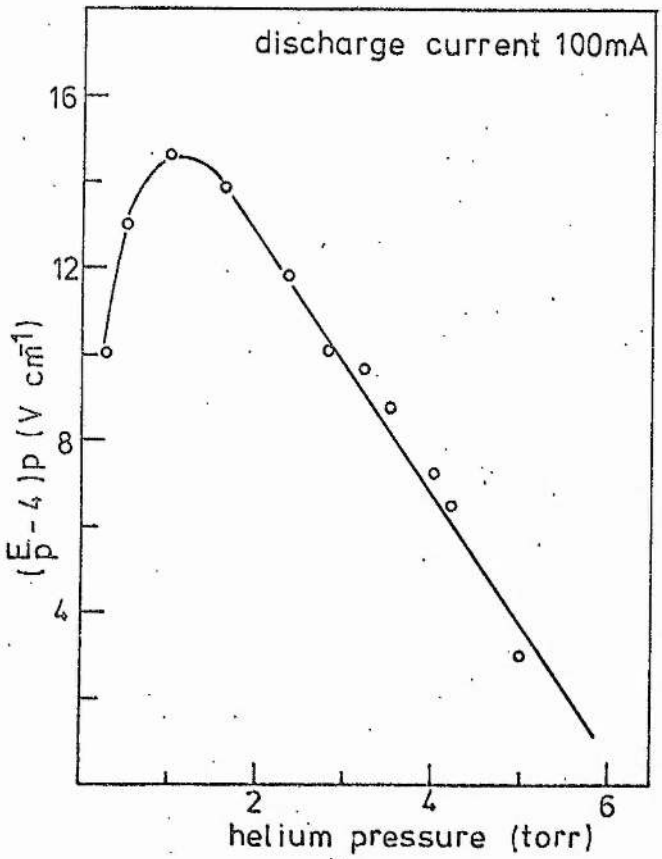

Fig. 3.11 The function $(\frac{E}{p} - 4)p$ against helium pressure, p, for a discharge in a 3 mm bore tube.

CHAPTER IV

EFFECTS OF CADMIUM VAPOUR ON THE METASTABLE POPULATIONS

4.1 Introduction

When cadmium vapour is introduced into the helium discharge by cataphoresis to produce discharge conditions similar to the active medium of the He-Cd laser, two effects on the metastable densities are observed. First, the metastable densities are reduced considerably, falling to almost half their original (no cadmium) values at the optimum cadmium partial pressure for laser oscillation. Second, the metastable populations do not now saturate until much higher discharge currents (60 - 120 mA). The changes in metastable densities with the partial pressures of helium and cadmium and the discharge current are correlated with the variations in laser output power also associated with these parameters.

The results reported here complement those of Silfvast (41) who described line absorption measurements in a He-Cd discharge at 10 mA in a 10 mm bore tube ($\sim$ 10 mA cm^{-2}). While the measurements of Silfvast provide information on the nature of the Penning collision process, the discharge conditions are unlike those pertaining to He-Cd lasers where currents of the order of 150 mA are passed through tubes of 3 - 5 mm bore ($\sim$1000 mA cm^{-2}).

4.2 Cadmium Neutral Density

To allow an unambiguous interpretation of the later results of this chapter it is necessary to know the parametric behaviour of the density of ground state cadmium atoms. Accordingly the absorption of the CdI intercombination resonance line at 3261Å ($5\ ^3P_1$ - $5\ ^1S_0$) has been measured by the line absorption technique. The complications introduced by isotope structure of the line have been taken into account by the methods described in Section 2.7.

The variation of the measured cadmium ground state neutral density with oven temperature is shown in Fig. 4.1 for several values

of helium pressure. The theoretical line shown is the number density calculated (42) from the measured oven temperature and the ideal gas laws. The difference between the measured and calculated densities is due to temperature variations in the oven, so that the thermocouple may not measure the minimum temperature inside the oven. Further, the details of the cataphoretic process also affect the ratio of the number density in the discharge tube to that in the oven. Fig. 4.1 also shows the relative values of the spontaneous emission at 4416Å. The cadmium ground state atomic density for optimum laser power is $\sim 2 \times 10^{13}$ cm^{-3}. Fig. 4.2 shows the current dependence of the cadmium ground state density, again with the 4416Å spontaneous emission included.

The important conclusion to be drawn from Figs. 4.1, 2 is that the cadmium ground state neutral density is determined principally by the cadmium oven temperature. The variations with discharge current and helium pressure are slight.

4.3 Metastable Densities in the Presence of Cadmium Vapour

Typical results for the variation of the metastable densities with increasing cadmium partial pressure (with discharge current and helium pressure constant) are shown in Fig. 4.3. Triplet and singlet metastable densities decrease rapidly as the amount of cadmium increases. The presence of cadmium in the discharge has two principal effects:

(i) The E/p value of the discharge decreases (Fig. 4.4) because the mean energy of the electrons is reduced by inelastic collisions with cadmium atoms. Further, the high energy tail of the electron energy distribution is depleted due to excitation of low-lying energy levels of CdI

(ii) An additional loss process for the helium metastable species is introduced - the process of Penning ionization.

The rate of Penning ionization, R_p, is given by

$$R_p = \langle\sigma_p v\rangle N_m N_{Cd}, \qquad (4.1)$$

where σ_p is the cross section for Penning ionization and v the relative velocity of the colliding particles and the average < > is over the thermal energy distribution. N_m and N_{Cd} are the densities of the helium (singlet or triplet) metastables and the ground state cadmium neutral atoms respectively. For the triplet metastables the ratio, f, of the loss of metastables by Penning processes to $\gamma n_e N_m$, the loss by electron collision de-excitation (the dominant loss mechanism after saturation in pure helium) is given by

$$f = \frac{\langle\sigma_p v\rangle N_{Cd}}{\gamma\, n_e} .$$

Using the value of 4.5×10^{-15} cm^2 found by Schearer and Padovani (6) and Riseberg and Schearer(7) for the total de-excitation cross-section of helium triplet metastables by cadmium ground state atoms, and putting $n_e \sim 10^{12}$ cm^{-3}, $N_{Cd} \sim 10^{13}$ cm^{-3} for typical lasing conditions, f is 0.1. Thus Penning collisions do not significantly alter the metastable populations. The decrease in metastable densities is due, therefore, to a decrease in their production rate by electron collisions.

If the electron energy distribution in the presence of cadmium were known, the above effects could be quantified. Vokaty and Masek (43) give some calculated distributions, but for conditions well removed from those appropriate to a laser. However, they also show the variation of the mean electron energy $\bar{E}$ as cadmium is introduced into the discharge. These data cover the range appropriate to a laser and from them a crude model of the effects of cadmium on the discharge may be constructed. If it is assumed that in the presence of cadmium the fraction of electrons with energy greater than 20 eV is largely unaltered (i.e. we underestimate the effects of cadmium on the electron energy distribution), then the production rate for

metastables may be written in terms of $\bar{E}$. From the data of Englert (28), Smit (25), and Heylen and Lewis (26), the value of E/p may be written

$$E/p = 4\bar{E} - 20$$

for $$\frac{E}{p} > 3 \text{ V cm}^{-1} \text{ torr}^{-1} .$$

The saturated metastable density becomes from equation (3.10)

$$(N_m)_{sat} = 8 \times 10^{12} \{\bar{E} - 6\}p,$$

for $\bar{E} > 6$ eV. The variation of $\bar{E}$ as cadmium is introduced into the discharge is shown in Fig. 4a of Vokaty and Masek (43) for various values of E/p. With starting conditions $E/p = 6\text{V cm}^{-1} \text{ torr}^{-1}$ in the absence of cadmium $\bar{E}$ is approximately 10 eV. When the optimum cadmium partial pressure for lasing is present ($\frac{N_{Cd}}{N_{He}} \sim 10^{-4}$), $\frac{E}{p}$ is reduced to 5 V cm^{-1} torr^{-1} and $\bar{E}$ to $\sim$ 8 eV. Thus the value for $(N_m)_{sat}$ is reduced by a factor of approximately 2 by the presence of the cadmium.

Since the laser power at 4416Å from a He-Cd discharge follows the shape of the spontaneous emission curve, the power limitations must occur as a result of limitations in the pumping rate of the upper laser level rather than through lower level effects such as direct electron excitation to this level or radiation trapping. To test for radiation trapping, absorption measurements were made on the 2265Å ($5\ ^2S_{1/2} - 5\ ^2P_{1/2}$ CdII) resonance transition from the lower level of the 3250Å laser transition (which shows the same parametric behaviour as the 4416Å laser). The absorption observed over 3 cm was not large, but care is needed in interpreting this because the motion of the ions in the longitudinal (and radial) electric fields of the discharge introduces large Doppler shifts so that the emission and absorption profiles do not necessarily coincide.

The excitation rate of the CdII upper laser levels is given by equation 4.1 where σ_p is now interpreted as the Penning cross-section for the <u>individual</u> level under consideration. Fig. 4.3 shows that

N_m is a decreasing function of the oven temperature while Fig. 4.1 shows that N_{Cd} is an increasing function. Thus the pumping rate must exhibit a maximum as the oven temperature is increased. The peak in the spontaneous emission at 4416Å (Fig. 4.1) and the associated peak in laser output power with increasing oven temperature is thus explained. The optimum pump rate for the 4416Å upper laser level by Penning collisions is then $\sim 3 \times 10^{16}$ cm^{-3} s^{-1} which implies a steady state population of the upper laser level (assuming radiative decay only) of 2×10^{10} cm^{-3}. This population is a minimum estimate since the effects of radiative cascade and electron collision excitation into the upper laser level have not been considered. The present value for the population of the upper laser level agrees reasonably well with the value for the optimum upper level population of 6.6×10^{10} cm^{-3} measured by Hodges (44) using a spectrometer which had been calibrated for absolute intensity measurements.

Fig. 4.5 shows the dependence of metastable densities and 4416Å spontaneous emission on helium pressure (with fixed discharge current and oven temperature). The peak in spontaneous emission corresponds to the peak in metastable density curves. This is to be expected since the neutral cadmium density is nearly independent of pressure (Fig. 4.1), so the pressure dependence of the Penning collision rate is the same as that of the metastables (Section 3.3).

The pressure peak of metastable densities is displaced to higher pressures than in the pure helium discharge (Fig. 3.3) because the present experiments were performed with the tube open to the vacuum system (of much larger volume) to allow the pressure to be varied quickly. The pure helium results on the other hand were taken with the tube closed-off from the vacuum system. Therefore, higher helium pressures are required to obtain the same number density of helium atoms in the

hot region of the discharge tube when the tube is open to the vacuum system which is at room temperature. The displacement of the peak to higher pressures may also be due to the changed production rate of the metastable species when cadmium is present such that the peak production rate need no longer occur at 2 torr.

The current dependence of the singlet and triplet metastable densities is shown in Figs. 4.6, 7 for two values of oven temperature. With the smaller amount of cadmium in the discharge the metastable densities reach much higher values at saturation (which occurs at a lower current) than when more cadmium is present. With the smaller amount of cadmium E/p (and hence $\bar{E}$) is reduced by a smaller amount than when the larger quantity of cadmium is present. Thus the value of the saturated metastable densities is higher with less cadmium present. Further, with the higher oven temperature, the fraction of high energy electrons (> 20 eV) is reduced by inelastic collisions so that higher currents (i.e. higher electron densities) are required to reach saturation.

Metastable densities and 4416Å spontaneous emission are only weakly dependent on current (for example, in Fig. 4.6 for the oven temperature of 250°C, there is a 10% variation in the triplet metastable density for the current range 60 - 160 mA). The broad maxima exhibited by the metastable densities must be regarded with caution since the apparent decrease at higher currents may still be caused by upper level effects. The weak dependence on current of the spontaneous emission at 4416Å (and the corresponding behaviour of laser power) may be explained by a saturation of the Penning excitation of the upper laser level, since at the higher currents both metastable densities and cadmium ground state neutral density are independent of current.

Thus the behaviour at 4416Å of the He-Cd laser with respect to its three important operating parameters is explained by the behaviour of the metastable densities and ground state cadmium atoms with these parameters, with the excitation rate of the upper laser level given by equation (4.1). These conclusions should be valid for other metal vapour systems (such as He-Zn and He-Se) in which upper laser levels are populated by Penning collisions between helium metastable species and ground state metal atoms.

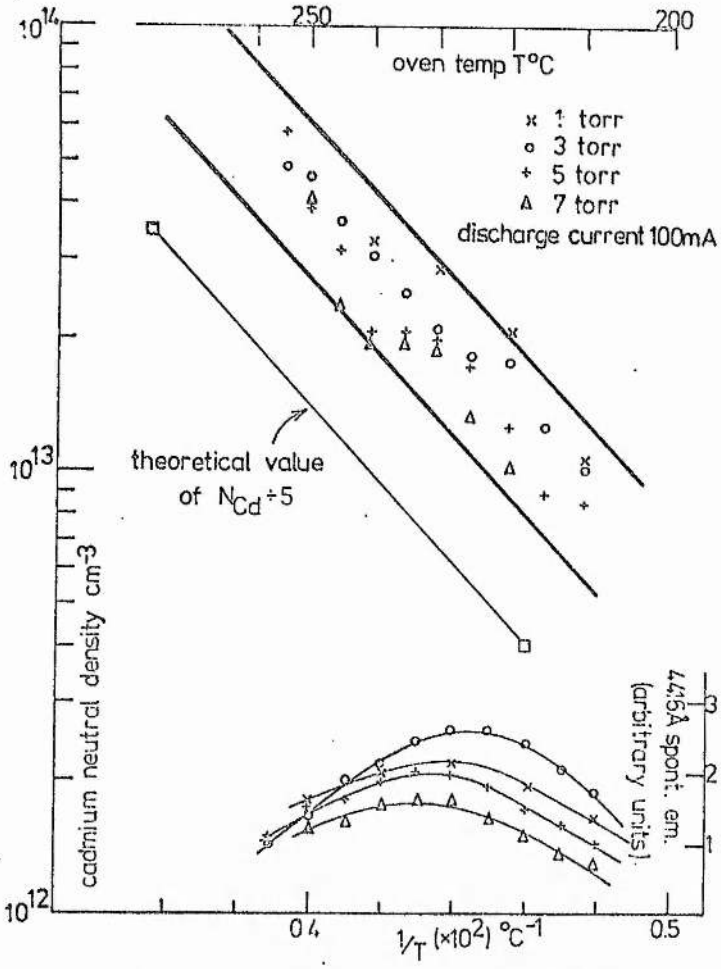

Fig. 4.1 The cadmium ground state neutral density as a function of oven temperature for various helium filling pressures. Spontaneous emission at 4416Å is shown for comparison.

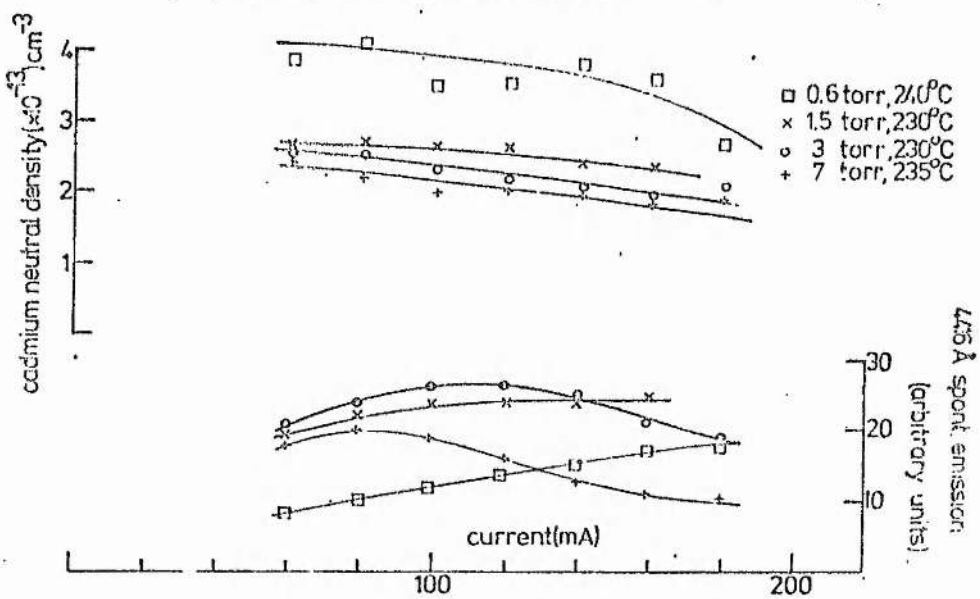

Fig. 4.2 The cadmium ground state neutral density as a function of current, for various oven temperatures and helium pressures. Spontaneous emission at 4416Å is shown for comparison.

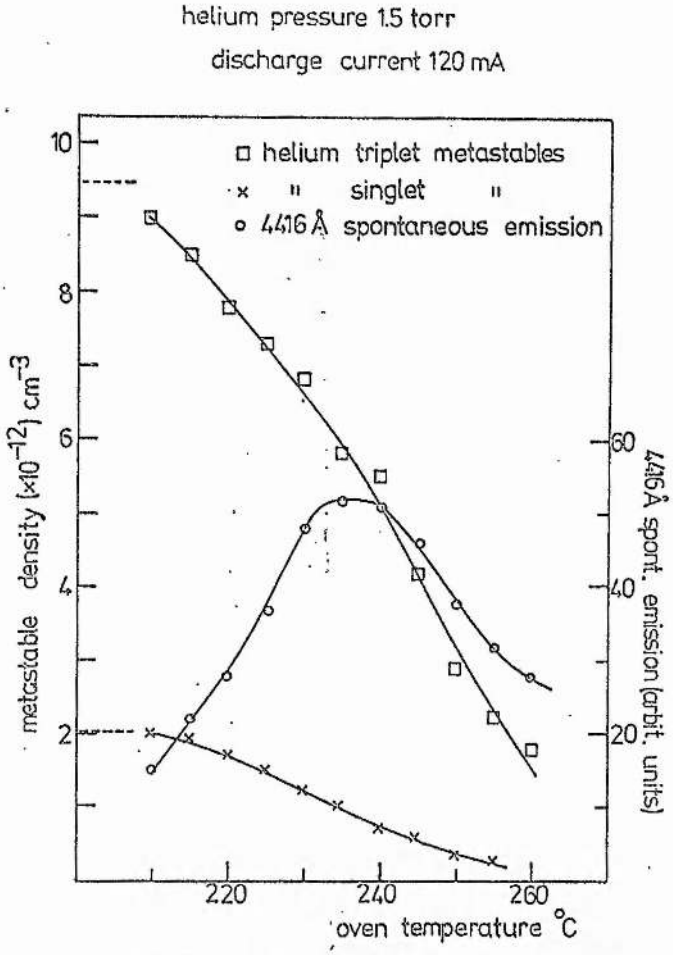

Fig. 4.3 Variation of reduced helium metastable densities with increasing cadmium concentration. Spontaneous emission at 4416Å is shown for comparison. Dashed lines show densities with no Cd present.

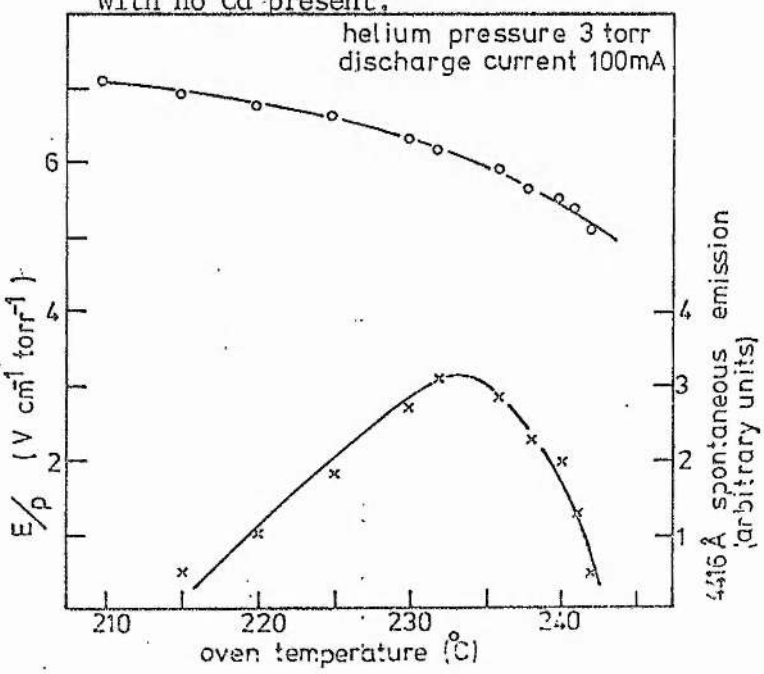

Fig. 4.4 Variation of E/p value and spontaneous emission at 4416Å with increasing cadmium concentration.

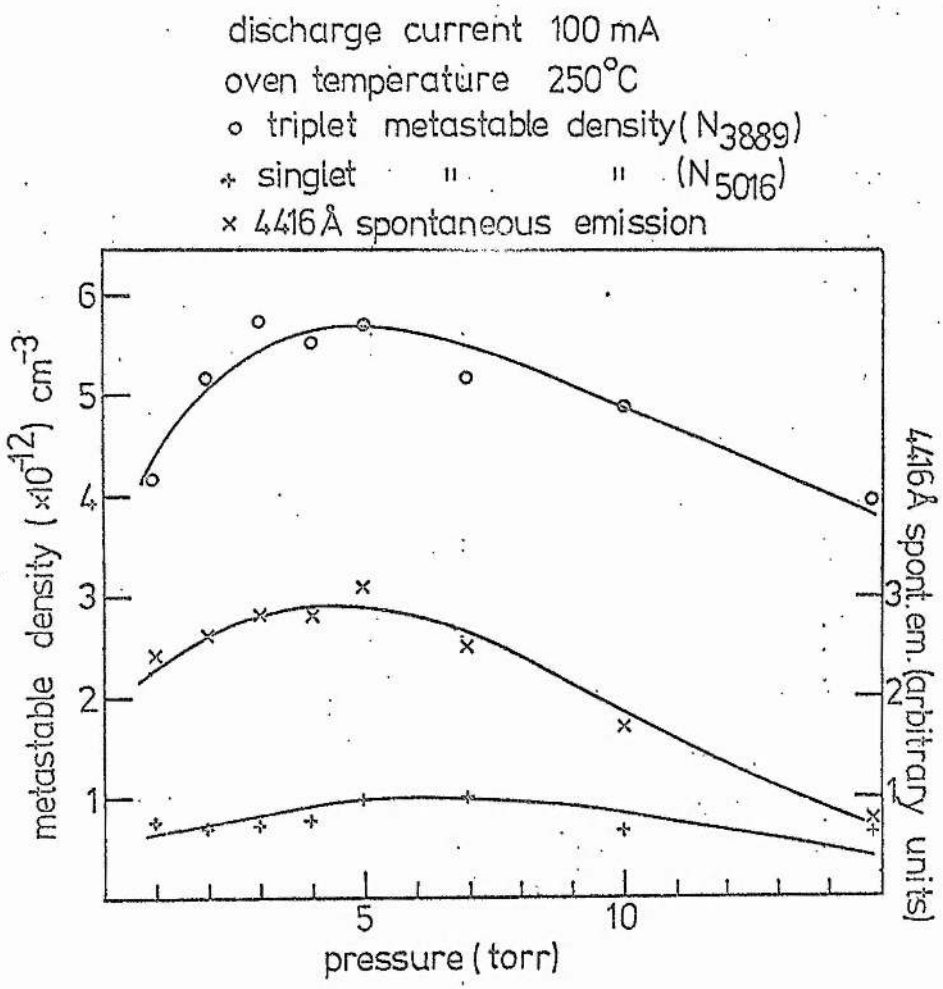

Fig. 4.5 Dependence of reduced helium metastable densities and spontaneous emission at 4416Å on the helium filling pressure. Oven temperature and discharge current are fixed.

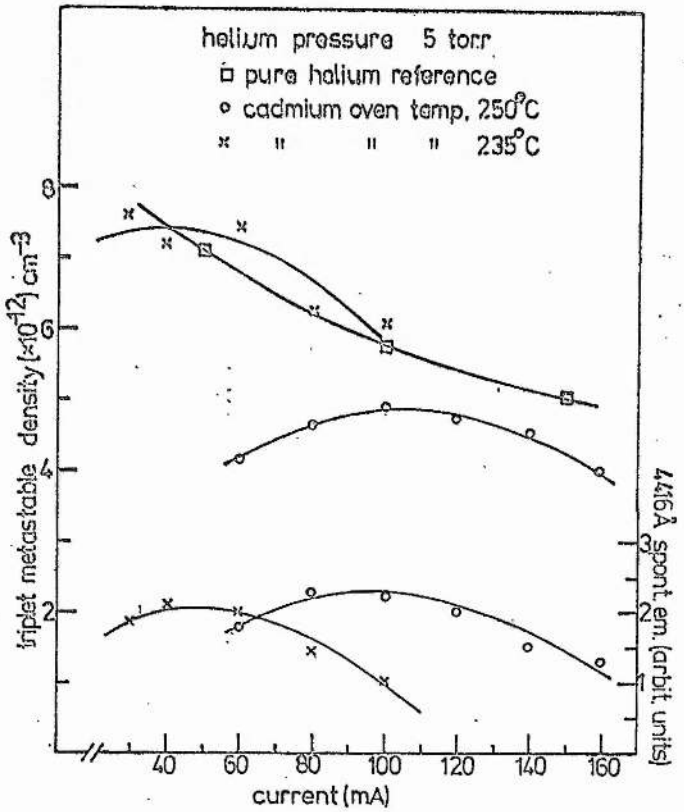

Fig. 4.6 Reduced helium triplet metastable densities (and spontaneous emission at 4416Å) as a function of current for fixed oven temperatures and helium pressure.

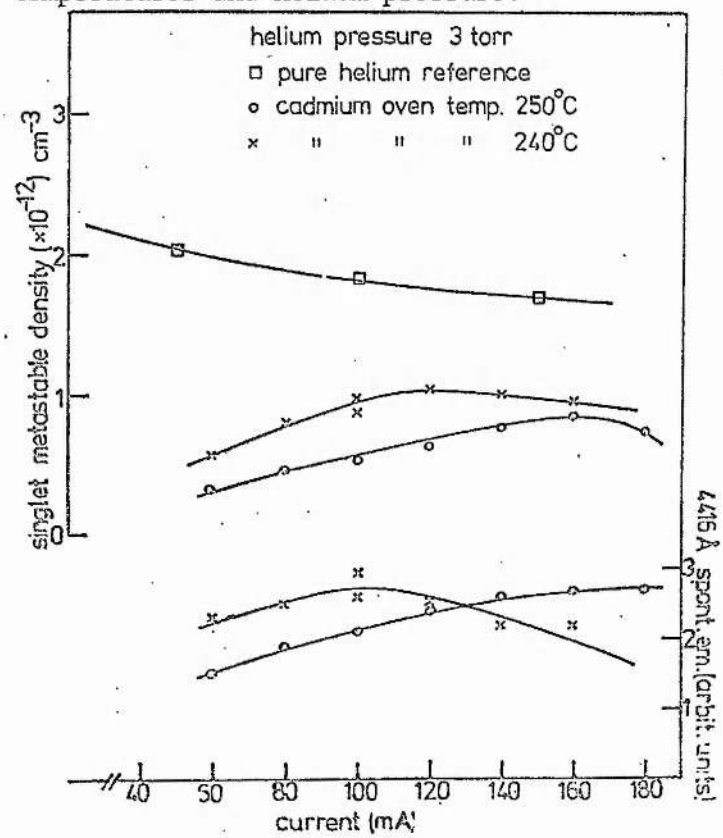

Fig. 4.7 Reduced helium singlet metastable densities (and spontaneous emission at 4416Å) as a function of current for fixed oven temperatures and helium pressure.

CHAPTER V

PERTURBATION SPECTROSCOPY OF THE HELIUM - CADMIUM DISCHARGE

5.1 Introduction

Having described the measurements of helium metastable densities which are pertinent to the calculation of excitation rates for the 4416Å upper laser level of Cd II the application of the technique of perturbation spectroscopy to the He-Cd laser system is now considered. This experiment allows, inter alia , the determination of the non-radiative destruction rate of the upper laser level.

In a gas discharge the populations of the excited states of the gas (or gases) are determined by the relevant creation and relaxation rates for collisional and radiative processes. If the discharge (in an appropriate optical cavity) supports laser oscillation on a transition between two energy levels, stimulated emission introduces an additional relaxation process for the upper laser level and may introduce an additional populating process for the lower laser level. Thus, if the laser field is switched on and off within the cavity only the populations of the upper and (possibly) lower laser levels are directly perturbed. If the sidelight spectrum is scanned for synchronous changes in the intensities of other spectral lines the resulting perturbation spectrum can be used to indicate collisional or radiative coupling mechanisms in the discharge. This technique has been applied to the He-Ne laser (45 - 52), the Xe laser (53), the CO_2-N_2-He laser (54) and the Ar ion laser (55).

This chapter describes the application of the technique of perturbation spectroscopy to the helium cadmium laser discharge. Chopping the 4416Å ($5s^2\ ^2D_{5/2}$ - $5p\ ^2P_{3/2}$, CdII) laser field in the cavity gives rise to changes in side-light intensity of the lines at 2144Å ($5p\ ^2P_{3/2}$ - $4s\ ^2S_{1/2}$, CdII) and 3250Å ($5s^2\ ^2D_{3/2}$ - $5p\ ^2P_{1/2}$, CdII) as well as at 4416Å. From the perturbations at 4416Å and 2144Å, the ratio of the radiative to non-radiative decay rates for the upper laser

level may be determined, as well as the relative excitation rates of the upper and lower laser levels. Perturbations at 3250Å may be used to obtain the relative pumping rates to the $5s^2\ ^2D_{3/2}$ level of CdII from the upper and lower laser levels ($5s^2\ ^2D_{5/2}$, $5p\ ^2P_{3/2}$ respectively) by electron collisions.

5.2 Preliminary Considerations

Before describing the experimental arrangement several background factors necessary for the interpretation of the results will be discussed. These factors are:

(a) spatial anisotropy in the sidelight emission

(b) calibration of the optical system for the range 2000Å -4500Å.

5.2.1 Spatial Anisotropy in the Sidelight

As the laser system used in this experiment was fitted with Brewster-angle windows, the laser radiation field was polarized. Thus the symmetry of the system about the tube axis is removed (56,59). In the absence of a magnetic field the quantization axis is along the electric field direction of the radiation (57) and so changes in the populations of the laser levels are exclusively generated via π transitions (58) (for which $\Delta m_J = 0$, where m_J is the magnetic quantum number). This results in a partial alignment of the ions in the laser levels. Owing to this partial alignment, changes in the sidelight may depend on the angle of observation relative to the polarization direction.

At the pressures used in the experiment (2-12 torr) collisional transfer within the m_J sublevels may destroy the alignment, but details of such processes for the He-Cd laser are unknown. However, the problem of spatial anisotropy may be avoided by the following considerations.

The sidelight intensity of any line comprises a mixture of π and σ transitions ($\Delta m_J = 0, \pm 1$ respectively) due to the structure of the

magnetic sublevels of the levels between which the transition occurs. Because of the partial alignment of the ions by transitions induced by the laser radiation, the relative proportions of π and σ transitions in the sidelight intensity will be altered. This implies an angular distribution in the intensity change, $\Delta I(\theta)$, measured in a plane perpendicular to the direction of propagation of the perturbing radiation, which may be written

$$\Delta I(\theta) = A \sin^2\theta + B \cos^2\theta \qquad (5.1)$$

since σ,π transitions have $\cos^2\theta$, $\sin^2\theta$ distributions respectively where θ is the angle between the quantization axis and the direction of observation. A and B are the appropriate maximum intensities.

Equation 5.1 may be rewritten as

$$\Delta I(\theta) = A + (B - A) \cos^2\theta$$

The mean change in sidelight, ΔI is then given by integrating $\Delta I(\theta)$ over θ to obtain

$$\Delta I = \frac{1}{\pi} \int_0^{\pi} \Delta I(\theta)\, d\theta = A + \tfrac{1}{2}(B - A) \qquad (5.2)$$

Thus, if $\Delta I(\theta)$ is measured for $\theta = 45^\circ$ (ie $\cos^2\theta = \frac{1}{2}$), the measured $\Delta I(\theta)$ is equal to the spatial average, ΔI. Thus the effects arising from spatial anisotropy are removed and the measured quantities are proportional to the total population changes.

The laser to be discussed in Section 5.3 had the plane of its Brewster-angle windows rotated about the tube axis by 45° from the vertical. Thus all the ancillary apparatus could be horizontal while observing the tube at an angle of 45° to the polarization direction of the laser field.

5.2.2 Calibration of the Optical System

As perturbations were expected at 2144Å and 4416Å the optical detection system was calibrated for relative intensity measurements

over the range 2000Å - 4000Å and at 4416Å. The sources for continuous radiation over this range were two deuterium lamps with quartz envelopes (Manufacturers Supply Co Type DF5S) which had been calibrated at the National Physical Laboratory (the ultimate standard for the calibration being synchrotron radiation from an electron accelerator). The lamps were calibrated for relative intensity measurements in two circumstances - first with the lamp radiating directly into a spectrometer, and second, with a UV achromat (Carl Zeiss f = 150 mm) imaging the lamp, the image being effectively a secondary source which was then calibrated.

Using one lamp, the present spectrometer - photomultiplier system was calibrated for relative sensitivity both with and without the lens. The sensitivity constants obtained from both methods agreed to $\pm$ 5%. The relative sensitivities at 4416Å, 2144Å and 3250Å were 1, $\frac{1}{109}$, $\frac{1}{1.8}$ respectively.

It is found that the quartz walls of metal-vapour lasers develop a dark deposit during operation. As this deposit may have varying transmission at the wavelengths of interest here, an arrangement must be provided to monitor the transmission of the tube walls during the course of the experiment. The tube itself is described in the next section - only the measurements of the transmission of the tube walls are described in this section.

With the deuterium lamp on the side of the tube opposite the spectrometer (Fig. 5.1), a second UV achromat (Carl Zeiss f = 75 mm) was used to image the lamp onto a stop at the tube wall. This stop acted as a second source, and was imaged onto the spectrometer slit with the calibrated f = 150 mm achromat. A reference spectrum from the deuterium lamp was then taken before any discharge was run in the tube. At various stages further spectra were taken. At a chosen wavelength the ratio of the later signal to the reference signal gave

the change in the fractional transmission of the two walls of the tube due to degradation of the surface. The square root of the fractional transmission for both walls gave the fractional transmission of one wall. After several hours of operation with the He-Cd discharge the transmissions at 3250Å and 2144Å were reduced to 70% and 60% respectively of that at 4416Å.

Thus the overall system was calibrated as the wall transmission could be monitored and the lens-spectrometer-photomultiplier system had been previously calibrated.

5.3 Experiment

The experimental arrangement is shown schematically in Fig. 5.1. Two quartz discharge tubes were used: the first, of active length 195 cm and diameter 4 mm, was maintained at the conditions for optimum laser power at 4416Å, while the conditions in the second tube, of active length 10 cm and diameter 5 mm could be widely varied. Two 2 m radius of curvature mirrors, of nominal 100% reflectivity at 4416Å, spaced 320 cm apart, formed the optical cavity. With the test cell inside the cavity higher radiation fields were obtainable to perturb the discharge than with the cell outside the cavity. Both tubes were of conventional cataphoretic design (4),used cadmium of natural isotopic composition, and had independent vacuum-filling systems, high voltage power supplies and oven temperature controllers. The Brewster-angle windows were inclined at 45° to the horizontal as described in section 5.2.1 to avoid spatial anisotropy in the perturbation signal. A 5Ω resistor in the anode circuit of the smaller test cell was included so that current changes at the chopping frequency could be observed. A toothed-wheel chopper, driven by a synchronous motor, chopped the radiation field in the cavity at 1600 Hz. The chopper was placed near the mirror furthest from the test cell.

The side light emitted by the cell was examined at a region where the curved wall of the tube had been ground away on opposite sides of the tube and replaced by quartz flats over a height of 1 mm (this made a negligible difference to the tube diameter). The lens effect of the tube walls was thus removed. The varying transmission of the flat sections of the tube wall was monitored using a calibrated deuterium lamp and lens arrangement as described in Section 5.2.2. The collection lens-monochromator-photomultiplier system was calibrated as described in the same section.

A Carl Zeiss SPM2 monochromator fitted with a quartz prism was used to select the lines of interest, and the light was detected by an EMI 9594 QUB photomultiplier. The output signal from the photomultiplier was either recorded directly as a steady d.c. signal level or connected to a Brookdeal Type 401 lock-in amplifier to obtain the perturbation signal. All measurements at 4416Å were corrected for stray laser light at the chopping frequency. This light gave a signal in antiphase to the population changes on the upper laser level. Such stray light corrections were at no time greater than 10% of the sidelight intensity changes at 4416Å. The measured perturbations and line intensities were corrected for tube wall transmission and spectrometer sensitivity using the results of Section 5.2.2.

5.4 Results and Discussion

5.4.1 General Remarks

In the experiment a spatial average of intensity changes across the tube is observed. Almost all parameters of the discharge, including the electron density, the metastable densities and the intensity of the laser field vary across the tube. It is important that the principle of superposition holds so that the equations describing the measured average quantities are the same as those describing the microscopic

changes in the discharge.

In the equations derived in this section for the interpretation of the results, the relationships between the population changes on various levels are linear. Thus, even though a spatial average of population changes is measured, the equations for local population changes apply to the spatial average.

The first check on the system was to observe the population changes on the upper laser level as a function of the laser power. Fig. 5.2 shows that the change in the population of the upper laser level is proportional to the laser intensity. This is to be expected as the change in upper level population is small compared to the steady state population, so that the cell is operating under conditions where the gain is not heavily saturated.

More important is Fig. 5.3, which shows the population changes of the $5s^2\ ^2D_{3/2}$ level (measured at 3250Å) against the changes of the $5s^2\ ^2D_{5/2}$ level. There is a linear relationship between the population changes on the level which is directly perturbed and the population changes on the level coupled to the former by collision processes. Thus the linear equations derived subsequently to describe the perturbations are valid, and the principle of superposition is applicable.

Each spectral line emitted by the He-Cd discharge (under optimum laser conditions) in the range 2000Å - 6000Å was then examined in turn for a perturbation signal when the laser field at 4416Å within the cavity was chopped. The only transitions to exhibit a perturbation, apart from that at 4416Å, were those at 2144Å ($5p^2\ P_{3/2}$ - $5s\ ^2S_{1/2}$, CdII) and 3250Å ($5s^2\ ^2D_{3/2}$ - $5p\ ^2P_{1/2}$). The other lines showed perturbations less than 0.5% of that at 4416Å, which was the limit of detection sensitivity set by discharge noise.

The interaction of the chopped laser radiation and the discharge

current was examined by connecting the voltage across the 5Ω anode resistor to the lock-in amplifier. The current change at the chopping frequency was less than 0.002mA in 100 mA, so that current-induced population changes may be ignored.

5.4.2 Perturbation at 2144Å

Consider a system of two levels 1, 2 coupled by a radiative transition with Einstein coefficient A_{12}. Level 1 represents the upper laser level and has a pump rate from all sources, population (in the absence of lasing) and non-radiative decay rate of R_1, N_1 and γ_1 respectively. Level 2 represents the lower laser level and similarly has a pump rate (apart from radiative cascade from the upper laser level), population (in the absence of lasing) and non-radiative decay rate of R_2, N_2 and γ_2 respectively. (Fig. 5.5).

In the absence of lasing the steady state populations N_1 and N_2 are given by the rate equations

$$R_1 = N_1(A_{12} + \gamma_1) \tag{5.3}$$

$$R_2 + N_1A_{12} = N_2(A_{20} + \gamma_2), \tag{5.4}$$

where A_{20} is the Einstein coefficient for radiative transitions from the lower laser level, and the upper laser level decays radiatively only to the lower laser level.

Laser oscillation introduces an additional loss rate L for level 1 due to stimulated emission, and an additional production rate L for level 2. If, as a consequence, the steady state population of level 1 is reduced by δN_1, and that of level 2 increased by δN_2, and if R_1 and R_2 do not change in the presence of the laser field then

$$R_1 = (N_1 - \delta N_1)\ (A_{12} + \gamma_1) + L \tag{5.5}$$

$$R_2 + (N_1 - \delta N_1)A_{12} = (N_2 + \delta N_2)\ (A_{20} + \gamma_2) - L \tag{5.6}$$

Subtracting (5.3) from (5.5), and (5.4) from (5.6) and eliminating L from the resulting equations gives

$$\frac{\delta N_1}{\delta N_2} = \frac{A_{20} + \gamma_2}{\gamma_1} \quad . \tag{5.7}$$

In the helium cadmium laser the lower level for the 4416Å laser transition is rapidly depopulated by radiative decay to the ion ground state, with a radiative lifetime of 3.4 ns (60). Since the gas-kinetic collision time in the discharge is of the order of 1 μs, the approximation $\gamma_2 << A_{20}$ may be made and equation (5.7) simplifies to

$$\frac{\delta N_1}{\delta N_2} = \frac{A_{20}}{\gamma_1} \tag{5.8}$$

The spectral line intensity changes are related to the population changes by

$$\begin{aligned} \delta I_1 &= h\nu_{12} A_{12} \delta N_1 \\ \delta I_2 &= h\nu_{20} A_{20} \delta N_2 . \end{aligned} \tag{5.9}$$

Substitution of (5.9) into (5.8) gives

$$\frac{\delta I_2}{\delta I_1} = \frac{\nu_{20}}{\nu_{12}} \frac{\gamma_1}{A_{12}} \quad . \tag{5.10}$$

Thus by measuring the relative intensity changes of lines arising from the upper and lower laser levels, the ratio of the non-radiative to radiative decay rates of the upper laser level may be determined. The ratio of the intensity changes at 2144Å and 4416Å (corresponding to δI_2 and δI_1 respectively) were measured over the range of operating conditions: helium pressure 2 - 7 torr, discharge current 80 - 160 mA and cadmium oven temperature 190° - 220°C.

No functional dependence of the ratio $\frac{\delta I_2}{\delta I_1}$ $\left(\frac{\delta I(2144Å)}{\delta I(4416Å)}\right)$ on either helium pressure or oven temperature was observed, and only slight variation with current (Fig. 5.4). The extrapolation of the current variation to zero current gives a non-zero intercept which implies that while electrons do play a part in destroying the upper laser level, other processes must also be considered. The average value of $\delta I_2/\delta I_1$

obtained over the range of operating conditions gives a value $\frac{\gamma_1}{A_{21}} = 0.9 \pm 0.2$. Thus the non-radiative destruction rate of the upper laser level is almost equal to the radiative decay rate.

This result is in agreement with the results of Klein and Maydan (61) who measured the decay rate of the upper laser level by using a fast cavity dumping technique. At a helium pressure of 3.5 torr the total decay rate varied in the range $1.5 - 1.9 \times 10^6\ s^{-1}$, with an approximately linear dependence on current in the range 75 - 170 mA. Dienes and Sosnowski (62) have also derived upper level decay rates from magnetic field dip measurements on the He-Cd laser. The values obtained were a factor of 2 - 3 higher than those of Klein and Maydan (61).

The constancy of the non-radiative decay rate of the upper laser level could be explained by the existence of another radiative decay path from the upper laser level, but the data of Shenstone and Pittenger (63) show that the 4416Å transition is the only one originating from the $5s^2\ ^2D_{5/2}$ level. The assumption $\gamma_2 << A_{20}$ could be invalidated by radiation trapping of the 2144Å line, but an 'at worst' calculation assuming single isotope cadmium and a ground state ion density equal to the ground state neutral density gives an imprisonment factor (64) of 0.1 for a tube of radius 0.2 cm. The effective Einstein coefficient with these assumptions is $50 \times 10^6\ s^{-1}$, which is still much greater than gas-kinetic collision rates.

In considering the non-radiative decay rate of the upper laser level, diffusion of cadmium ions to the tube wall, as well as volume losses, must be considered. Assume that a cadmium ion produced at the centre of the tube is accelerated to the walls by the ambipolar field established by the electrons and the helium ions. With a mean free path of 0.2 mm at 1 torr, the ion has an average of 10 collisions before

arriving at the wall, in each of which is loses 7% of its acquired energy. Thus, to a first approximation, the loss of an ion to the wall may be considered as a free fall. The value of the potential difference between the tube centre and the walls (neglecting the sheath) may be calculated (65) to be approximately 5V (electron mean free path = 0.5 mm, tube radius = 2 mm). Assuming a uniform field distribution the transit time of an ion to the tube wall is of the order of 1 μs. Thus diffusion in the radial field represents a significant loss process for the cadmium ions in the $5s^2\ ^2D_{5/2}$ level as the diffusion time is similar to the radiative lifetime. As the helium pressure increases the diffusion losses decrease but volume destruction processes increase, which results in the non-radiative decay rate of the upper laser level showing little variation with discharge conditions.

In a recent paper Lis (66) estimates a non-radiative decay rate of the upper laser level of $40 \times 10^6\ s^{-1}$ compared to the present value of $1 \times 10^6\ s^{-1}$. The discrepancy between these two values for the non-radiative decay rate of the $5s^2\ ^2D_{5/2}$ level of CdII will now be discussed in detail.

The method of Lis is similar to that of the present experiment, although only relative perturbations under one set of experimental conditions are measured. To interpret his results, Lis uses an equation similar to equation (5.8). In the present notation Lis's equation becomes

$$\gamma_1 = A_{20} \frac{\delta N_2}{\delta N_1}$$

$$= A_{20} \frac{N_2}{N_1} \frac{\delta N_2/N_2}{\delta N_1/N_1} . \qquad (5.11)$$

As Lis was unable to calibrate his system for relative intensity measurements he could determine only the ratio $\frac{\delta N_2/N_2}{\delta N_1/N_1}$. The value found by Lis for this ratio under the one set of experimental conditions agrees with values found in the present work (∿0.2). In order to calculate γ_1, Lis uses a value for $\frac{N_2}{N_1}$ of 0.46 found by Hodges (67). This value is

obtained for a tube containing cadmium of natural isotopic composition by combining gain measurements (which enable $(\frac{N_1}{g_1} - \frac{N_2}{g_2})$ to be deduced) with absolute intensity measurements at 4416Å (which enable $\frac{N_1}{g_1}$ to be deduced).

If Hodges' gain of 6% m^{-1} is taken as the gain at line centre of a purely Doppler broadened line (of full width at half-maximum equal to 1.5 GHz) a value of the lower laser level population of $\sim 3 \times 10^{10}$ cm^{-3} is obtained. This is the value deduced by Hodges. Therefore it appears that Hodges has not considered the isotope structure of the gain curve.

For a given population inversion the gain at 4416Å is smaller ($\sim$6% m^{-1} (67)) in a laser containing cadmium of natural isotopic composition than in a laser containing a single isotope ($\sim$20% m^{-1} (2)) due to the different shapes of the gain profiles. Treating the gain of 6% m^{-1} in a laser containing cadmium of natural isotopic composition as arising from a single isotope profile then leads to an overestimate of the population of the lower laser level.

The present experiment allows the ratio of the populations of the upper and lower laser levels to be measured from the ratio of spontaneous emission intensities at 2144Å and 4416Å, since

$$\frac{N_2}{N_1} = \frac{I_2}{I_1} \frac{A_{12}}{A_{20}} \frac{\nu_{12}}{\nu_{20}} .$$

Typical results are shown in Figs. 5.5, 5.6 as a function of current and helium pressure. The ratio $\frac{N_2}{N_1}$ is $\sim 10^{-2}$, which is to be expected if both levels have similar pump rates while their radiative lifetimes differ by two orders of magnitude.

Using a value of $\frac{N_2}{N_1} = 0.03$ and the measured value of $A_{20} = 3 \times 10^8$ s^{-1} (60) to re-interpret the results of Lis, γ_1 is found to be 1.8×10^6 s^{-1}, in agreement with the present results of $1.2 \pm 0.3 \times 10^6$ s^{-1}. Thus the present result, and those of Lis, Klein and Maydan (61), and Dienes and Sosnowski (62) are all consistent if the ratio of the populations

of the upper and lower laser levels found by Hodges is not included in the calculations.

From equations (5.3) and (5.4) the ratio of the pump rates $R_{1,2}$ for the laser levels may also be obtained:

$$\frac{R_2}{R_1} = \frac{N_2(A_{20} + \gamma_2) - N_1 A_{12}}{N_1(A_{12} + \gamma_1)}$$

$$= \frac{\frac{N_2}{N_1}\frac{A_{20}}{A_{12}} - 1}{1 + \frac{\hat{\gamma}_1}{A_{12}}} \qquad (5.12)$$

if γ_2 is small compared to A_{20}. Expressing $N_{1,2}$ in terms of $I_{1,2}$ using equation (5.9), equation (5.12) becomes

$$\frac{R_2}{R_1} = \frac{\frac{I_2}{I_1}\frac{\nu_{12}}{\nu_{20}} - 1}{1 + \frac{\gamma_1}{A_{12}}} \qquad (5.13)$$

(Recall that R_2 specifically excludes cascade from the upper laser level according to its definition earlier in this section.)

From equations (5.9), (5.3) if γ_1 is constant,

$$R_1 \propto N_1 \propto I_1 .$$

Therefore if R_1 is obtained in arbitrary units from the spontaneous emission at 4416Å, R_2 may be obtained in the same units from equation (5.13). Typical results are shown in Figs. 5.7, 5.8 as a function of current and helium filling pressure.

Fig. 5.7 shows that, with increasing pressure, the pumping rate, R_1, of the upper laser level reaches a maximum and then decreases. This is explained by the behaviour of the Penning collision rate as described in Section 4.3 . From that section the following relation between R_1 and the helium metastable density, N_m, is obtained (equation 4.1)

$$R_1 = \kappa_1 N_m$$

where κ_1 is the appropriate rate constant. However, the excitation rate, R_2, of the lower laser level is seen to increase steadily with pressure. The processes which contribute to R_2 comprise direct-excitation by collisions with electrons, ions, or metastable species and radiative cascade from higher lying levels of CdII (but excluding cascade from the upper laser level).

Direct excitation of the lower laser level by Penning or charge transfer processes does not occur (68) in view of the large energy defects for such processes. Further, direct electron excitation to the lower laser level is not significant for the following reason. As the pressure increases the mean electron energy decreases so that, although the total electron density increases, the fraction of electrons with sufficient energy (at least 6 eV) to excite the lower laser level decreases. (This point is discussed more fully in the following section in connection with the perturbation at 3250Å.)

Radiative cascade to the lower laser level, which must therefore be the principal contribution to R_2, arises predominately (>80%) (68) from levels of the cadmium ion which are excited by charge transfer collisions with helium ions. Thus R_2 may be expressed as follows:

$$R_2 = \kappa_2 N_i$$

where N_i is the helium ion density and κ_2 the appropriate rate constant.

At the conditions for optimum intensity at 4416Å in Fig. 5.7 (ie helium pressure 4 torr) $\frac{R_2}{R_1}$ equals 3, while N_m is approximately 5×10^{12} cm^{-3} (Fig. 4.3) and the helium ion density is 3×10^{12} cm^{-3} assuming it is equal to the electron density (10). Thus $\frac{\kappa_2}{\kappa_1}$ equals 5.

This ratio may be compared with the results obtained by Turner-Smith (68) from a flowing afterglow, under conditions where $N_m \gtrsim N_i$ (the precise relationship between N_m and N_i is not noted in (68)). The principal cascade transitions to the lower laser level, at

2749Å, 2313Å, 2321Å and 3536Å, were found to have (68) relative rates of 350, 240, 22 and 96 respectively, giving a total cascade rate of ∿800 units. These transitions arise from levels populated by charge transfer processes except for the transition at 3536Å whose upper level is populated by Penning collisions. Also approximately one quarter of the intensity at 2749Å is due to Penning excitation. In the same units the pump rate of the upper laser level was found to be 1000. Thus, under the conditions of the afterglow experiment

$$\frac{\kappa_2}{\kappa_1} = \frac{R_2}{R_1}\frac{N_m}{N_i} \geqslant \frac{R_2}{R_1} = 0.8 \ .$$

A similar estimate may be made if the total cross-section of 3.7×10^{-15} cm^2 (69) for the de-excitation of helium ions by ground state cadmium atoms is used. As two thirds of the cadmium ions excited by charge transfer decay radiatively via level 2 (68), the ratio $\frac{\kappa_2}{\kappa_1}$ becomes

$$\frac{\kappa_2}{\kappa_1} \sim \frac{\frac{2}{3}\sigma_{ce}}{\sigma_p}$$

where σ_{ce} and σ_p are the total charge transfer cross-section and the Penning cross-section to level 1 respectively. Thus, with $\sigma_p \sim 1 \times 10^{-15}$ cm^2 (6,7,8), $\frac{\kappa_2}{\kappa_1}$ is 2.5.

The two estimates $\frac{\kappa_2}{\kappa_1} \geqslant 0.8$ and $\frac{\kappa_2}{\kappa_1} \sim 2.5$ are in reasonable agreement with the present result of $\frac{\kappa_2}{\kappa_1} \sim 5$.

At constant current, as the pressure increases the metastable population falls while the ion density increases. Thus the rate of excitation to the lower laser level increases with pressure as the radiative cascade from higher states of the cadmium ion increases with the ion density.

The current behaviour of R_2 (Fig. 5.8) is consistent with this explanation as the increase in R_2 with current reflects the increase in helium ion density with current. The behaviour of R_1 with current has

been explained previously in Section 4.3.

Finally, the rate of excitation of the lower laser level by cascade from the upper laser level, $N_1 A_{12}$, and the rate by all other processes combined in R_2 may now be compared. In Section 4.3, R_1 was found to be $\sim 3 \times 10^{16}$ cm^{-3} s^{-1} for optimum laser conditions. Thus the rate of decay to the lower laser level is $\sim 1.5 \times 10^{16}$ cm^{-3} s^{-1}. With $\frac{R_2}{R_1} \sim 3$, R_2 is approximately 6×10^{16} cm^{-3} s^{-1}. Thus radiative cascade from the upper laser level is a comparatively minor pump process for the lower laser level.

5.4.3 Perturbation at 3250Å

The upper level of the 3250Å transition ($5s^2\ ^2D_{3/2}$) is about 1 eV above the upper level of 4416Å laser transition ($5s^2\ ^2D_{5/2}$). When the population of the latter level is decreased by laser oscillation, that of the former is also observed to decrease. The ratio of the intensity changes on the two transitions is shown in Figs. 5.10, 11, 12 as a function of discharge current, helium pressure, and cadmium oven temperature respectively. Typical experimental accuracy is shown on the graph of the oven temperature dependence (Fig. 5.12). The current behaviour of the ratio (Fig. 5.10) is consistent with electron collisions being the principal cause of coupling, as there is a linear relationship between the ratio of perturbations and the current (ie the electron density). The pressure behaviour (Fig. 5.11), however, shows an extrapolated zero perturbation at a non-zero pressure. This indicates that coupling to the lower ($5p\ ^2P_{3/2}$) as well as the upper laser level of the 4416Å transition must be taken into account.

An analysis of the perturbation at 3250Å is now described which leads to a very large cross-section ($\sim 7 \times 10^{-13}$ cm^2) for excitation of $5s^2\ ^2D_{3/2}$ CdII level from the $5p\ ^2P_{3/2}$ CdII level by electron collisions. As shown on pages 5.20-21 this cross-section implies a much larger de-excitation rate of the $5s^2\ ^2D_{5/2}$ level than is observed (Section 5.4.2). The results of this section must therefore be regarded as tentative.

If the couplings between the $5s^2\ ^2D_{3/2}$ level and the $5s^2\ ^2D_{5/2}$ and $5p\ ^2P_{3/2}$ levels (levels 3, 1, 2 respectively - see Fig. 5.9) are included explicitly, then the rate equation describing the population

N_3 of the $5s^2\ ^2D_{3/2}$ level in the absence of laser radiation is

$$R_3 + N_2\gamma_{23} + N_1\gamma_{13} = N_3(A_3 + \gamma_3) \qquad (5.14)$$

where γ_{23} and γ_{13} are the rates for electron excitation to level 3 from levels 2 and 1 respectively, and R_3, A_3, γ_3 are the excitation rate (excluding γ_{13}, γ_{23}), total radiative decay rate and total non-radiative decay rate respectively of level 3, (Fig. 5.9). In the presence of laser radiation the rate equation becomes

$$R_3 + (N_2 + \delta N_2)\gamma_{23} + (N_1 - \delta N_1)\gamma_{13} = (N_3 - \delta N_3)(A_3 + \gamma_3) \qquad (5.15).$$

Subtracting (5.14) from (5.15) and rearranging gives

$$\frac{\delta N_3}{\delta N_1} = \frac{1}{A_3+\gamma_3}\{\gamma_{13} - \gamma_{23}\frac{\delta N_2}{\delta N_1}\} \qquad (5.16).$$

If (5.16) is rewritten in terms of line intensities using (5.9), and the following values for the Einstein coefficients substituted : $A_{20} = 3 \times 10^8\ s^{-1}$ (60), $A_{12} = 1.3 \times 10^6\ s^{-1}$ (70,71), $A(5s^2\ ^2D_{3/2} - 5p\ ^2P_{1/2}) = 2.2 \times 10^6\ s^{-1}$ (60, 71), it becomes

$$\frac{\delta I_3}{\delta I_1} = \frac{3}{A_3+\gamma_3}\{\gamma_{13} - 10^{-3}\ \gamma_{23}\frac{\delta I_2}{\delta I_1}\} \qquad (5.17).$$

By extrapolating the pressure variation shown in Fig.5.11, it is seen that $(\delta I_3/\delta I_1)$ becomes zero at a pressure of 1.5 - 2 torr (E/p = 10V cm^{-1} $torr^{-1}$), so that for these conditions we have

$$\gamma_{13}/\gamma_{23} = 10^{-3}\ (\frac{\delta I_2}{\delta I_1}).$$

The value of $(\delta I_2/\delta I_1)$ is of the order of 1.8 (see previous section) so that at 1.5 - 2 torr, the ratio γ_{13}/γ_{23} is approximately 10^{-3}. If the coupling is due to electron collisions the rates $\gamma_{13,23}$ can be written

$$\gamma_{13} = n_e \langle\sigma_{13}v_e\rangle$$
$$\gamma_{23} = n_e\langle\sigma_{23}v_e\rangle\ , \qquad (5.18)$$

where n_e is the electron density, σ_{13} and σ_{23} are the cross-sections for electron impact excitation from levels 1 and 2 respectively and the average < > is carried out over the electron energy distribution. The

threshold energy for σ_{13} is about 1 eV, while that for σ_{23} is about 5 eV. At an E/p value of 10 V cm^{-1} $torr^{-1}$, in a pure helium discharge, the majority of electrons have an energy in excess of 1 eV, while the fraction with an energy exceeding 5 eV is about 0.6 (25), and hence the ratio σ_{13}/σ_{23} is of the order of 10^{-3}. Thus the cross section for electron excitation from the lower laser level, which corresponds to an allowed optical transition , is much greater than that from the upper laser level.

The increase in the ratio $(\delta I_3/\delta I_1)$ with increasing pressure above 1.5 - 2 torr may be explained as follows. As the pressure increases the E/p value of the discharge decreases, so that the electron energy distribution shifts to lower energies (25). This favours the excitation process from the $5s^2\ ^2D_{5/2}$ level as opposed to the $5p\ ^2P_{3/2}$ level and so the ratio $(\gamma_{13}/\gamma_{23})$ increases with pressure. Since the total electron density also increases with pressure (10),the ratio $(\delta I_3/\delta I_1)$ rapidly increases.

Before considering the behaviour of $(\delta I_3/\delta I_1)$ at pressures above 4 torr, the influence of cadmium vapour must be discussed. Fig. 5.12 shows that as the cadmium partial pressure in the discharge increases with oven temperature the ratio $(\delta I_3/\delta I_1)$ rapidly decreases. The most likely cause of this decrease is that both excitation processes $(\gamma_{13},\gamma_{23})$ decrease with increasing cadmium partial pressure.

The decrease in the rate of excitation (γ_{13}) from the $5s^2\ ^2D_{5/2}$ level is due to the increasing fraction of electrons with energies less than 1 eV as cadmium is introduced. Vokaty and Masek (43) have computed the electron energy distribution in a helium-cadmium discharge. Their figure 2 (reproduced here as Fig. 5.13) illustrates this increase in the fraction of electrons with energies less than 1 eV as cadmium is introduced at a constant E/p value of 1.5 volts cm^{-1} $torr^{-1}$. While the

value of E/p for the initial conditions of Fig. 5.12 is 5 volts cm^{-1} $torr^{-1}$, it decreases as the oven temperature increases. The decrease in E/p and the increase of cadmium partial pressure both lead to an increase in the fraction of electrons with energies less than 1 eV. Since the total electron density is but weakly dependent on cadmium partial pressure (10), the excitation rate γ_{13} must decrease. Similar arguments applied to γ_{23} indicate an even stronger decrease in the fraction of electrons with energies greater than 5 eV with increasing cadmium partial pressure.

The behaviour of the ratio $(\delta I_3/\delta I_1)$ at pressures above 4 torr is now considered. With increasing pressure the total electron density increases but the E/p value decreases. Fig. 5.11 shows that at pressures above 4 torr a condition is reached where the change in E/p, through increasing the fraction of electrons with energies less than 1 eV, is the more important factor in determining the excitation rates γ_{13} and γ_{23}, and the ratio $\delta I_3/\delta I_1$ saturates or decreases.

Cross-sections σ_{13} and σ_{23} can be estimated by considering equation (5.17) at the higher pressures when the term involving γ_{23} may be neglected. The ratio $(\delta I_3/\delta I_1)$ reaches a value of 0.07 at 4 torr when the electron density is $\sim 10^{12}$ cm^{-3} for electrons with energy above 1 eV (10,25). Taking a value for A_3 of 3×10^6 s^{-1} and neglecting γ_3 gives a value of $\sigma_{13} \sim 7 \times 10^{-16}$ cm^2 and hence a value of $\sigma_{23} \sim 7 \times 10^{-13}$ cm^2.

The value of σ_{13} is typical of gas kinetic collision cross sections, but the value of σ_{23} is very large for an atomic collision process. It is of interest to note that very large cross sections have been reported recently by Green et al (73) for electron collisions with excited states of the zinc ion. A cross section of $\sim 2 \times 10^{-12}$ cm^2 was obtained for the transfer of energy from the 6p ^2P level of ZnII to other levels of the zinc ion, while approximately the same value was obtained for the

cross section for electron induced energy transfer between the 5d ^2D and 4f ^2F levels of ZnII.

Large cross sections are characteristic of collisions involving a resonance (74), so that the cross section $\sigma_{23} \sim 7 \times 10^{-13}$ cm^2 implies the possible existence of a resonance interaction, via an intermediate state, in the collision of electrons with cadmium ions in the 5s $^2P_{3/2}$ level.

Such an intermediate state is formed if the collision takes place according to the reaction

$$(Cd^+)_{^2P_{3/2}} + e \rightarrow (Cd^{**}) \rightarrow (Cd^+)_{^2D_{5/2}} + e,$$

where Cd** is a state of neutral cadmium whose total excitation energy is higher than the ionization potential of CdI, ie an autoionizing state. Such autoionizing states of CdI are known to exist (72), the series limits of these states having energies coincident with the $^2D_{3/2,5/2}$ levels of CdII. Thus the colliding electron may form an autoionizing state of CdI by temporary recombination when it collides with the cadmium ion. (The recombined state is necessarily short-lived since in a two-body recombination process energy and momentum are not conserved simultaneously). For autoionizing states near the $5s^2\ ^2D_{3/2}$ series limit, thermal energies are sufficient to cause decay into the $5s^2\ ^2D_{3/2}$ level of CdII.

On the basis of a plausibility argument, however, the magnitude of σ_{23} is now shown to lead to a value of the non-radiative decay rate of the $5s^2\ ^2D_{5/2}$ level which is much larger than observed. The value $\sigma_{23} = 7 \times 10^{-13}$ cm^2 implies a rate γ_{23} (equ 5.18) under typical laser conditions ($n_e \sim 10^{12}$ cm^{-3}, $v_e \sim 10^8$ cm s^{-1}) of $\gamma_{23} = 7 \times 10^7$ s^{-1}. Therefore the rate of excitation, γ_{21}, of the $5s^2\ ^2D_{5/2}$ level from the 5p $^2P_{3/2}$ level is expected to be of the same magnitude as γ_{23} (if not

larger in view of the ratio of Einstein coefficients for the optical transitions corresponding to γ_{21} and γ_{23}). Thus the reverse process, electron collisional destruction of the 4416Å upper laser level to the 5p $^2P_{3/2}$ level, is, by the principle of detailed balance, expected to have a rate $\gamma_{12} \geqslant \gamma_{21}$. (The neglect of exponential terms and statistical weights in this argument makes no difference to this inequality). Thus we have $\gamma_{12} \geqslant 70 \times 10^6\ s^{-1}$, which is inconsistent with the results of the previous section where a value for the total non-radiative decay rate for the $5s^2\ ^2D_{5/2}$ upper laser level of $\gamma_1 \sim 10^6\ s^{-1}$ was obtained. At present it is not possible to see how this inconsistency may be removed.

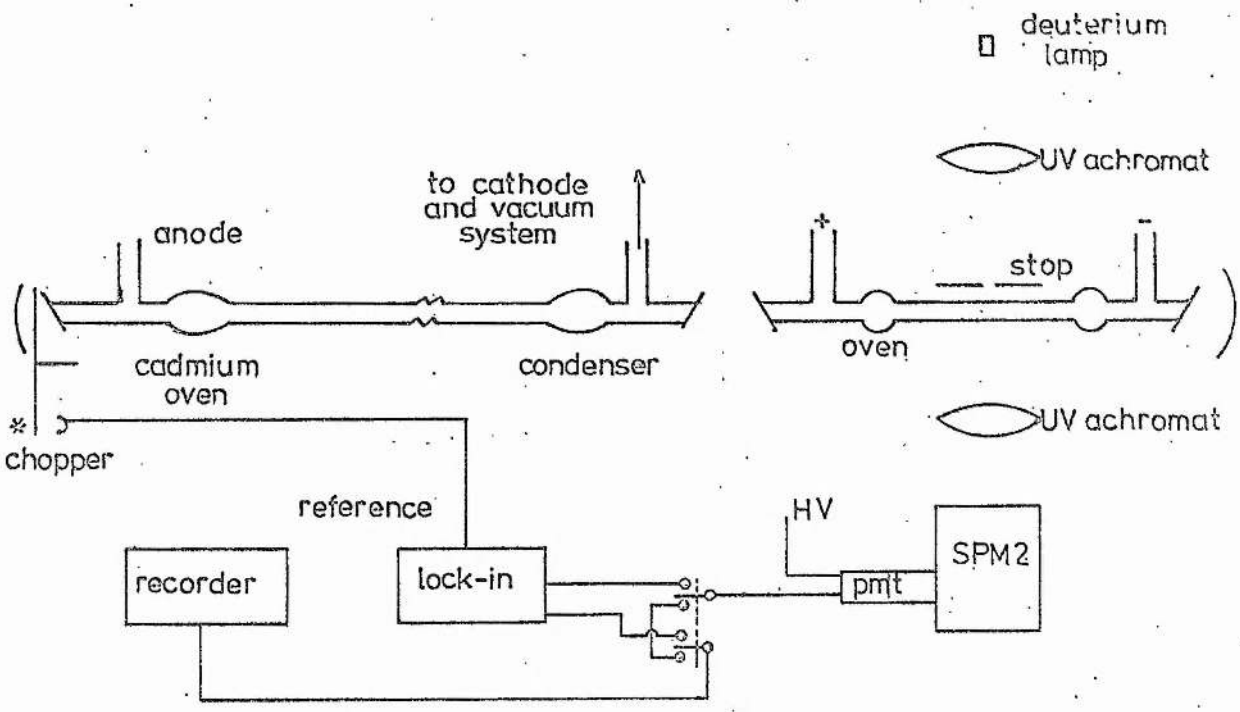

Fig. 5.1 Schematic diagram of the perturbation spectroscopy experiment (including apparatus for measuring the transmission of the tube walls).

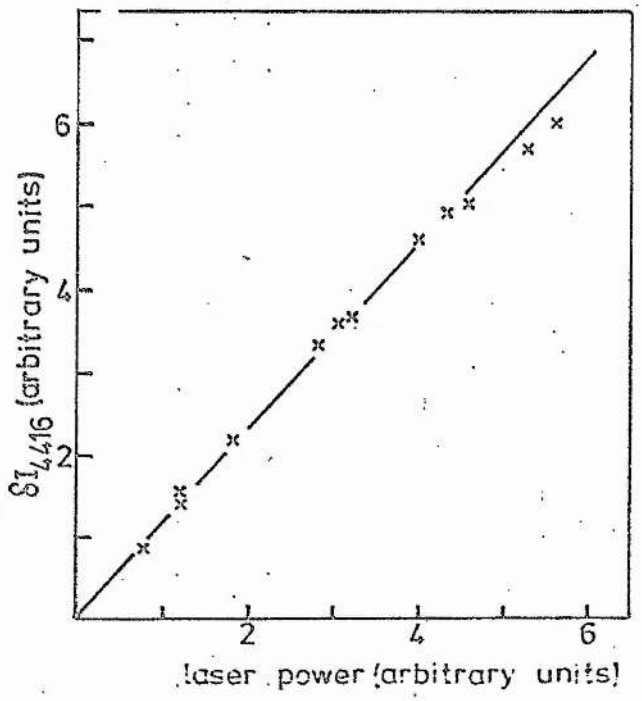

Fig. 5.2 Perturbation signal at 4416Å (δI_{4416}) as a function of the laser power.

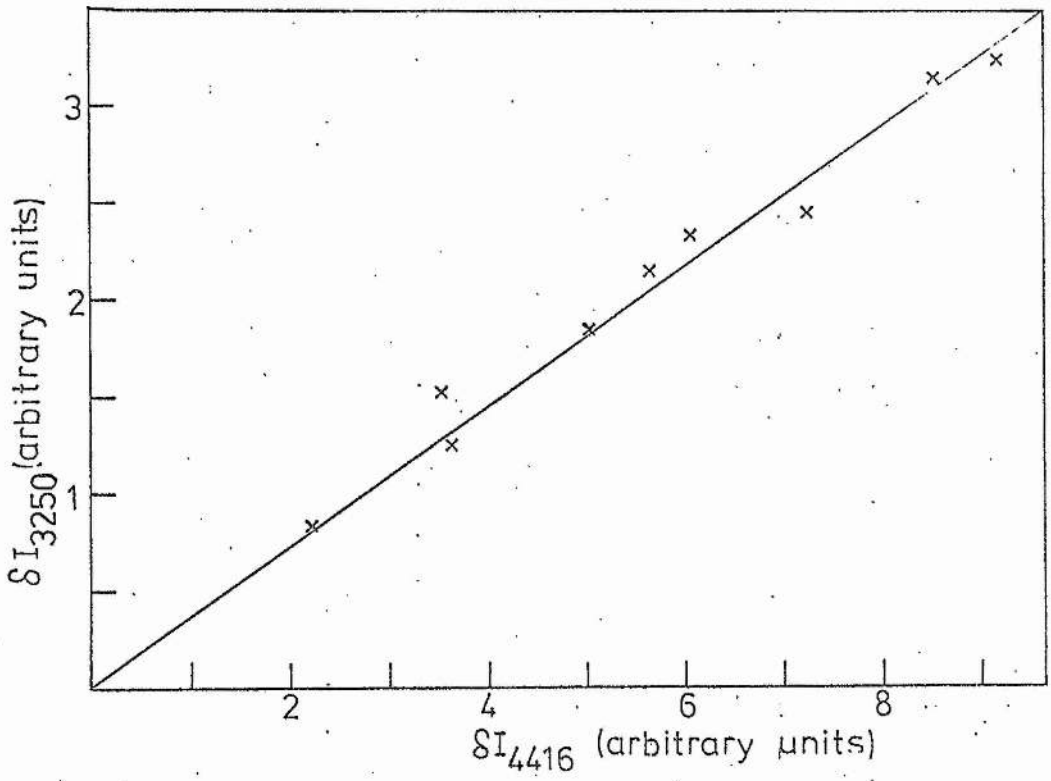

Fig. 5.3 Perturbation signal at 3250Å against perturbation signal at 4416Å.

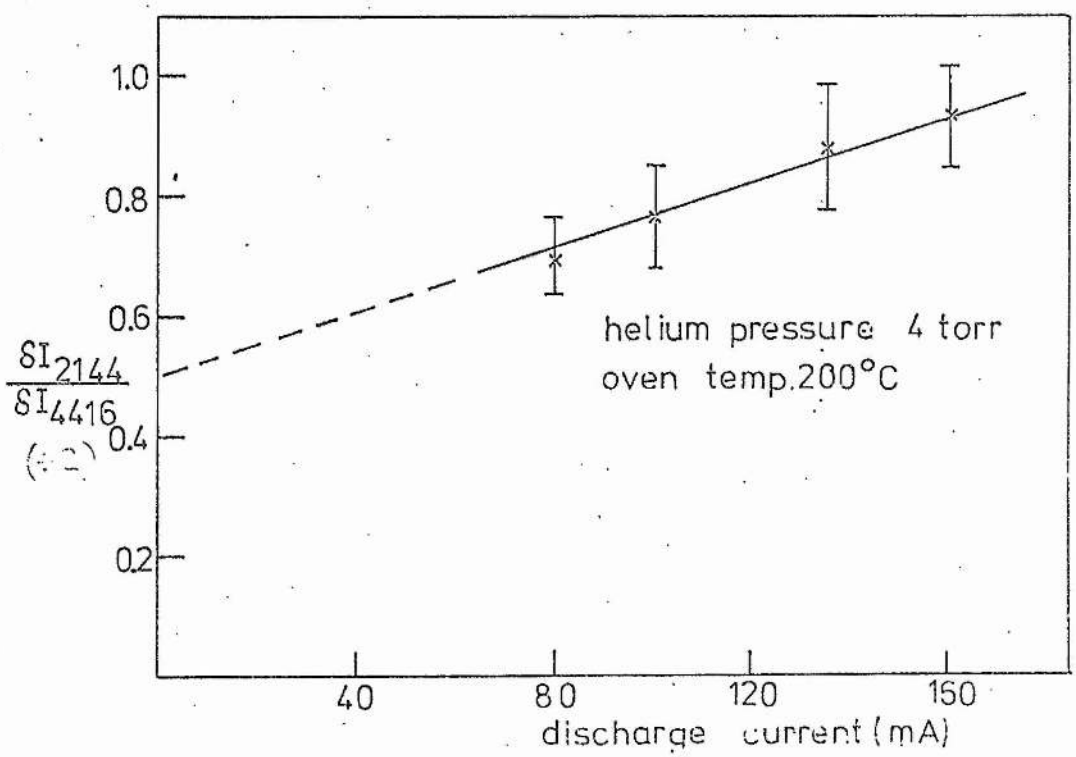

Fig. 5.4 The ratio of the intensity changes at 2144Å and 4416Å as a function of current.

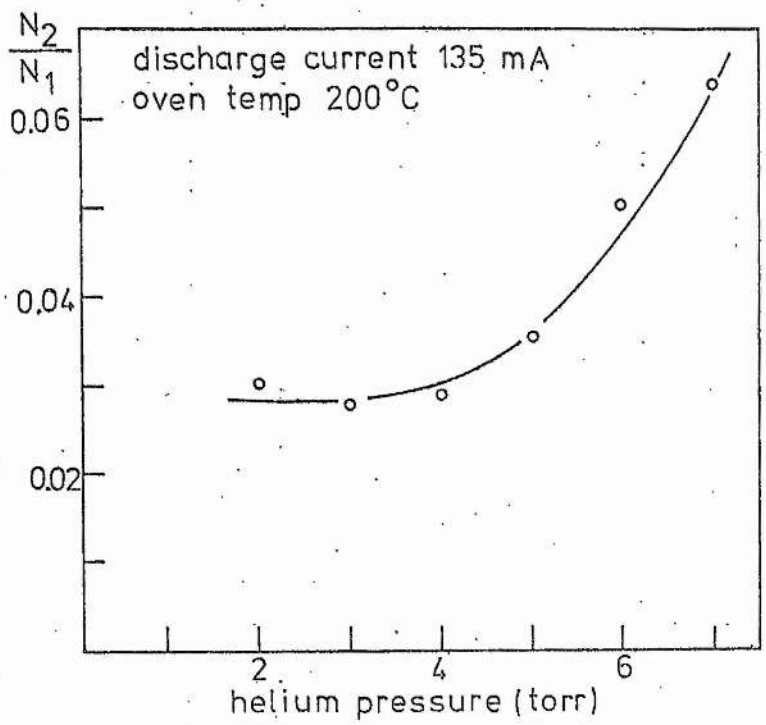

Fig. 5.5 The ratio of the populations of the lower (N_2) to the upper (N_1) levels of the 4416Å laser transition as a function of helium pressure.

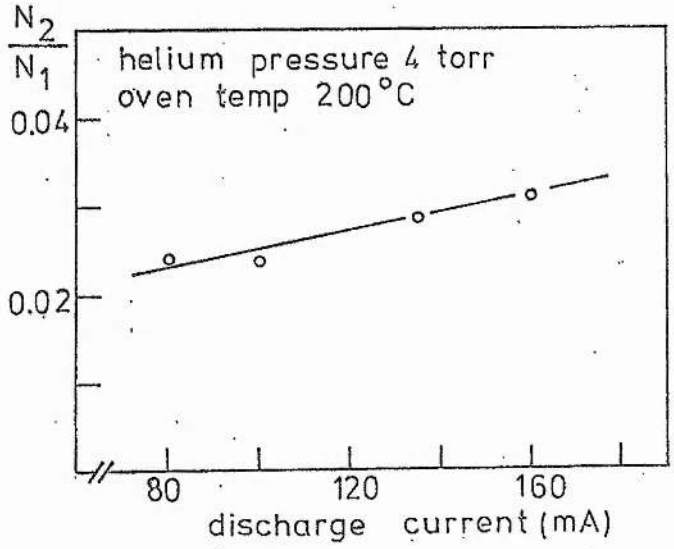

Fig. 5.6 The ratio of the populations of the lower (N_2) to the upper (N_1) levels of the 4416Å laser transition as a function of the discharge current.

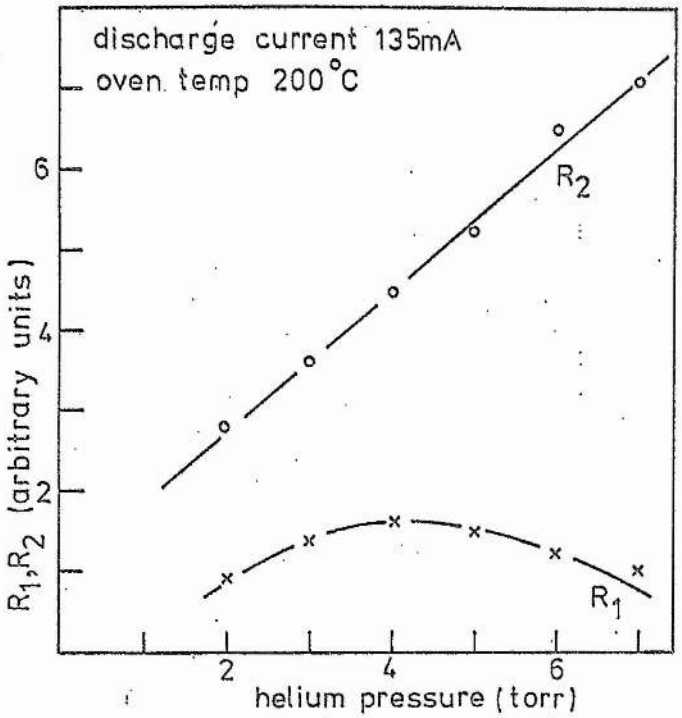

Fig. 5.7 The relative pumping rates of the upper (R_1) and lower (R_2) laser levels of 4416Å transition as a function of the helium filling pressure.

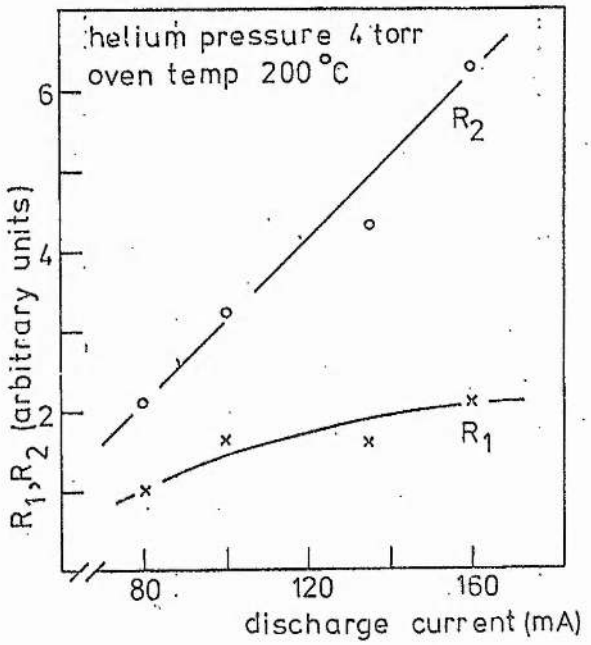

Fig. 5.8 The relative pumping rates of the upper (R_1) and lower (R_2) laser levels of the 4416Å transition as a function of the discharge current.

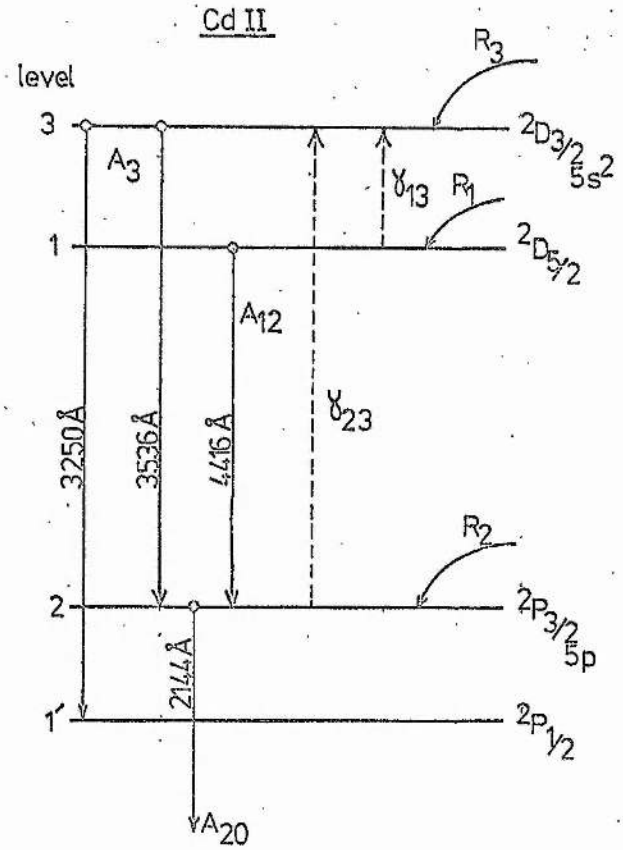

Fig. 5.9 Energy levels and optical transitions in CdII pertinent to the analysis of the perturbation spectrum.

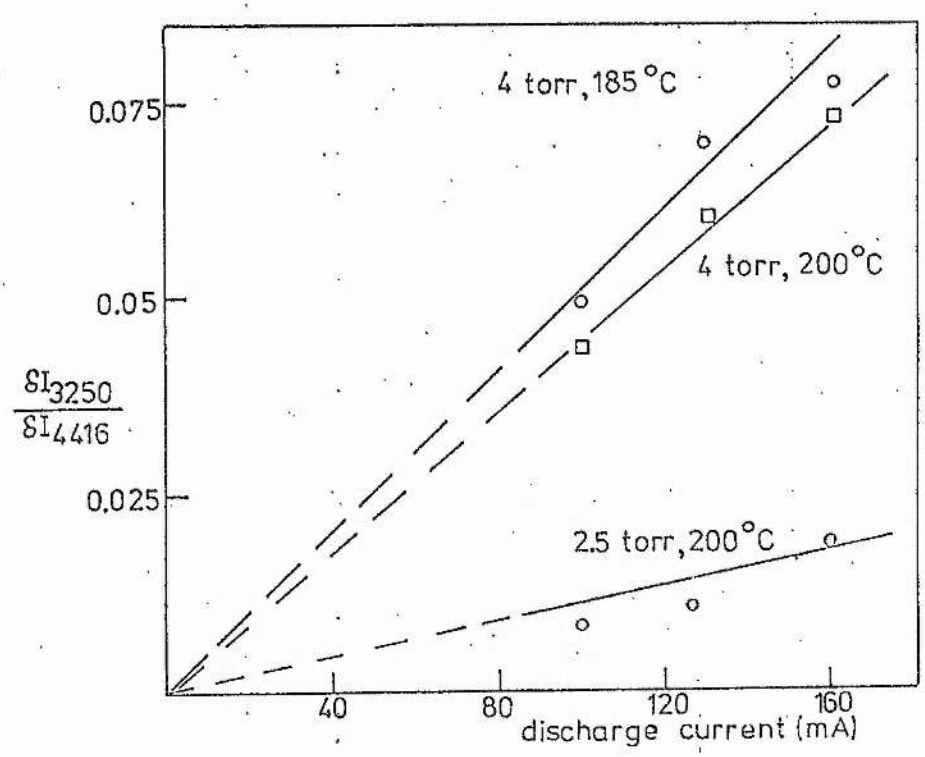

Fig. 5.10 The ratio of the perturbation signals at 3250Å and 4416Å as a function of current for various conditions.

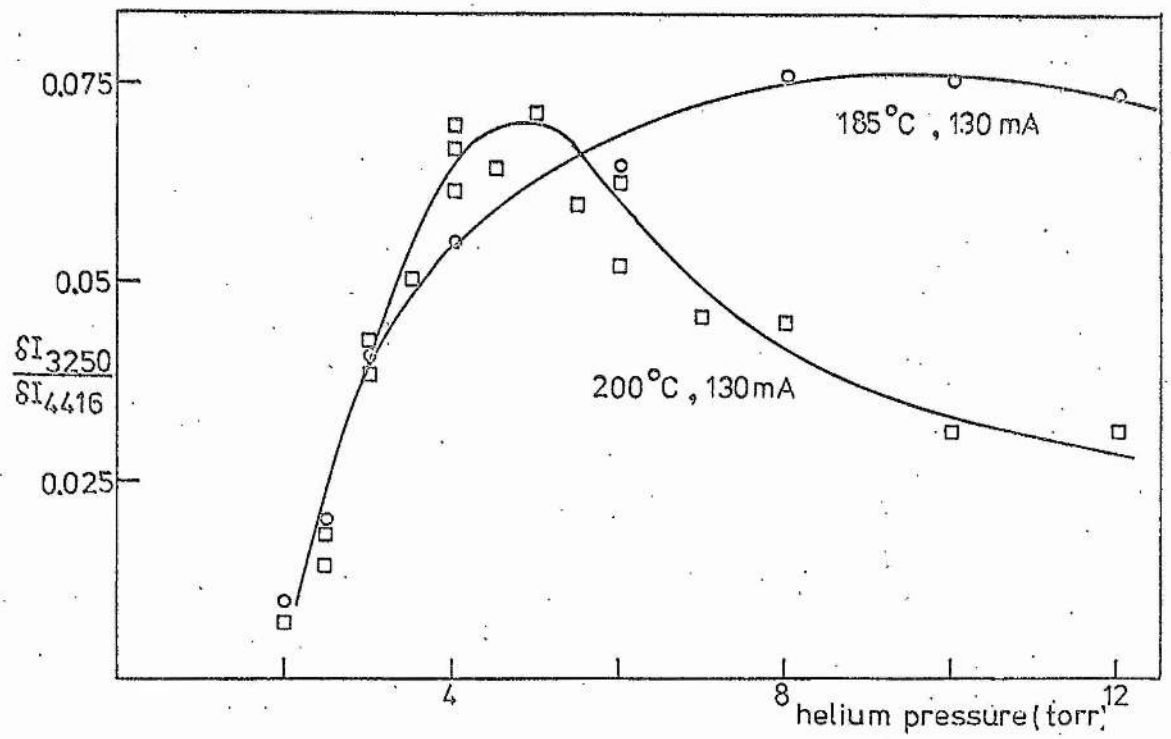

Fig. 5.11 The ratio of the perturbation signals at 3250Å and 4416Å as a function by helium pressure for two conditions.

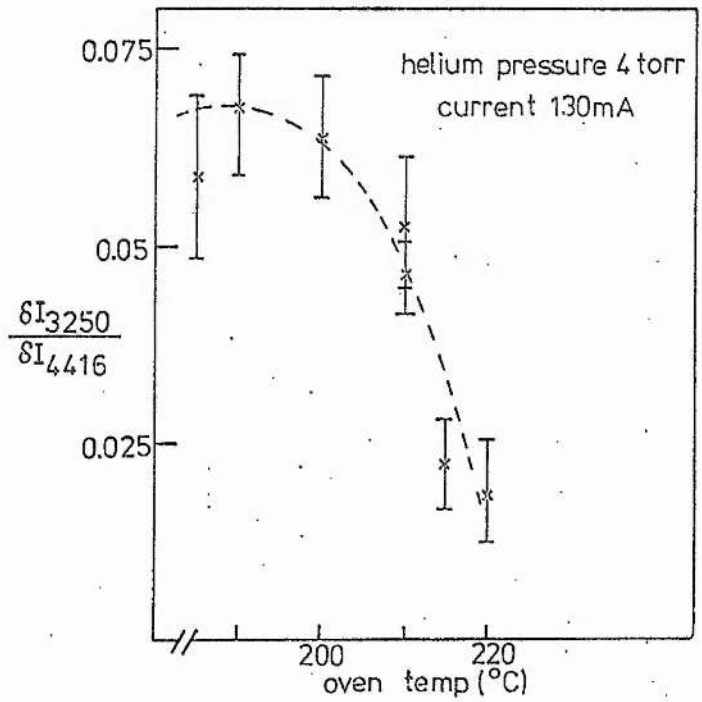

Fig. 5.12 The ratio of the perturbation signals at 3250Å and 4416Å as a function of oven temperature.

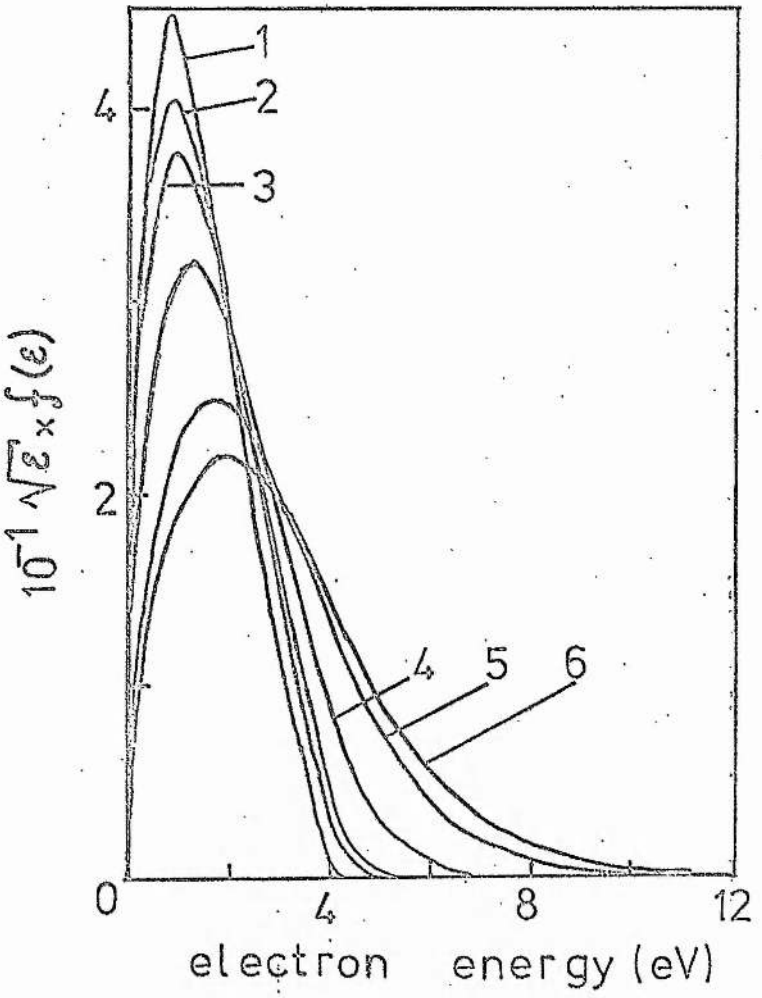

Fig. 5.13 Reproduction of Fig. 2 of Vokaty and Masek . .) showing calculated electron distribution functions for E/p = 1.5 V cm^{-1} $torr^{-1}$ with increasing fractional Cd concentration (N_{Cd}).

1 : $N_{Cd} = 5 \times 10^{-2}$, 2 : $N_{Cd} = 1 \times 10^{-2}$,

3 : $N_{Cd} = 5 \times 10^{-3}$, 4 : $N_{Cd} = 1 \times 10^{-3}$,

5 : $N_{Cd} = 1 \times 10^{-4}$, 6 : $N_{Cd} = 1 \times 10^{-5}$.

CHAPTER VI

SUMMARY AND CONCLUSIONS

6.1 Introduction

In this thesis investigations of the positive column helium-cadmium laser have been described. The experimental techniques comprised absorption spectroscopy and perturbation spectroscopy. Absorption spectroscopy was used to determine the population densities of the helium singlet (2^1S) and triplet (2^3S) metastable states and the cadmium ground state (5^1S). In particular the behaviour of these densities with discharge parameters was examined, and the production rate by Penning collisions of the $5s^2\ ^2D_{5/2}$ level of CdII estimated. Perturbation spectroscopy was used to determine the non-radiative destruction rate of the $5s^2\ ^2D_{5/2}$ level of CdII (the upper level of the 4416Å laser transition), the relative pump rates of the upper and lower ($5p\ ^2P_{3/2}$) laser levels, and collisional processes linking excited levels of the cadmium ion. The results of these experiments are summarised in turn.

6.2 Absorption Spectroscopy

Absorption spectroscopy was applied first (Chapter III) to the measurement of the singlet (2^1S) and triplet (2^3S) metastable densities in a pure helium discharge in a capillary tube of diameter 3 mm.

The density of the singlet metastable level (2^1S) was determined from absorption measurements at 5016Å (3^1P - 2^1S, HeI) and 3965Å (4^1P - 2^1S, HeI) while the density of triplet metastable level (2^3S) was determined from absorption measurements at 3889Å (3^3P - 2^3S, HeI). The effects of the fine structure of the 3889Å line on the analysis of the absorption experiment were taken into account (Section 2.7).

The pressure dependence of the metastable densities (Section 3.3) shows pronounced maxima around 2 torr (for a constant discharge current). The maximum densities are 2×10^{12} cm^{-3} for singlet and 9×10^{12} cm^{-3}

for triplet metastables. A model of the helium discharge is constructed (Section 3.4) in which all reported production and loss processes for the helium triplet metastable level are considered. The principal production mechanism for the triplet metastable level is electron excitation from the helium ground state (1^1S), either directly or by radiative cascade from higher excited levels, while the principal loss process is electron collisional excitation of the metastable states to ionized states. Other less important loss processes are diffusion of metastables to the tube walls, metastable-metastable collisions and metastable-helium ground state collisions. This model explains the appearance of a maximum in the dependence of triplet metastable density on current and predicts densities which are a factor of 2-3 higher than the measured densities. In view of the wide range of values reported for some of the cross-sections required in the model, some difference between model and experiment is expected.

Both triplet and singlet metastable densities saturate with increasing current for pressures below 1 torr. The discharge model discussed in Section 3.4 illustrates this behaviour for the 2^3S metastables since a point is reached where electron-collisional destruction of the triplet metastable level dominates the other loss processes mentioned above. Since the principal production and loss processes are then both proportional to the discharge current, the metastable density is independent of this parameter. The model further predicts the current at which saturation should occur. The predicted currents for saturation and those observed in the experiment agree to within a factor of 2. The model further predicts the observed behaviour that with increasing pressure the current at which saturation occurs rapidly decreases.

For pressures above 1 torr a slow decrease of singlet and triplet metastable densities with current is observed. This is shown to be

caused by the presence of significant populations, ie > 10% of the metastable populations, in the upper levels of the transitions for which the absorption is measured. These levels are the 3^1P, 4^1P and 3^3P levels of HeI. Calculations of the population of the 3^1P level were made (Section 3.4) using a procedure similar to that for calculating metastable densities. The principal excitation process is electron excitation from the helium ground state and the 2^1S metastable level, while the major destruction process is radiative decay at 5016Å (3^1P - 2^1S). The populations calculated in this way ($\sim 4 \times 10^{10}$ cm^{-3} for helium pressure 2 torr, current 100 mA) are in poor agreement with the values of $\sim 10^{12}$ cm^{-3} implied by the present experiment. The principal cause of this discrepancy is uncertainty in the cross-section for excitation of the 3^1P level from the metastable level. Populations of the 3, 4^1P levels of helium of $\sim 10^{12}$ cm^{-3} have been reported also by Kruse (21) for helium discharges under conditions close to those studied in this work (helium pressure 1 torr, discharge diameter 1 cm, currents 0-500 mA).

A possible consequence of the large populations ($\sim 10^{12}$ cm^{-3}) in the higher levels of helium is that they too may contribute to the Penning excitation of the upper laser levels $5s^2\ ^2D_{3/2,5/2}$ of the cadmium ion.

When cadmium vapour is admitted to the absorption cell (Chapter IV) the parametric behaviour of the spontaneous emission at 4416Å shows the same characteristics as are observed in a laser (Appendix I), namely distinct maxima in the dependence of the spontaneous emission on discharge current, helium pressure and cadmium oven temperature.

The cadmium neutral density in the discharge was determined (Section 4.2) by measuring the absorption of the CdI intercombination resonance line at 3261Å (5^3P_1 - 5^1S_0). The cadmium neutral density was found to vary little with the discharge current and the helium pressure,

but to be controlled by the oven temperature, which determines the vapour pressure of the cadmium within the oven. For optimum spontaneous emission at 4416Å (and hence optimum laser power) the cadmium neutral density is $\sim 2 \times 10^{13}$ cm^{-3}.

The presence of cadmium vapour has two effects on the metastable populations (Section 4.3).

First, these populations are reduced by a factor of 2 when the optimum cadmium partial pressure for lasing is present. This reduction is due to a decrease in the production rate of the metastable species since the presence of cadmium lowers the E/p value of the discharge and hence lowers the mean energy of the electrons. The high energy tail of the electron energy distribution is further depleted due to excitation of low-lying levels of CdI. The introduction of an additional loss process, Penning ionization, for the helium triplet metastables does not significantly alter the population of this level, since the ratio of the loss by Penning ionization to that by electron collisional de-excitation is 0.1 for typical lasing conditions (Section 4.3).

The second effect of cadmium vapour on the metastable populations is that the currents at which saturation occurs are higher (60-120 mA) than for the pure helium discharge (10-50 mA). The presence of cadmium vapour, by reducing the E/p value of the discharge, reduces the production rate and electron de-excitation rate for metastables. Inspection of equation (3.9) (Section 3.4) shows that higher currents are then required before electron collisional de-excitation dominates the other loss processes, ie the current at which saturation occurs is higher. In view of the lowered production rate for metastables when cadmium is present, their densities at saturation are also reduced.

The spontaneous emission at 4416Å as a function of current and pressure (for a fixed oven temperature, ie constant density of cadmium

ground state neutrals, Section 4.2) is found to follow the dependence of the triplet metastable densities on these parameters. The variation of spontaneous emission at 4416Å with oven temperature shows a pronounced maximum for an oven temperature of 240°C. As the cadmium neutral density steadily increases with oven temperature (Section 4.2) while the metastable densities steadily decrease (Section 4.3) the maximum in the spontaneous emission at 4416Å is consistent with the view (1,2) that the production rate of the upper level of this transition ($5s^2\ ^2D_{5/2}$, CdII) is proportional to the product of the helium metastable density and the cadmium ground state neutral density.

From the measured densities of metastable and neutral species in the He-Cd discharge (Chapter IV) and the decay rates of the $5s^2\ ^2D_{5/2}$ level of CdII (the upper level of the 4416Å laser transition) (Chapter V) the population of this level is now calculated as 1×10^{10} cm^{-3} under typical lasing conditions (helium pressure 2-4 torr, discharge current 120 mA, and oven temperature giving $N_{Cd} \sim 2 \times 10^{13}$ cm^{-3}). The calculation does not include excitation of the $5s^2\ ^2D_{5/2}$ level by collisions with helium atoms in states above the metastable levels. This may explain the difference between the present estimation and the value 6×10^{10} cm^{-3} obtained by Hodges (44). The behaviour at 4416Å of the He-Cd laser with respect to its three important operating parameters (helium filling pressure, cadmium oven temperature and discharge current) is thus explained by the behaviour of the metastable densities and ground state cadmium atoms with these parameters, with the excitation rate of the upper laser level proportional to the product of the metastable density and the ground state metal density. These conclusions should be valid also for other metal vapour laser systems such as He-Zn and He-Se where upper laser levels are populated by Penning collisions.

6.3 Perturbation Spectroscopy

In the perturbation spectroscopy experiments (Chapter V) the radiation field within the cavity of a He-Cd laser operating at 4416Å is chopped at 1600 Hz. Synchronous changes in the sidelight are observed at 4416Å ($5s^2\ ^2D_{5/2}$ - $5p\ ^2P_{3/2}$, CdII), 2144Å ($5p\ ^2P_{3/2}$ - $5s\ ^2S_{1/2}$, CdII) and 3250Å ($5s^2\ ^2D_{3/2}$ - $5p\ ^2P_{1/2}$, CdII).

Analysis of the perturbations at 2144Å and 4416Å (Section 5.4.2) yield an average value for the non-radiative decay rate, γ_1, of the $5s^2\ ^2D_{5/2}$ level of CdII of $\gamma_1 = 1.2 \pm 0.3 \times 10^6\ s^{-1}$. A slight variation of this non-radiative decay rate with current was seen, but no functional dependence on oven temperature or helium pressure. Slight variations of γ_1 with pressure and oven temperature have been observed (61,62) but for pressures below 1.5 torr where the discharge is less noisy. In the present experiments small changes in γ_1 could easily be masked by discharge fluctuations. While taking the average of the values of γ_1 over the range of conditions appropriate to laser oscillation conceals small variations, the value obtained may be used as an estimate in the analysis of the laser system. The most significant contribution to γ_1 is diffusion of ions in the radial field of the discharge to the tube walls. The transit time to the walls for an ion initially at the centre of a tube of radius 2 mm is approximately 1 μs (Section 5.4.2) which is similar to the radiative lifetime of $\sim$ 0.8 μs (70,71) for the $5s^2\ ^2D_{5/2}$ level of CdII.

The present result, $\gamma_1 = 1.2 \pm 0.3 \times 10^6\ s^{-1}$, is in agreement with the results of Klein and Maydan (61) who found that the total decay rate varied in the range $1.5 - 1.9 \times 10^6\ s^{-1}$ and with the results of Dienes and Sosnowski (62) whose values for γ_1 were a factor of 2-3 higher than those of Klein and Maydan.

There is however a large discrepancy between the present result for

γ_1 and that of Lis (66) who found a value $\gamma_1 = 40 \times 10^6\ s^{-1}$. This is shown (Section 5.4.2) to be due to the use by Lis of the ratio of the populations of the upper and lower laser levels of the 4416Å transition ($5s^2\ ^2D_{5/2}$, $5p\ ^2P_{3/2}$ respectively) which was derived by Hodges (67). The value derived by Hodges for this ratio is ~ 0.5, while the present experiments indicate a much lower value, ~ 0.03. Using this latter value for the ratio of population to re-interpret the results of Lis gives a value of $\gamma_1 = 1.8 \times 10^6\ s^{-1}$, in agreement with the present value.

A crucial test of the differing values for the ratio of the populations of the $5s^2\ ^2D_{5/2}$ and $5p\ ^2P_{3/2}$ levels would be a search for laser oscillation at 3536Å ($5s^2\ ^2D_{3/2}$ - $5p\ ^2P_{3/2}$, CdII). According to Hodges this transition should not lase because of the large population of the lower $5p\ ^2P_{3/2}$ level, in contradiction to the conclusions of the present work. Two main difficulties would be present in such a search. First, oscillation at 3250Å would have to be quenched (as the 3250Å laser transition has the same upper level as the transition at 3536Å) and second, the losses in the system would have to be less than the gain of $\frac{1}{2}\%\ m^{-1}$ in a tube containing a single isotope of cadmium.

From the ratio of the spontaneous emission intensities at 2144Å and 4416Å the excitation rates of the lower and upper levels of the 4416Å laser transition are in the ratio 3:1 under typical conditions for lasing. The excitation to the lower laser level is via radiative cascade from levels of the cadmium ion which are excited by charge transfer collisions. The upper laser level is excited by Penning collisions.

A perturbation at 3250Å ($5s^2\ ^2D_{3/2}$ - $5p\ ^2P_{1/2}$, CdII) is found (Section 5.4.3) to have a parametric behaviour which necessitates the inclusion of coupling to the $5s^2\ ^2D_{3/2}$ level (the upper level of the

3250Å transition) from both the upper ($5s^2\ ^2D_{5/2}$) and lower ($5p\ ^2P_{3/2}$) level of the 4416Å transition. This coupling is via electron collisions. The cross-section for excitation to the $5s^2\ ^2D_{3/2}$ level from the $5s^2\ ^2D_{5/2}$ level is 7×10^{-16} cm^2, a value typical of gas kinetic cross-sections. The cross-section for excitation from the $5s\ ^2P_{3/2}$ level to the $5s^2\ ^2D_{3/2}$ level is found to be 7×10^{-13} cm^2, which is extremely large for an atomic collision process. A plausibility argument based on this cross-section and applying the principle of detailed balance shows that the electron de-excitation rate of the $5s^2\ ^2D_{5/2}$ upper laser level should be far higher ($\sim 70 \times 10^6\ s^{-1}$) than is observed ($\sim 1 \times 10^6\ s^{-1}$, Section 5.4.2). At present, however, it is not possible to resolve this inconsistency.

Very little is known about electron collisions with levels which are already excited, but if the present large cross-section of 7×10^{-13} cm^2 for transitions between the $5s^2\ ^2D_{3/2}$ and $5s\ ^2P_{3/2}$ levels is valid, it could indicate a collision involving a transient intermediate state, for example an autoionizing level of neutral cadmium.

APPENDIX I

CONSTRUCTION OF A CATAPHORETIC HELIUM-CADMIUM LASER

A1.1 Introduction

The technology associated with the helium-cadmium laser is very similar to that of the well established helium-neon system except that somewhat higher current densities are needed as well as the means for introducing into the discharge a uniform vapour pressure of cadmium. Goldsborough (4) and Sosnowski (3) found that if cadmium vapour is continuously introduced into the helium capillary discharge at the anode end then cataphoresis causes a flow of metal ions towards the cathode at a controlled even rate. The positive column of the discharge becomes thereby a region where the metal vapour density is uniform, and by adjusting the vapour pressure in the cadmium source it is possible to obtain cadmium densities of the correct magnitude for laser oscillation. The construction of the laser system will be discussed in three sections : the laser tube and the vacuum system, the oven design, and the cathode processing and performance. Typical output power curves are shown as a function of the parameters: discharge current, helium filling pressure and cadmium oven temperature.

A1.2 The laser tube and vacuum system

The laser tube is shown schematically in Fig. AI.1. The capillary tube, electrode envelopes, Brewster angle window assemblies and tee sections were quartz. The capillary tube was 2.5 mm i.d., 5.1 mm o.d. and 60 cm long. The tube had been specially selected by the suppliers (Jencons) for straightness and uniformity of bore.

The two hollow electrodes were turned from 94% Al - 6% Cu alloy and were supported by the tungsten to quartz seals which provided electrical connection. The electrodes were made identical so that either could be used as the cathode. This allowed the direction of the cadmium flow to be reversed.

Spirals made from pyrex tube of 5 mm bore and length 150 cm were

attached at one end to electrode envelopes through quartz to pyrex seals, and at the other to stainless steel valves (Hoke Type H72 G4Y) by pyrex to Nilo-K seals. These spirals prevented the discharge running to the metal vacuum system on the other side of the valves.

Enlarged sections of the tube (approximately 2 cm diameter and 3 cm long) were provided at each end of the quartz capillary. The one near the anode contained a few pellets of cadmium metal of natural isotopic composition (BDH 'Analar' grade) and was enclosed by the oven. The other was not covered and was therefore cooled by convection. As the discharge heating of the tube wall was much reduced by the larger diameter the cadmium vapour condensed in this region. The discharge heating in the capillary, however, maintained a sufficiently high wall temperature, without the need for heaters or extra insulation, to prevent condensation of the cadmium in this section of the tube.

No special procedure was adopted to accurately align the Brewster angle windows at the tube ends. The presence of the helium was most effective in preventing diffusion of cadmium to the windows.

The vacuum and gas filling system, shown schematically in Fig. AI.2, was constructed from stainless steel with gold 'O'-ring seals. Connection to the laser tube was made with short sections of ¼" o.d. stainless steel pipe. A stainless steel system was used since it could be left open to the laser tube (to monitor pressure) for extended periods, while sealed off from the pump, with little outgassing.

The system was pumped by a two-stage rotary pump (Metrovac GDR 1) with a zeolite-filled oil vapour trap (Vacuum Generators RT 1). The system reached a base pressure of 10^{-2} torr, measured with a Pirani gauge (Edwards M6A, range 0.001 - 0.5 torr). Gas filling pressure was monitored with a 0 - 10 torr capsule gauge (AEI). The two valves on the laser tube were arranged so that helium could be flushed through the system (with or without a discharge). This facility was found to

be unnecessary and was eliminated from later tubes. Helium of 4N5 purity was used (BDH 'Labgas').

The laser discharge was run from a 0-15 kV, 0-1A power supply of conventional design (three phase bridge rectification followed by smoothing capacitors). As this supply was not current regulated a 40 kΩ ballast resistor was placed in series with the tube for stability of the discharge.

A1.3 Cadmium Oven Design

The first design of the oven used to heat the cadmium at the anode end of the discharge consisted of two semi-cylindrical asbestos sections with a hole in each end through which the discharge tube passed. The inside was of such diameter that the heating element fitted closely to the enlarged section of the tube holding the cadmium. The two sections fitted over the tube and were bolted together to give a small (3" diameter x 2" long) robust oven. The heating elements (one to each semi-cylindrical section) consisted of five turns of nichrome wire (2 mm x 0.16 mm) wound over a quartz former with notched ends to keep the turns separated.

A chromel-alumel thermocouple monitored the oven temperature. The thermocouple was placed on the enlarged section of the tube and covered with thin asbestos sheet to avoid direct contact with the heater turns. The output of the thermocouple was connected to the temperature controller (Ether 'Transitrol' type 991 G). The required oven temperature was set and maintained to $\pm$ 1C^{o} by the controller.

Subsequent tubes were constructed using flexible ovens (Electro-thermal), capable of dissipating 400 W at up to 1000°C.

A1.4 Cathode Requirements

Prior to operation in helium the cathode required processing. This was carried out by running a discharge in air at a pressure of a few torr and a current of 50 mA for thirty minutes. The tube was then

evacuated to the base pressure of the pump and filled with 3-4 torr of helium and a 100 mA discharge initiated. Due to outgassing during this first discharge the system was pumped out and refilled after a further thirty minutes.

For a cathode of the dimensions in Fig. AI.1 and processed in the above way, sputter free operation in helium at 3 torr was obtained up to 100 mA. Operation above 100 mA was accompanied by pronounced sputtering, and a thin film of aluminium slowly formed on the quartz envelope around the cathode. Above 120 mA the rate of deposition was considerable as an opaque film formed in one hour.

Larger cathodes (8" long x 1¼" o.d.) were subsequently made from aluminium alloy (HE15TF). These cathodes have been run up to 400 mA with little sputtering or surface degradation. Further, the need for processing the cathode before operation in helium was found to be unnecessary.

A1.5 Operating Characteristics and Laser Power

When operated at 100 mA in pure helium at a pressure of 2-10 torr the discharge voltage was 2.3 kV. As the oven temperature was increased to the value which provided optimum cadmium concentration for laser power at 4416Å the discharge voltage dropped to 1.7 kV. The discharge took only a few minutes to reach equilibrium when the cadmium oven was in operation. The power dissipated in the quartz capillary was about 3 W/cm.

The effects of varying the three important operating parameters were studied. These parameters are the oven temperature (which controls the cadmium vapour pressure), discharge current, and the helium filling pressure. Figs. AI.3 a, b, c show the effects of keeping two of the three parameters constant while measuring the laser output power at 4416Å as a function of the third. These results indicate the form of the dependence of the laser power on the parameter varied and the range of the parameter over which laser oscillation occurs. Note that the

power scale has arbitrary units - the maximum power obtained with this laser (active length 60 cm) was 20 mW. No attempt was made to obtain optimum coupling through the laser output mirror.

The pronounced optimum behaviour of the laser power with respect to the three operating parameters is a characteristic feature of the behaviour of laser transitions excited by Penning collisions.

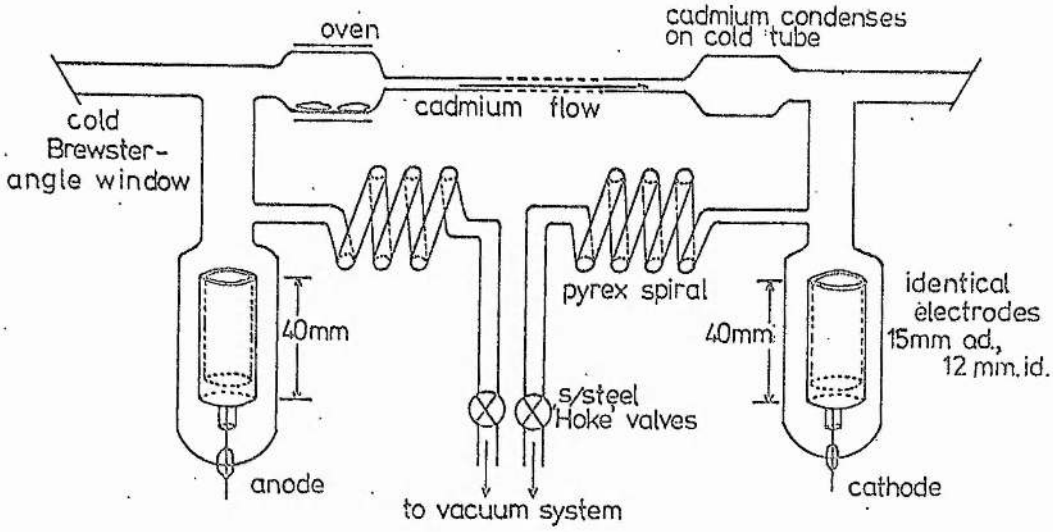

Fig. AI.1 Schematic diagram of the He-Cd laser tube

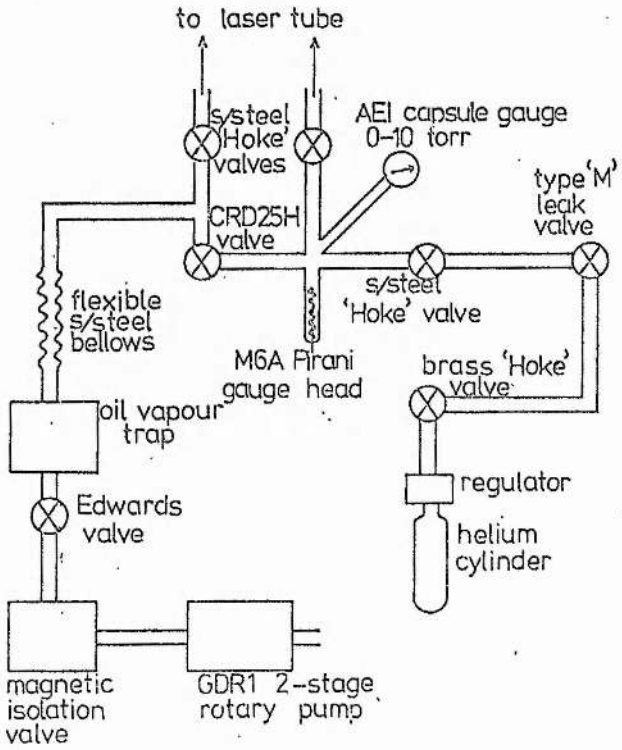

Fig. AI.2 Schematic diagram of vacuum and gas-filling system

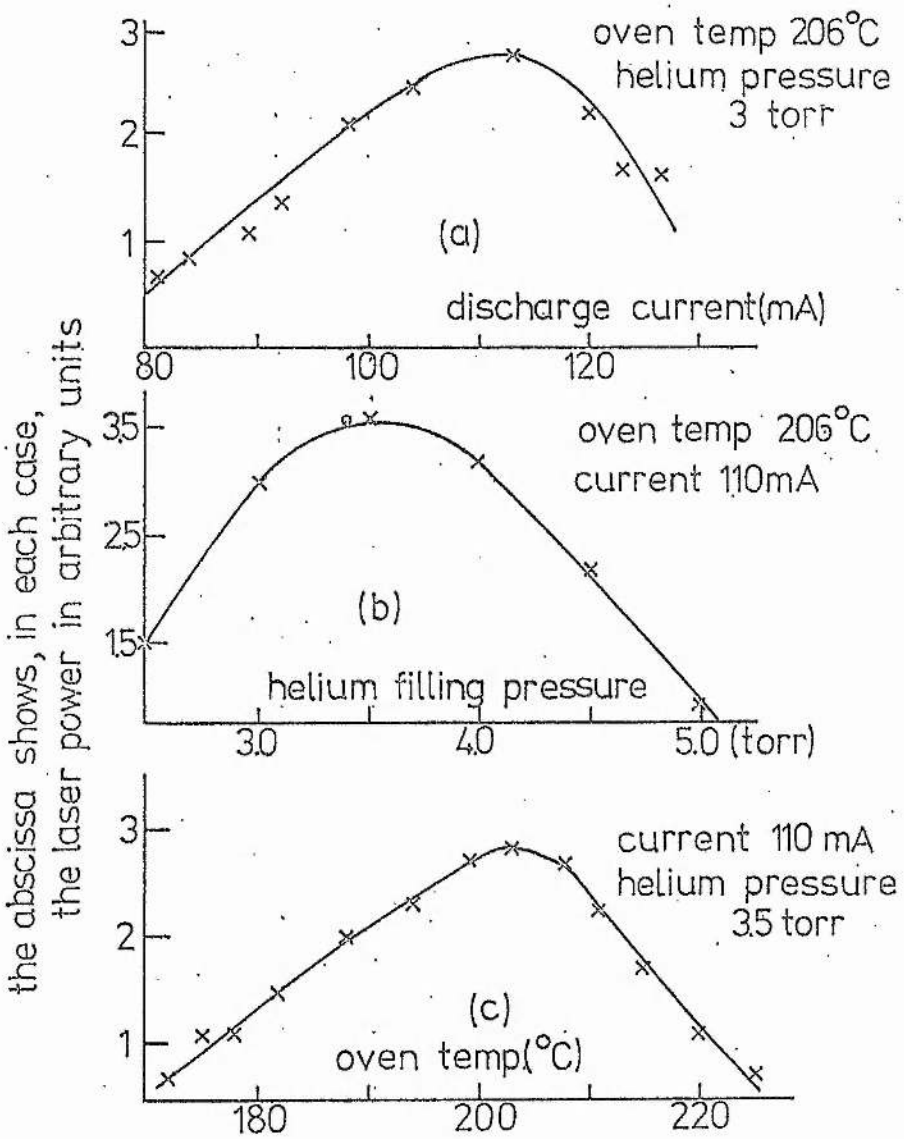

Fig. AI.3 Laser power at 4416Å as a function of

(a) discharge current, with oven temperature and helium pressure fixed

(b) helium filling pressure, with oven temperature and discharge current fixed

(c) oven temperature, with discharge current and helium pressure fixed.

APPENDIX II

COMPUTER CALCULATION OF THE ABSORPTION FOR A LINE WITH OVERLAPPING COMPONENTS

The stepwise integration of the absorption functions (1 - A)A and (1 - A) (where $A = \exp(-k_\nu d)$ (Section 2.4)) for a complex line shape is now described. Five hundred points are generated across a frequency interval of 20 GHz and the centre frequencies of each of the components of the line are arranged about the centre of this interval. The value of the absorption coefficient, k_ν, resulting from the overlapping Doppler profiles of each component is calculated at each of the five hundred points.

The value of the product of the absorption length and the density of the absorbing species (N1) is varied over a range of 100 in increments of 2. For each value the above integrals are determined and values of the absorption ($\frac{I_R}{I_o}$, Section 2.4) are printed against the values of the N1 product.

Listings for the programmes to calculate the absorption at 3889Å in HeI and 3261Å in CdI are shown in Figs AII.1, AII.2 respectively. The programme for the helium line will be explained in detail - the programme for the cadmium line is completely analogous and as far as possible the same names for variables have been used.

The programme begins by reading the centre frequencies (HZ1, HZ2, HZ3) of the components of the 3889Å line, their relative fractional intensities (R1, R2, R3), the frequency HZS at which the 20 GHz interval starts (usually 0 GHz) and the value of the increment (HZA) of frequency required to give five hundred points across the 20 GHz interval.

The constants WDTH and A are given by

$$\mathrm{WDTH} = \frac{4\ln^2}{\Delta\nu_D^{\,2}}$$

$$A = \frac{\lambda_o^{\,2}}{8\pi}\sqrt{\frac{\ln 2}{\pi}}\cdot\frac{g_u}{g_1}\,\frac{2}{\Delta\nu_D}\,A_{ul}\quad (\times 10^n)$$

(For simplicity some of the powers of 10 from the N1 product are included in A at this stage so that the N1 range which occurs later in the programme is 0 - 100).

The last quantities read in are the starting value of the N1 product (DES) in the increment (DEA) required to cover the N1 range.

First, five hundred points along the frequency axis are generated and stored as CYCLE (I) values (Statement 29). At each of the five hundred points the absorption coefficient is determined by summing the contributions from the Doppler profiles of each of the components. These coefficients are stored (Statement 30) as TRP(I) values (TRP abbreviates 'triplet', the second programme uses CDR to abbreviate 'cadmium resonance').

The required values of the N1 product are calculated and stored (Statement 35).

Finally, for each of these N1 values, the absorption integrals are evaluated step by step across the five hundred points of the absorption profile and the value of the required function

$$\frac{\int_{\nu} (1 - \exp(-k_{\nu} d)) \exp(-k_{\nu} d)\, d\nu}{\int_{\nu} 1 - \exp(-k_{\nu} d)\, d\nu}$$

is printed with the corresponding N1 value.

```
// FOR
*IOCS(CARD,TYPEWRITER)
*LIST SOURCE PROGRAM
      DIMENSION CYCLE(500),TRP(500),DE(100)
      READ(2,24)HZ1,HZ2,HZ3,WDTH,HZS,HZA
      READ(2,24)A,R1,R2,R3,DES,DEA
      CYCLE(1)=HZS
      DO29I=2,500
29    CYCLE(I)=CYCLE(I-1)+HZA
      DO30I=1,500
      TRP1=A*R1*EXP(-WDTH*(CYCLE(I)-HZ1)**2)
      TRP2=A*R2*EXP(-WDTH*(CYCLE(I)-HZ2)**2)
      TRP3=A*R3*EXP(-WDTH*(CYCLE(I)-HZ3)**2)
30    TRP(I)=TRP1+TRP2+TRP3
      DE(1)=DES
      DO35J=2,100
35    DE(J)=DE(J-1)+DEA
      DO36J=1,100
      ABSA=0.0
      ABSB=0.0
      DO31I=1,500
      ABSA=ABSA+(1.-EXP(-DE(J)*TRP(I)))**2
31    ABSB=ABSB+(1.-EXP(-DE(J)*TRP(I)))
      ANS=1.-ABSA/ABSB
36    WRITE(1,25)DE(J),ANS
24    FORMAT(6F10.5)
25    FORMAT(2F10.5)
      CALL EXIT
      END
```

Fig. AII.1 Listing of the programme used for relating absorption at 3889Å (HeI) to the reduced helium triplet metastable density.

```
// FOR
*IOCS(CARD,TYPEWRITER)
*LIST SOURCE PROGRAM
      DIMENSION CYCLE(500),CDR(500),DE(100)
      READ(2,24)HZ1,HZ2,HZ3,HZ4,HZ5,HZ6
      READ(2,24)HZ7,HZ8,HZ9,HZ10,HZS,HZA
      READ(2,24)WDTH,A,R1,R2,R3,R4
      READ(2,24)R5,R6,R7,R8,R9,R10
      READ(2,25)DES,DEA
      CYCLE(1)=HZS
      DO29I=2,500
29    CYCLE(I)=CYCLE(I-1)+HZA
      DO30I=1,500
      CDR1=A*R1*EXP(-WDTH*(CYCLE(I)-HZ1)**2)
      CDR2=A*R2*EXP(-WDTH*(CYCLE(I)-HZ2)**2)
      CDR3=A*R3*EXP(-WDTH*(CYCLE(I)-HZ3)**2)
      CDR4=A*R4*EXP(-WDTH*(CYCLE(I)-HZ4)**2)
      CDR5=A*R5*EXP(-WDTH*(CYCLE(I)-HZ5)**2)
      CDR6=A*R6*EXP(-WDTH*(CYCLE(I)-HZ6)**2)
      CDR7=A*R7*EXP(-WDTH*(CYCLE(I)-HZ7)**2)
      CDR8=A*R8*EXP(-WDTH*(CYCLE(I)-HZ8)**2)
      CDR9=A*R9*EXP(-WDTH*(CYCLE(I)-HZ9)**2)
      CDR10=A*R10*EXP(-WDTH*(CYCLE(I)-HZ10)**2)
30     CDR(I)=CDR1+CDR2+CDR3+CDR4+CDR5+CDR6+CDR7+CDR8+CDR9+CDR10
      DE(1)=DES
      DO35J=2,50
35    DE(J)=DE(J-1)+DEA
      DO36J=1,50
      ABSA=0.0
      ABSB=0.0
      DO31I=1,500
      ABSA=ABSA+(1.-EXP(-DE(J)*CDR(I)))**2
31    ABSB=ABSB+(1.-EXP(-DE(J)*CDR(I)))
      ANS=1.-ABSA/ABSB
36    WRITE(1,25)DE(J),ANS
24    FORMAT(6F10.5)
25    FORMAT(2F10.5)
      CALL EXIT
      END
```

Fig. AII.2 Listing of the programme used for relating absorption at 3261Å (CdI) to the cadmium ground state neutral density.

REFERENCES

1. Silfvast W T, Appl Phys Lett 13, 169-171, 1968
2. Silfvast W T, Appl Phys Lett 15 , 23-25, 1969
3. Sosnowski T P, J Appl Phys 40, 5138-44, 1969
4. Goldsborough J P, Appl Phys Lett 15, 159-61, 1969
5. Francis G, Handbuch der Physik, Springer-Verlag, Berlin, Vol XXII, pp 53-208, 1956
6. Schearer L D and Padovani F A, J Chem Phys 52, 1618-19, 1970
7. Riseberg L A and Schearer L D, Phys Lett 35A, 269-270, 1971
8. Čermak V, Collection Czechoslov Chem Comm 36, 948-950, 1971
9. Varshavskii S P, Mityureva A A and Penkin N P, Opt Spectrosc 29, 341-343, 1970
10. Dunn M H, J Phys B : Atom Molec Phys 5, 665-672, 1972
11. Webb C E, Turner-Smith A R and Green J M, J Phys B : Atom Molec Phys 3, L134-138, 1970 and 6, 114-130, 1973
12. Harrison J A, Proc Phys Soc 73, 841-848, 1959
13. Mitchell A G C and Zemansky M W, Resonance Radiation and Excited Atoms, Cambridge : University Press, 1961
14. Griem H R, Plasma Spectroscopy, McGraw-Hill, New York, 1964
15. Fugol I Y, Myshkis D A and Grigorashchenko O N, Opt Spectrosc 31, 282-5, 1971
16. Gibbs R C and Kruger P G, Phys Rev 37, 1559-61, 1931
17. Brix P and Steudel A, Z Phys 128, 260-68, 1950
18. Kelly F M and Tomchuk E, Proc Phys Soc 74, 689-692, 1959
19. Kuhn H G and Ramsden S A, Proc Roy Soc A237, 485-95, 1956
20. Dunn M H, University of St Andrews, Scotland, unpublished work.
21. Kruse M, Z Phys 109, 312-331, 1938
22. Chester A N, Phys Rev 169, 172-184 and 184-193, and references therein
23. Corrigan S J B and von Engel A, Proc Phys Soc 72, 786-790, 1958
24. Miller P A, Verdeyen J T and Cherrington B E, Phys Rev A4, 692-700, 1971

25. Smit J A, Physica 3, 543-560, 1936

26. Heylen A E D and Lewis T J, Proc Phys Soc 271A, 531-550, 1963

27. Reder F H and Brown S C, Phys Rev 95, 885-889, 1954

28. Englert G W, Z Naturf 26A, 836-848, 1971

29. Phelps A V, Phys Rev 99, 1307-1313, 1955

30. Long D R and Geballe R, Phys Rev A1, 260-5, 1970

31. Fugol I Y, Grigorashchenko O N and Myshkis D A, Sov Phys JETP 33, 227-35, 1971

32. Arrathoon J, Bell Telephone Labs, NJ, USA, private communication.

33. Morrison D J T and Rudge M R H, Proc Phys Soc 91, 565-73, 1967

34. Phelps A V and Molnar J P, Phys Rev 89, 1202-8, 1953

35. Bell K L, Dalgarno A and Kingston A E, J Phys B: Atom Molec Phys 1, 18-22, 1968

36. Miller P A, Verdeyen J T and Cherrington B E, Phys Rev A4, 692-700, 1971

37. Fugol I Y, Grigorashchenko O N and Myshkis D A, Sov Phys - Dokl 16, 560-2, 1972

38. van Eck J and de Jongh J P, Physica 47, 141-158, 1970

39. Kim Y K and Inokuti M, Phys Rev 181, 205-13, 1969

40. Phelps A V, Phys Rev 110, 1362-68, 1958

41. Silfvast W T, Phys Rev Lett 27, 1489-92, 1971

42. Honig R E, RCA Revue 23, 567-589, 1962

43. Vokaty E and Masek K, Czech J Phys B22, 776-789, 1972

44. Hodges D T, Appl Phys Lett 17, 11-13, 1970

45. Waksburg A L and Carswell A I, Appl Phys Lett 6, 137-138, 1965

46. Parks J H and Javan A, Phys Rev 139, A 1351-1358, 1965

47. Weaver L A and Freiberg R J, J Appl Phys 37, 1528-1538, 1966

48. Lis L, Acta Phys Polonica A42, 307-318, 1972

49. Lis L, Acta Phys Polonica A43, 453-459, 1973

50. Khaikin A S, Sov Phys JETP 24, 25-32, 1967

51. Khaikin A S, Sov Phys JETP 27, 28-33, 1968

52. Lilley R A, J Opt Soc Amer 62, 1023-1026, 1972

53. Freiberg R J and Weaver L A, J Appl Phys 38, 250-262, 1967

54. Crane R A and Waksberg A I, Appl Phys Lett 10, 237-239, 1967

55. Dunn M H and Maitland A, Proc Phys Soc 92, 1106-1114, 1967

56. Hansch T and Toschek P, Phys Lett 20, 273-75

57. Heisenberg W, Z Phys 31, 617-26, 1926

58. Hansch T and Toschek P, Phys Lett 22, 150-51, 1966

59. Abrams R L, PhD thesis, Cornell University, New York, 1968

60. Baumann S R and Smith W H, J Opt Soc Amer 60, 345-347, 1970

61. Klein M B and Maydan D, Appl Phys Lett 16, 509-511, 1970

62. Dienes A and Sosnowski T P, Appl Phys Lett 16, 512-514, 1970

63. Shenstone A G and Pittenger J T, J Opt Soc Amer 39, 219-225, 1949

64. Phelps A V, Phys Rev 110, 1362-68, 1958

65. Cobine J D, Gaseous Conductors, Dover, New York, 1958, p256.

66. Lis L, Acta Phys Polonica A44, 173-175, 1973

67. Hodges D T, Appl Phys Lett 17, 11-13, 1970

68. Turner-Smith A R, PhD thesis, Oxford University, 1971

69. Collins G J, Jensen R C and Bennett W R, Appl Phys Lett 19, 125-128, 1971

70. Geneux E and Wanders-Vincenz B, Helv Phys Act 33, 183-215, 1960

71. Barrat M and Barrat J P, Comptes Rendus 257, 1463-65, 1963

72. Beutler H, Z Phys 87, 19-27, 1934

73. Green J M, Collins G J and Webb C E, J Phys B : Atom Molec Phys 6, 1545-1555, 1973

74. Bransden B H, Atomic Collision Theory, Benjamin, New York, 1970, Chapter 7.